Discharge Characteristics of Auditory Nerve Fibers for Pulsatile Electrical Stimuli

by

Scott Budd Chapman Dynes

Submitted to the Department of Physics
in partial fulfillment of the requirements for the degree of

Doctor of Philosophy

at the

MASSACHUSETTS INSTITUTE OF TECHNOLOGY

February 1996

Author .....
Department of Physics
December 12, 1995

Certified by .....
Bertrand Delgutte
Associate Professor of Otolaryngology
Thesis Supervisor

Certified by .....
George B. Benedek
Alfred H. Caspary Professor of Physics
Thesis Supervisor

Certified by .....
Richard J. Cohen
Professor of Health Sciences and Technology
Reader

Accepted by .....
George F. Koster
Chairman, Departmental Committee on Graduate Students

Discharge Characteristics of Auditory Nerve Fibers for Pulsatile Electrical Stimuli

by

Scott Budd Chapman Dynes

Submitted to the Department of Physics
on December 12, 1995, in partial fulfillment of the
requirements for the degree of
Doctor of Philosophy

Abstract

Human cochlear implant subjects show improved speech perception when their implanted electrode arrays are stimulated using interleaved pulses rather than continuous analog signals. Current interleaved pulse stimulation schemes result in temporal interactions, where one stimulus affects the neural response to subsequent stimuli. This work characterizes temporal interactions occurring in single auditory nerve fibers in cat using pulsatile stimuli. A conditioner, consisting of one or more pulses of equal amplitude, was used to modify the state of the resting neuron. This was followed at various delays by a single pulse used to probe the state of the modified neuron. The neural threshold and relative spread (normalized dynamic range) were measured from the neural response to the probe pulse. Subthreshold pulses result in a short period of sensitization immediately after the conditioning pulse, followed by a longer desensitization period. Sensitization decreased with increasing numbers of conditioning pulses. The relative spread of the neural response is increased during sensitization. Suprathreshold conditioners lead to a relative refractory period, with probe threshold resuming the resting value after 4 msec. Following a suprathreshold conditioner, the relative spread is decreased for short probe delays. Modeling efforts show that these experimental phenomena can be qualitatively reproduced using standard Hodgkin-Huxley-like models. Of the five systems whose model parameters were examined, the Hodgkin-Huxley model of the squid giant axon and the Rothman-Manis-Young model of a cochlear nucleus bushy cell provided simulations that fit well with the observed data. Models of mammalian systems (rat and rabbit sciatic nerve) provided poor simulations of the data. It is hypothesized that the overall effect of temporal interactions is to increase the dynamic range of neural response to electric pulsatile stimulation, and that this change in dynamic range may improve the nerve's ability to code changes in stimulus amplitude, possibly resulting in increased speech perception by human cochlear implant users.

Thesis Supervisor: Bertrand Delgutte

Title: Associate Professor of Otolaryngology

Thesis Supervisor: George B. Benedek
Title: Alfred H. Caspary Professor of Physics

Acknowledgments

This work has benefited from the support and input of many kind, knowledgeable individuals. Foremost, I must thank my advisor for his endless efforts to corral my efforts into a focused, coherent piece of research. Also, this work would not have been possible without the challenging, rich environment of the Eaton-Peabody lab and Nelson Kiang, who always was able to place the day's travails into the context of the scientific ideal.

I would like to recognize the able assistance of Jennifer Melcher and Don Eddington in my quest for closure, and to Ed Mroz who brought the true meaning of the grad school experience to my attention.

In the years that I have worked at EPL, there were/are many individuals who have made life quite interesting. I thank them all.

Finally, I thank my wife Linda for her love and support, and to my son Jason, who probably did not help me finish quickly, but provided many enlightening hours about the meaning of life.

This work was supported by research grant number DC00361 from the National Institute on Deafness and Other Communication Disorders, National Institutes of Health.

Contents

Chapter 1

Introduction

In the normally-functioning ear an acoustic stimulus, consisting of pressure variations in the air, results in motions of elements of structures in the ear. Specialized sensory cells in the inner ear transduce these mechanical vibrations into neural impulses traveling along auditory nerve fibers from the ear to the brain; the death of these cells results in profound deafness. **Cochlear prostheses**, also known as **cochlear implants**, restore a sense of hearing to the profoundly deaf by using electrodes implanted in the inner ear to directly stimulate the auditory nerve using electric currents.

One stimulus commonly used in cochlear implants consists of a train of short electric pulses interleaved in time so that each implanted electrode is stimulated in turn. Typical pulse durations are about 100 μsec, with intervals between pulses on each electrode being about 0.5 msec. The issue is whether these interleaved pulses give rise to **temporal interactions**, where previous pulses affects the neural response to subsequent pulses. These temporal interactions can come about either from consecutive pulses on the same electrode or from closely-spaced pulses on separate electrodes affecting the same neuron.

The questions that are addressed in this work are:

- Do temporal interactions exist in electrically-stimulated auditory nerve fibers?
- Do existing models of the neural membrane provide reasonable simulations of temporal interactions?

- Do the observed temporal interactions have implications for existing cochlear implant stimulus schemes?

These questions will be addressed using experimental data collected from individual auditory nerve fibers in cat, with pulsatile electrical stimulation provided by an electrode implanted in the cat's cochlea.

The remainder of this introduction provides a framework in which to think about the issues associated with temporal interactions. First, cochlear implants are introduced, along with the interleaved pulse stimulus. Following is a discussion of the neuron, and how it responds to electrical stimulation.

With this background, the experimental results and results of modeling studies are discussed.

1.1 Function of the Auditory Periphery

The peripheral auditory system is customarily divided into three parts: the outer, middle, and inner ears. These are shown in Figure 1-1.

The external ear, consisting of the pinna and the external auditory meatus serves to modify the free-field acoustic signal in a manner that aids in source localization. The middle ear consists of three ossicles. The first one, the malleus, is attached to the tympanic membrane, and moves with the membrane in response to pressure changes in the external ear. The motion of the malleus is transferred through the second ossicle, the incus, to the last ossicle, the stapes, which fills an opening into the cochlea.

The cochlea, also known as the inner ear, can be stylized as two fluid-filled tubes (the scalae tympani and vestibuli) which are collinear and separated along their length by a flexible membrane called the basilar membrane. Each tube opens to the middle ear near the basal end; the opening of the scala tympani is called the round window and is covered by a thin membrane. The opening from the scala vestibuli, the oval window, is filled with the footplate of the stapes. At the apical end, the two scalae are connected by a small opening, allowing the passage of fluid. The scalae are coiled

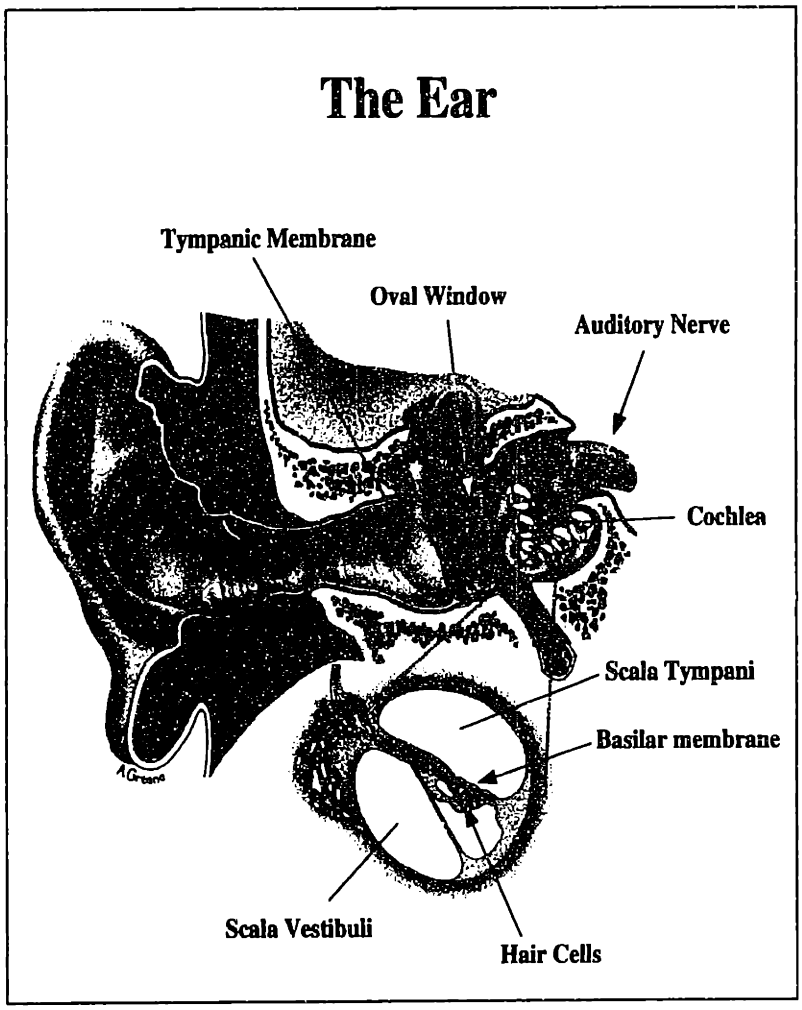

Figure 1-1: An overview of the ear.

about each other, resulting in the familiar snail shape.

The basilar membrane acts as a substrate for sensory cells, called hair cells, which are specialized for detecting movement of that membrane via protruding tufts of hairs. In cat, approximately 3,000 of these hair cells lie in a line extending the length of the basilar membrane. The function of these hair cells is to transduce the motions of the basilar membrane into neural impulses which travel along auditory nerve fibers to the brain. The means by which these cells communicate movements of the basilar membrane is through the release of neurotransmitters, which can cause a propagating signal in each of the 15 to 20 auditory nerve fibers whose endings lie close to each cell body. These auditory neurons consist of peripheral dendrites, which synapse with the hair cells, a cell body, and an axon, which terminates in the cochlear nucleus in the brainstem. These nerve fibers are collectively known as the auditory nerve.

1.1.1 Activity of the normally functioning inner ear

An oscillatory motion of the tympanic membrane, caused by an acoustic stimulus impinging on the outer ear, results in motion of the stapes footplate. This causes a displacement of the basilar membrane and the attached hair cells. Through the action of the hair cells, this mechanical displacement is transduced into neural impulses which travel along auditory nerve fibers from the ear to the brain. The mechanics of the basilar membrane are such that for a sine-wave stimulus, the amplitude of this displacement is maximal at one longitudinal location along the basilar membrane whose position depending on the frequency. The basal part of the basilar membrane responds maximally to high frequencies, the apical part maximally to low frequencies. Thus, acoustic signals can activate localized populations of neural fibers independently. The patterns of activity in the nerve fibers as a function of their cochlear place of innervation provide information about the spectral content of the acoustic input. These **rate-place** cues are thought to play an important role in the encoding of speech by the auditory periphery, in part because this tonotopic organization of the cochlea is carried on through the higher levels of the auditory system up to the auditory cortex [73].

1.2 Cochlear Implants

If, for some reason, the ear lacks hair cells, there will be no mechanical-to-neural spike transduction, and there will be no neural signal from the ear to the brain. To restore a sense of hearing, devices have been developed which directly stimulate the nerve fibers using electrodes implanted into the scala tympani of the inner ear. These **cochlear prostheses** or, more typically, **cochlear implants**, attempt to replicate the functions of the ear peripheral to the auditory nerve, and then stimulate the auditory nerve in such a manner that the activity patterns of the nerve mimic the natural pattern closely enough that the brain can interpret the input pattern. A brief discussion of the points of interest for this work will be given here; a more detailed survey of cochlear implants can be found in Wilson ([92]). These devices consist of a microphone for sensing the acoustic stimulus, a processor for computing the electric stimulus to the implanted electrodes, and the implanted electrode array, as shown in Figure 1-2. Multiple electrodes are implanted with the hope of stimulating independently localized populations of neural fibers, as is the case with normal acoustic stimulation. In one common processor, each electrode is stimulated by short pulses that are interleaved in time with pulses to other electrodes so that two electrodes are never simultaneously active. The amplitude of the individual pulse depends on the short time spectrum of the acoustic input. The duration of each pulse is about 100 μsec. Pulse rates are typically such that the interval between pulses on each electrode is about 0.5 msec, while the interval between pulses across electrodes can be as small as 50 μsec. Processors that use this stimulation method are known as continuous interleaved sampling (**CIS**) processors. An example of CIS waveforms for each electrode due to two speech utterances ("aw", and "t") is shown in Figure 1-3.

The pulse rate of CIS processors is increasing as technical improvements are made; this is being done to increase the temporal resolution available to the user. It has been shown that human speech comprehension increases as the pulse rate increases (Eddington, pers. comm.).

Now that we know something of the waveforms used to stimulate auditory nerve

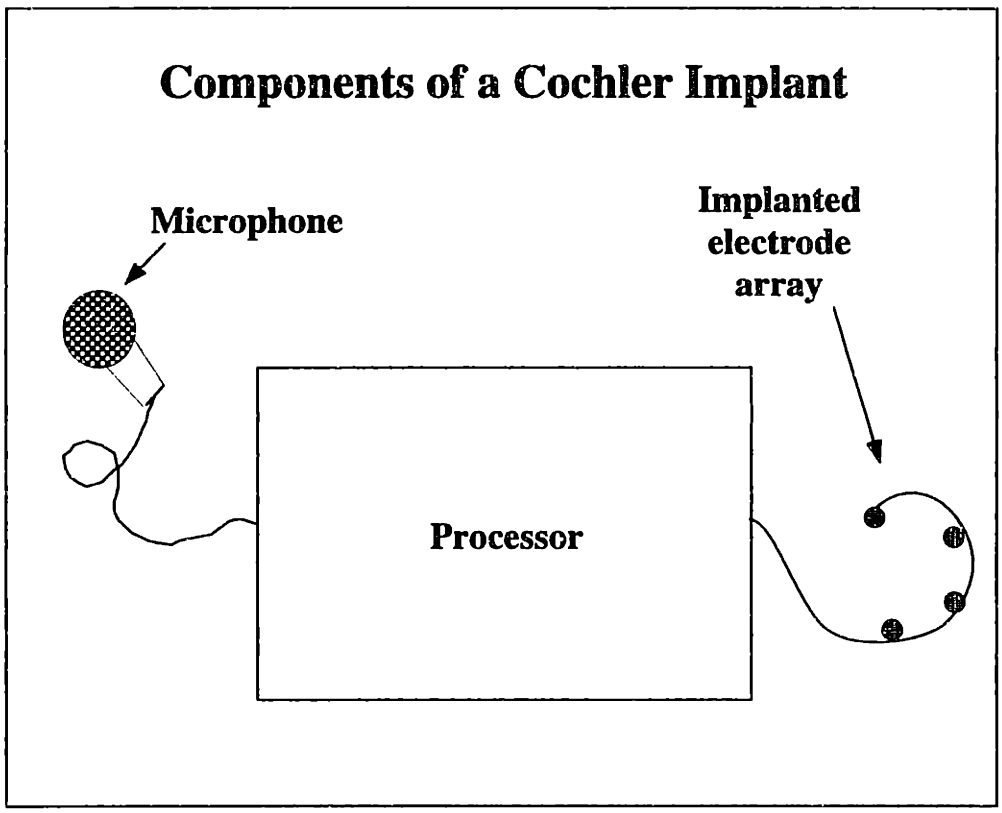

Figure 1-2: A schematic diagram of a cochlear prosthesis. A microphone is used to measure the local sound field. The output from the microphone is processed in some manner, and the implanted electrode array is stimulated based upon the results of that processing.

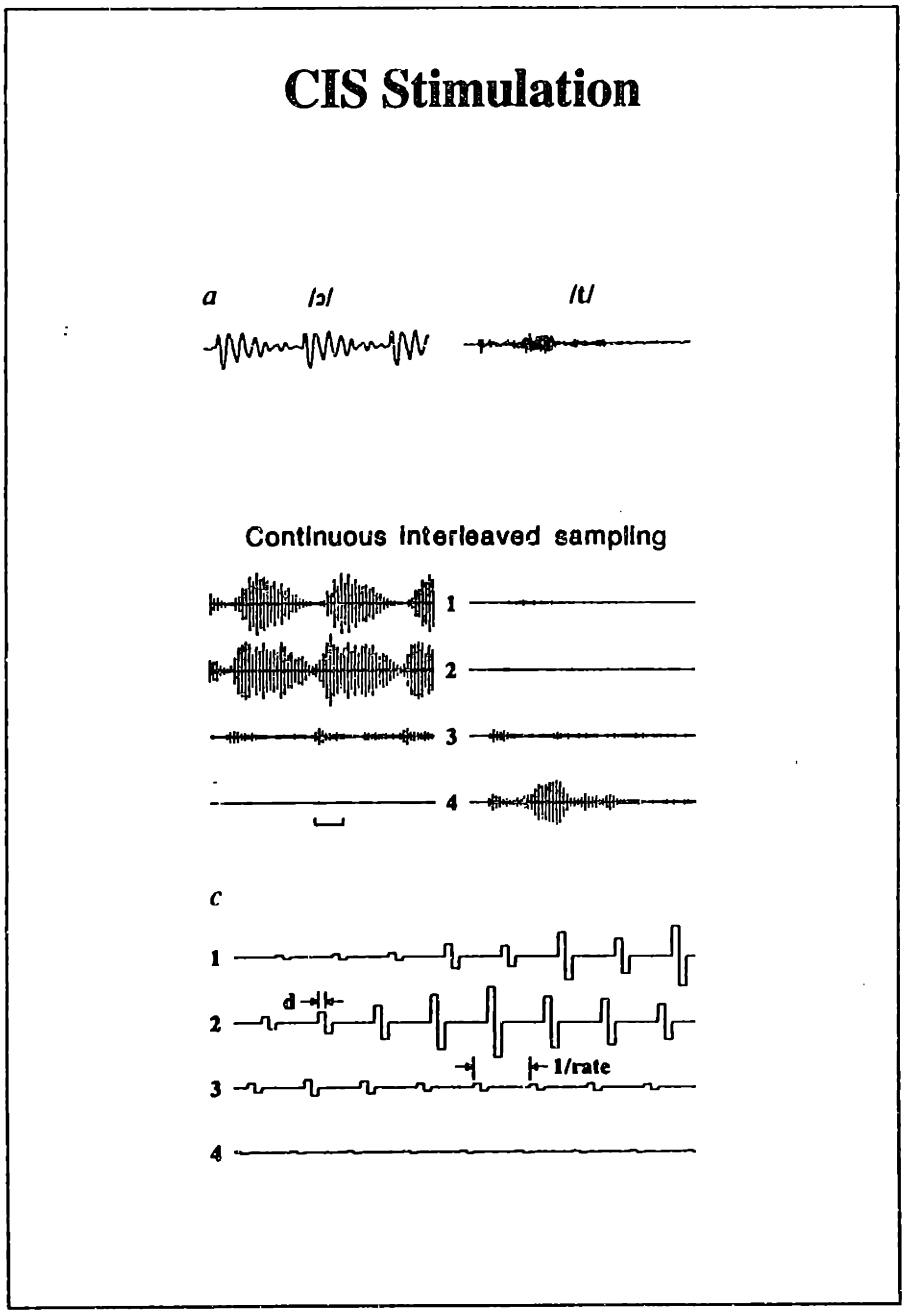

Figure 1-3: Continuous Interleaved Sampling stimulation methods. The waveforms of two speech utterances ("aw" and "t") are shown at the top of the figure. The waveforms of the two utterances were processed using the CIS scheme: the resulting waveforms for each electrode are displayed, with electrode 1 being the most apical. The pulse amplitudes reflect the envelope of the amplitudes of the filtered waveforms.

fibers, we will introduce the important elements of these neurons, and discuss how electrical stimuli can cause neural responses.

1.3 Functional Elements of Neurons

Neurons are the primary means for conducting information from one point to another in the nervous system. They consist of a tubular membrane which extends between the two points. Fluids containing ions fill and surround this membrane, the ionic concentrations differing between the internal and external plasmas. In particular, the sodium concentration is higher in the external fluid, and the potassium concentration is higher in the interior fluid. There are also ionic channels specific for the sodium and potassium ions whose conductances depend on the transmembrane potential. A schematic neuron is shown in Figure 1-4. As a result of these concentrations and permeabilities,the neural interior at rest is at a potential roughly 50–80 mV less than the exterior. The potassium and sodium channel permeabilities result in a system that, for a sufficiently strong depolarizing stimuli, results in a sudden, almost complete depolarization of the neural membrane followed by a gradual repolarization. The depolarization of one region of the neuron affects neighboring regions, resulting in a propagating wave of depolarization. This neural spike, or action potential, is the means by which neurons transmit information. Experimentally, this propagating neural spike is used to measure the neural response to a stimulus.

Figure 1-5 shows how the transmembrane potential V_m changes following depolarizing pulses of different strengths. For the smaller pulses V_m returns to the resting value. For one pulse strength some pulse presentations result in V_m returning to the resting value while others result in the sudden depolarization of the neural membrane. All stronger pulses result in a neural spike.

The probabilistic behavior for some range of stimulus levels can be used to define a **neural threshold level**, the stimulus level at which the neuron responds with a spike to half the stimulus presentations. An additional measure of the neural response is the **relative spread (RS)** [89], which is a measure of the dynamic range of the

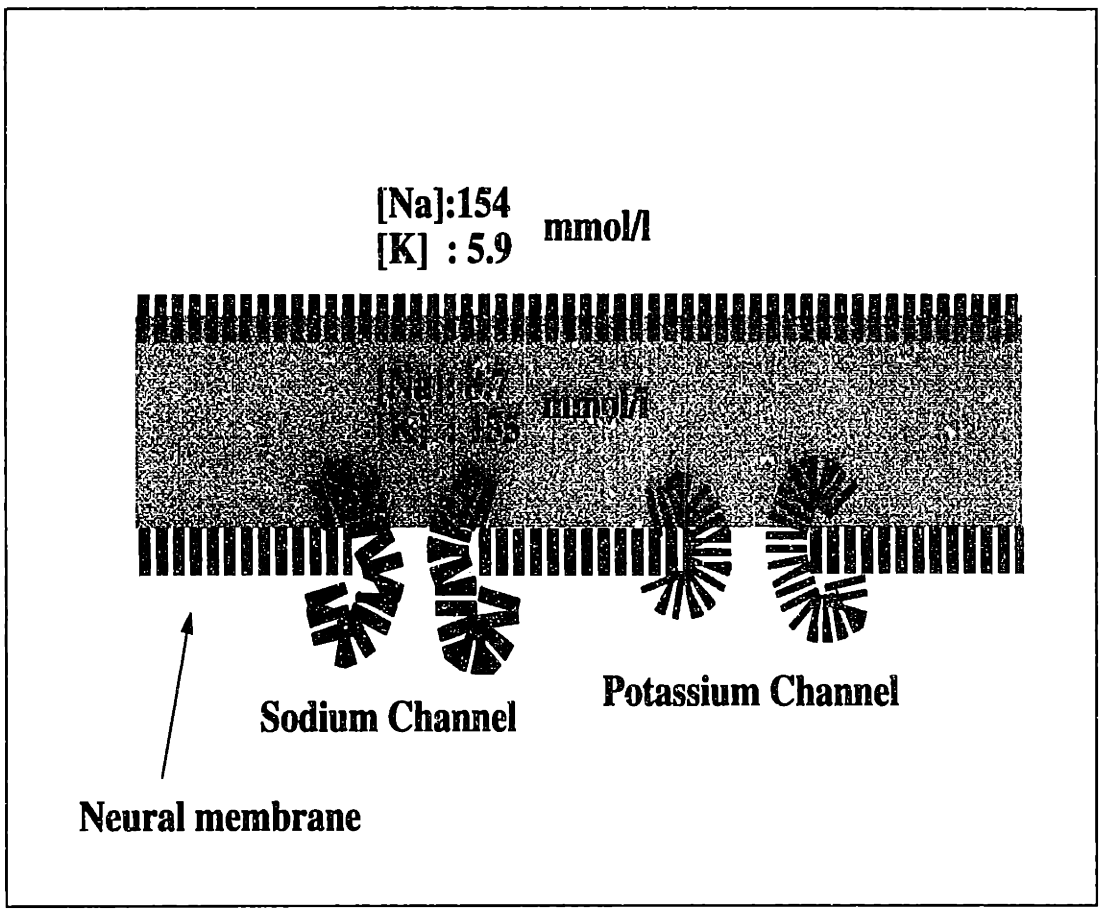

Figure 1-4: The main elements of an axon. The interior and exterior consist of ionic solutions; the ionic concentrations of sodium and potassium ions from Schwartz and Eikhof ([76]) are given. The differences in ionic concentrations gives rise to a resting transmembrane potential V_m of -80 mV. Ionic channels in the membrane can allow the transport of selected ionic species across the membrane; the permeability can depend on the transmembrane potential V_m

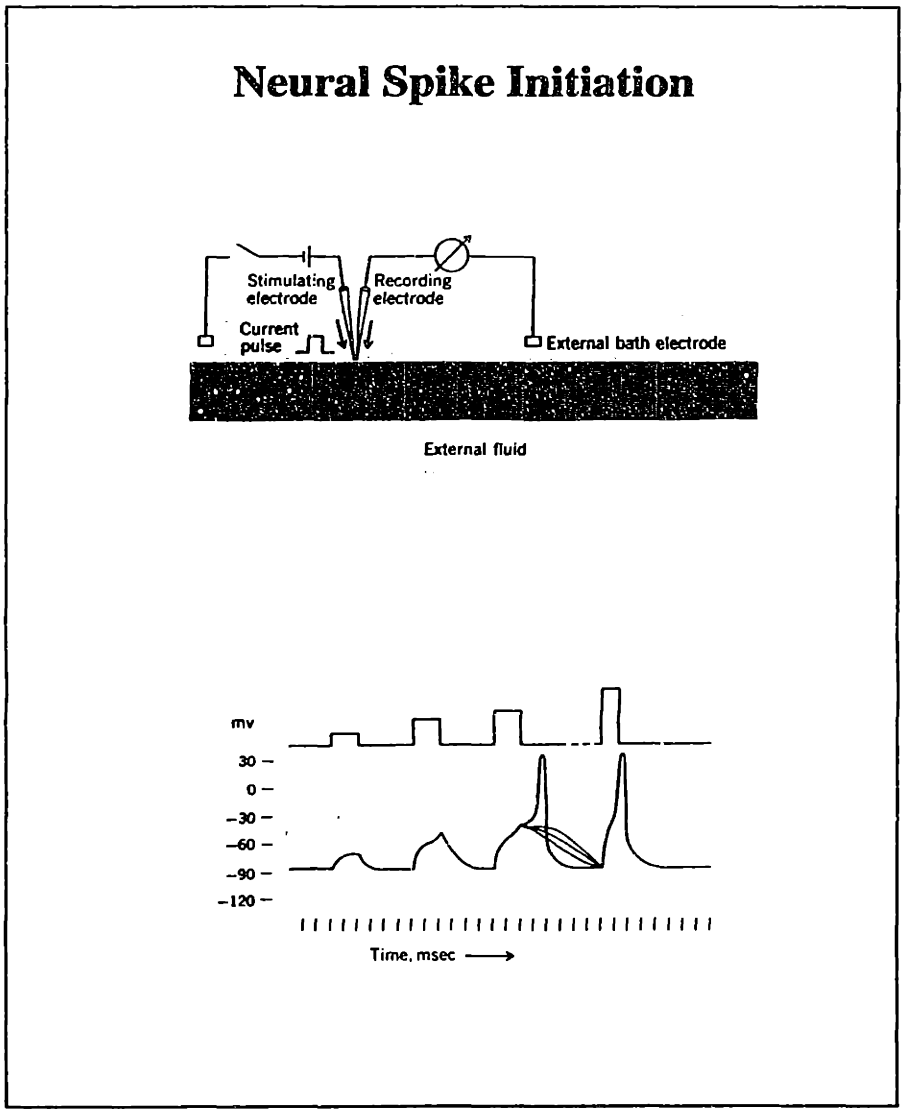

Figure 1-5: The initiation of neural spikes. The top panel shows the transmembrane potential V_m plotted as a function of time for depolarizing stimuli of different strengths. For small pulses, V_m returns to the resting value. For the pulse near threshold strength some pulse presentations result in V_m returning to the resting value, while other presentations result in the sudden depolarization of the neural membrane. The pulse injection and V_m recording points are as shown.

fiber, ie; the range of stimulus intensities over which the probability of neural response varies appreciably. Both of these measures will be described further in the Methods chapter.

1.4 Electrical stimulation of neural fibers

Understanding that action potentials are initiated by a threshold depolarization of the neural membrane, the mechanism for neural stimulation by the implanted electrodes is straightforward. A potential is created between two electrodes of an implanted electrode array. This potential will cause currents to flow; part of that current will enter the neuron far from the electrode and leave the neuron closer to the electrode. This situation is shown in Figure 1-6. The top panel depicts a neuron in a homogeneous infinite medium, along with a cathodic electrode with a far-field ground. At the sites where the current enters the neuron, the membrane becomes hyperpolarized, that is, V_m becomes larger. At the points where current exits the neuron, the membrane is depolarized. The bottom panel if Figure 1-6 shows changes in the transmembrane potential calculated by a cable model of the situation in the top panel. The change in V_m is greatest at the point nearest the electrode and decreases rapidly with lateral distance; for the cathodic stimulus shown, the increase in V_m depolarizes the fiber. If the depolarization is large enough, a neural spike will be generated as described previously. This is the mechanism by which electrical stimulation can cause neural activity.

A short distance along the neuron away from the point closest to the electrode, the change in V_m goes from positive to negative; the maximum decrease in V_m is much smaller and broader than the peak increase at the nearest-electrode point. Since neural responses are initiated only at depolarized nodes, this leads to the conclusion that neural thresholds are lower for cathodic stimulation, and that the spike initiation site is much better defined for cathodic stimulation, since there are many fewer nodes near the maximum depolarization at the nearest-electrode point than for the maximum depolarization for an anodic stimulus, which is far from the electrode.

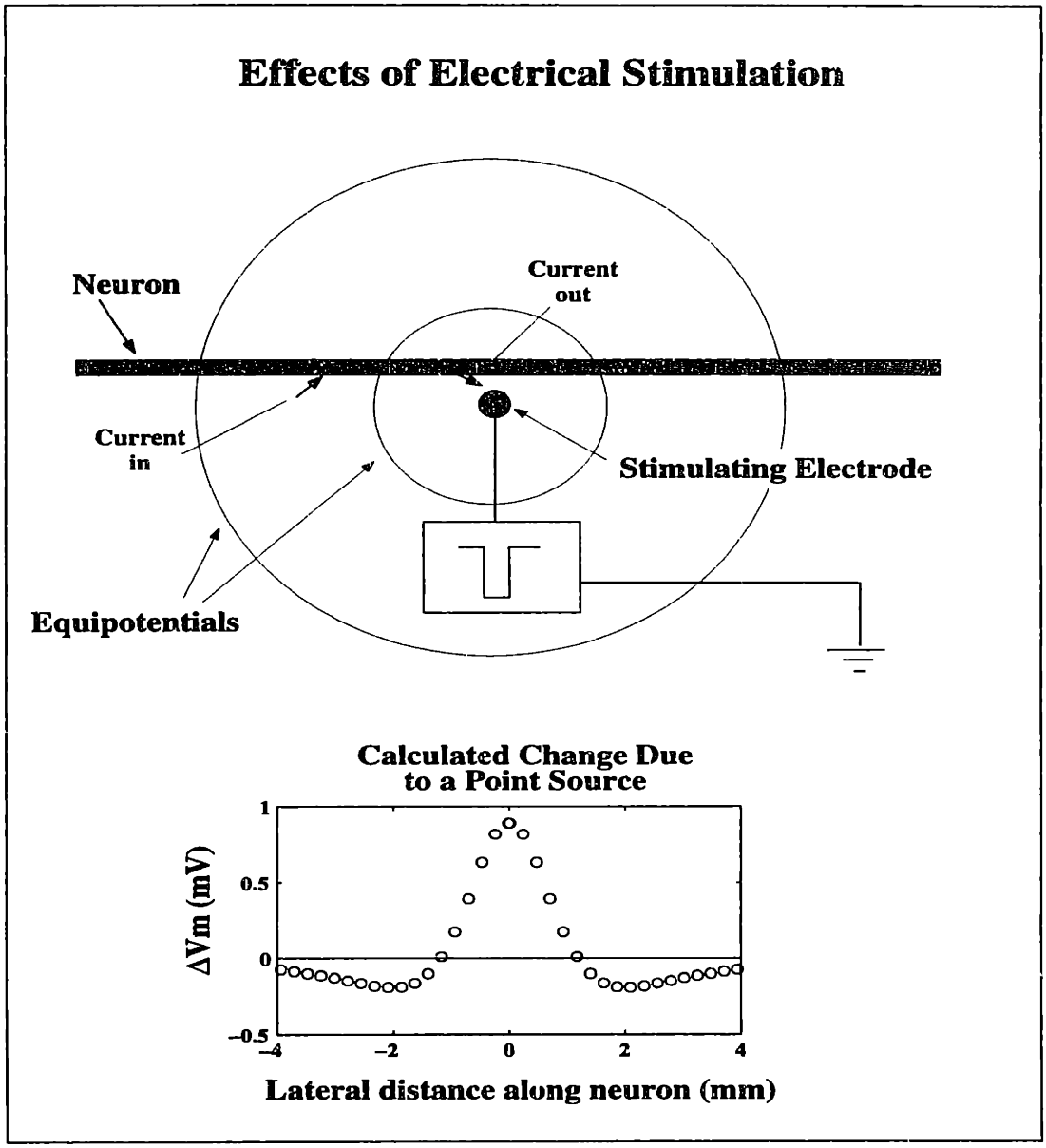

Figure 1-6: Electrical stimulation of a nerve fiber. The top panel shows a single nerve fiber in an infinite homogeneous medium along with a single cathodic electrode referenced to a far-field ground. Arrows represent the currents that flow due to the cathodic electrode. The bottom panel shows the change in the transmembrane potential V_m as calculated using a cable model for the situation shown in the top panel. Plotted is the change in V_m as a function of distance along the neural membrane from the closest point to the electrode. Note that the neural membrane is depolarized near the electrode.

1.5 The results of Hodgkin and Huxley

In order to understand in more detail how electric current causes the neural depolarization, the results of Hodgkin and Huxley will be presented. In a series of papers published in 1952 ([27], [28], [29], [30]), Hodgkin and Huxley describe a functional model of how action potentials are produced. This model was the result of their studies of sodium and potassium currents through the neural membrane in response to step changes in the transmembrane potential V_m. In their studies, the neuron was voltage clamped, which means that the transmembrane potential was constant along the neuron. These studies resulted in a description of how the membrane sodium and potassium conductances depend on both the transmembrane potential V_m and time. A series of plots showing the sodium and potassium conductance for different voltage steps is shown in Figure 1-7.

The circles in the left column show experimentally-determined sodium conductances of the squid giant axon ([31]) as a function of time for several voltage steps. The initial effect is for a sharp increase in the conductance, followed by a slower decrease in conductance to near the initial level. The rate of change and the maximum conductance both increase with the size of the depolarizing voltage step. The initial increase in the conductance is caused by the "activation" or opening of the sodium channels; the decrease is caused by the channels "inactivating", or closing.

The right panel depicts the potassium conductance. Here, the experimental data (circles) shows an S-shaped curve monotonically rising from the starting value to the final value. The potassium channel has only activating components, so that the change in conductance following a voltage step is a monotonic function of time.

To model the dependence of these conductances on the transmembrane potential V_m and time, Hodgkin and Huxley assumed that each ion channel was controlled by a set of particles. These particles are in one of two orientations, and for the channel to be open, all particles have to be in the correct orientation. The probability that an individual particle is in the correct position is governed by a pair of first-order differential equations describing, as a function of the transmembrane potential V_m,

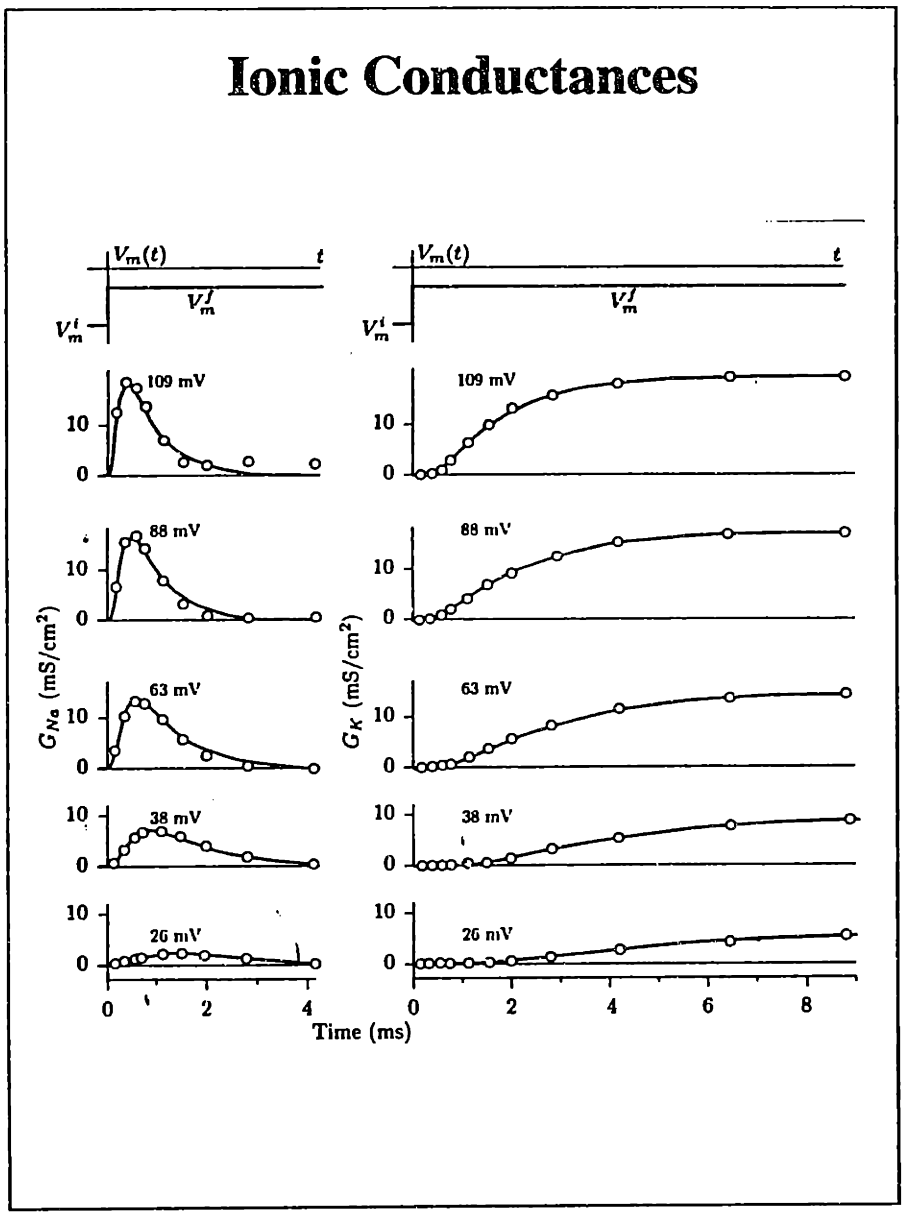

Figure 1-7: Experimental and model sodium and potassium conductances as a function of time shown for several voltage steps. The experimental data (circles) are from voltage-clamp experiments on the giant squid axon ([31]). The model results (line) is from the Hodgkin-Huxley model of the conductances ([30]) The numbers above each curve represent the amount V_m was displaced from rest.

the rate of transition of each particle between the "open" and "closed" states, α describing the rate to the open state, and β to the closed state:

$$\text{"1 - n"} \underset{\beta(V_m)}{\overset{\alpha(V_m)}{\rightleftharpoons}} \text{"n"}$$

where n is the probability tat the particle is in the "open" orientation.

Using their data from the squid axon, Hodgkin and Huxley determined empirical fits for α and β as a function of V_m for the particles describing the sodium and potassium conductances. The above rate equations and parameters completely describe the dynamics of the ion channels:

$$\frac{dn}{dt} = \alpha_n(1 - n) - \beta_n n$$

Hodgkin and Huxley found the best fit to the experimental conduction data was given by using four particles controlling the conductances of each sodium and potassium channel.

The sodium conductance is controlled by three indistinguishable particles controlling the channel activation and a single particle controlling the inactivation. The probability that any one activation particle is in the position corresponding to an open channel is given by the parameter m, the corresponding probability for the inactivation particle is given by the parameter h. There is a separate pair of rate equations for each variable. It follows that the probability that any given channel is in the open state is given by m^3h. Using the equations they empirically determined for the rate constants, Hodgkin and Huxley calculated the sodium conductance for the data shown in Figure 1-7; their results are given by the lines in that figure. The sodium current can be calculated from the probabilities, the maximum sodium conductance $\overline{g_{Na}}$, and the difference between V_m and the sodium Nernst potential V_{Na}:

$$I_{Na} = \overline{g_{Na}} m^3 h (V_m - V_{Na}) \tag{1.1}$$

The potassium conductance is controlled by four indistinguishable particles. The probability that any given particle is in the "open" condition is given by the parameter n. The model conductances as calculated by Hodgkin and Huxley are again shown by the lines in the right-hand panels of Figure 1-7. Thus, the potassium current can be calculated in a manner analogous to the sodium current:

$$I_K = \overline{g_K} n^4 (V_m - V_K) \tag{1.2}$$

The HH model also includes a non-specific leak current, whose conductance is fixed:

$$I_L = g_L (V_m - V_L) \tag{1.3}$$

where V_L is an empirically-determined quantity.

Taking into account all the ionic currents, the capacitive current, the non-specific leakage current, and the external (stimulus) current, one obtains a differential equation for the transmembrane potential V_m:

$$I_{stim} = C\frac{dV_m}{dt} + \overline{g_K} n^4 (V_m - V_K) + \overline{g_{Na}} m^3 h (V_m - V_{Na}) + g_L (V_m - V_L) \tag{1.4}$$

Starting from initial values for V_m, m, h, and n, V_m can be calculated as a function of time for arbitrary stimuli. Hodgkin and Huxley demonstrated that their model recreates the main features of neural spikes: a spike that exhibits a sharp threshold as a function of stimulus level, a spike waveform that has the same temporal characteristics as that recorded experimentally, and a refractory period, where the threshold for subsequent spikes following an initial spike is elevated for a period of time. An example of a neural spike calculated using their model is shown in Figure 1-8. Note that the transmembrane potential and the state variables m, h, and n do not return to their resting values until many msec following the end of the stimulus pulse. These changes in the state variables can result in temporal interactions, where a stimulus

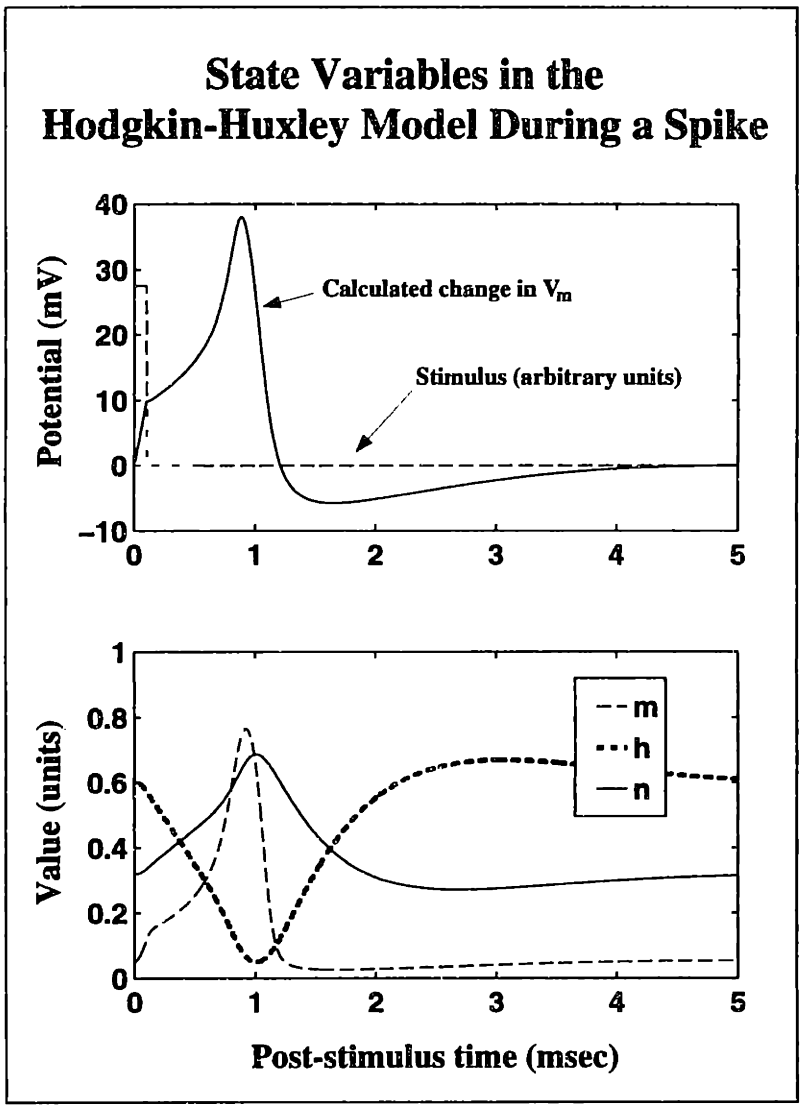

Figure 1-8: A neural spike calculated using the Hodgkin-Huxley model ([30]). The top panel plots the stimulus and the resulting model spike as a function of time. The stimulus (dashed line) is a current pulse of barely suprathreshold strength; the amplitude is not indicated. The solid line represents the change in the membrane potential from its resting value; positive numbers reflect a depolarization of the neuron. The bottom panel plots as a function of time the values of the m, h, and n state variables used in the HH model

affects the neural response to subsequent pulses. In this particular case, since the initial pulse results in a spike, the nerve is in the well-known refractory state, where the threshold for subsequent pulses will be elevated for a period of time.

From these results it is apparent that during a spike the channels at the spike initiation site open in a manner to depolarize the nerve at that site. This depolarization causes a decrease in the transmembrane potential at neighboring sites; if the depolarization is large enough, the channels open in the same manner as at the initial site. The resulting traveling wave of depolarization is the manner by which spikes propagate along the neuron.

1.5.1 Other models of neural membranes

The methods and model developed by Hodgkin and Huxley were based on experimental data from the giant squid. Despite the success of their model, the squid neuron, being unmyelinated, may not be the best model for other types of fibers. Other investigators have since modeled ionic conductances and used the Hodgkin-Huxley model framework to arrive at membrane models for other systems. These include: a model of the myelinated frog sciatic nerve, developed by Frankenhaeuser and Huxley [16]; a model of the myelinated rabbit sciatic nerve, developed by Chiu *et al.* [7]; a model of the myelinated rat sciatic nerve from Schwarz and Eikhof [76]. Additionally, a model of bushy cells, which are in the cat cochlear nucleus and integrate the responses of the auditory nerve fiber axons which synapse upon their dendrites, has been developed by Rothman, Young and Manis [69]. These models differ only in the dynamics of the ion channels and the membrane parameters; they share a common base model.

1.6 Outline of the Presented Work

With this background, we can now present a detailed outline of the presented study.

This work explores temporal interactions for electrical pulses from a physiological viewpoint using a stimulus consisting of one or more pulses to condition the nerve, and then probing the state of the conditioned nerve using a single probe pulse at

several time intervals following the conditioning pulses. From the neural responses, the neural threshold and relative spread are calculated for several probe delays.

The conditioning stimuli consist of cathodic current pulses, of both sub- and suprathreshold intensity. The pulses are cathodic because of the issues discussed on page 18: many more sites experience near-maximal depolarization for anodic stimuli than for cathodic stimuli. Using cathodic stimuli gives a much greater chance that all spikes will be initiated at the same site. For this reason, the pulse used to probe the state of the conditioned neuron is a single cathodic pulse.

For this work, the simplest stimuli consists of a single conditioning pulse; this gives a fundamental measure of the temporal interactions seen in electrically-stimulated auditory neurons. The number of conditioning pulses as well as the conditioning pulse level were varied to determine how changing these parameters affect the observed temporal interactions and to better approximate the situation encountered in cochlear implants.

With the experimental results characterizing the temporal interactions, Hodgkin-Huxley-like models were used to see if the observed temporal interactions could be simulated using existing models of the neural membrane. The models were stimulated with the identical stimuli used experimentally to see if the observed behaviors could be qualitatively explained. A stochastic extension of the Hodgkin-Huxley model of the giant squid axon was developed to determine if the observed changes in the relative spread could also be qualitatively explained.

Chapter 2

Methods

The response of individual auditory nerve fibers to electrical stimuli was recorded using glass microelectrodes inserted into the auditory nerve of anesthetized cats. Generally, a threshold response to a single 100-μsec cathodic pulse was first determined, followed by the response to various conditioner-probe stimuli.

2.1 Animal Preparation

Animal preparation and techniques to record from single auditory-nerve fibers are essentially as described in Kiang *et al.* [40]. In brief, adult cats were injected peritoneally with daillyl barbituric acid in urethane solution (dosage 75 mg per kg weight). A cannula was inserted into the trachea, the cartilaginous external auditory meatus was cut near the tympanic membrane, and the bulla opened to expose the round window.

The posterior fossa of the cranial cavity was opened dorsally and the cerebellum retracted medially to expose the auditory nerve. The animal was placed in a soundproof, vibration-isolated, electrically-shielded chamber. An acoustic cavity containing a calibrated sound transducer (Radio Shack model 40-1377) was sealed in the meatus. Neural activity was recorded through micropipettes placed in the nerve under visual control.

Electrical stimulation was provided through either a single teflon- coated plat-

inum wire (.005 in wire diameter) or a UCSF cat electrode array consisting of four longitudinally-spaced electrodes (Snyder *et al.* [82] [83], Leake *et al.* [45]), in which case the most apical electrode was used. The apical tip of platinum wire electrodes passed about 4–5 mm through the round window; the apical electrode of the UCSF cat array extended further, part way around the basal turn. In all cases, the indifferent electrode was an 18-gauge needle placed in the ipsilateral forelimb.

The electrical search stimulus was a train of 100-μsec cathodic pulses presented at a rate of 10/sec. The search stimulus amplitude was varied, but was typically 15 dB below 1 mA. Single units were detected by monitoring the neural potentials on an oscilloscope.

Efforts were made to eliminate spontaneous activity, since these spikes could change the neural responsiveness in an uncontrolled fashion. Even though the insertion of the implanted electrodes usually resulted in a cessation of spontaneous activity, further efforts were taken. These efforts initially consisted of piercing the basilar membrane with forceps; later, cats were systemically deafened using a kanamycin/ethacrynic acid protocol [95]. There was occasional spontaneous activity following mechanical deafening; following systemic deafening it was very rare. No systematic difference in results between the mechanically- and chemically-deafened cats were noted.

2.2 Reduction of Stimulus Artifact

Neural activity was recorded through glass micropipettes. Since the stimulus artifact[1] is proportional to the difference in potential between the recording and reference electrodes, minimizing the distance between these electrodes should result in a smaller stimulus artifact. A two-electrode configuration was used to accomplish this. A pair of 2M KCl-filled microelectrodes were placed so their tips were as close as practical ([58]). One electrode was advanced so as to record a single unit, while the other

[1]**Stimulus Artifact** is that part of the recorded potential that is directly due to currents produced by the stimulating electrodes.

remained in the extracellular space. The extracellular electrode measured only the artifact, while the other electrode measured both the artifact and the propagating spike. The measured signal was the difference between the two signals; the individual microelectrode signals were filtered so that the artifact waveforms optimally canceled. The signal was also gated during and for a short period (0.15 msec) immediately following a pulse stimulus. This procedure yielded waveforms whose spikes could be reliably detected.

2.3 Stimuli

Stimuli consisted of pulse waveforms produced by a computer-controlled D-A converter capable of 10μsec. resolution. These waveforms were delivered to the implanted electrodes by a custom constant-current optically-isolated stimulator. The stimulus amplitude could be changed in 0.1 dB increments.

Stimuli are conceptually divided into two components: the conditioner, consisting of one or more equal-amplitude pulses used to modify the state of the nerve, and the probe, consisting of a single pulse following the conditioner at some delay which is used to probe the response characteristics of the modified nerve (see Figure 2-1). Each stimulus pulse was rectangular and of 100-μsec duration. The repetition rate of the stimuli was such that there was at least 80 msec between the end of one stimulus and the start of the next. The conditioner pulses can be of sub-threshold or suprathreshold amplitude: subthreshold pulses never result in a spike, while suprathreshold pulses always result in a spike.

The probe is without exception a single 100 μsec cathodic pulse. This is done for a very specific reason: there are theoretical (Reilly, Freeman and Larkin [67], Rattay [63], Rubinstein [70]) and experimental (van den Honert and Stypulkowski [86], Parkins [59]) reasons to believe that the spike initiation site for cathodic stimulation remains constant. Having a constant spike initiation site simplifies the interpretation of the data by eliminating effects due to changes in the initiation site.

Typically, once a unit was obtained, the threshold to a single pulse was measured.

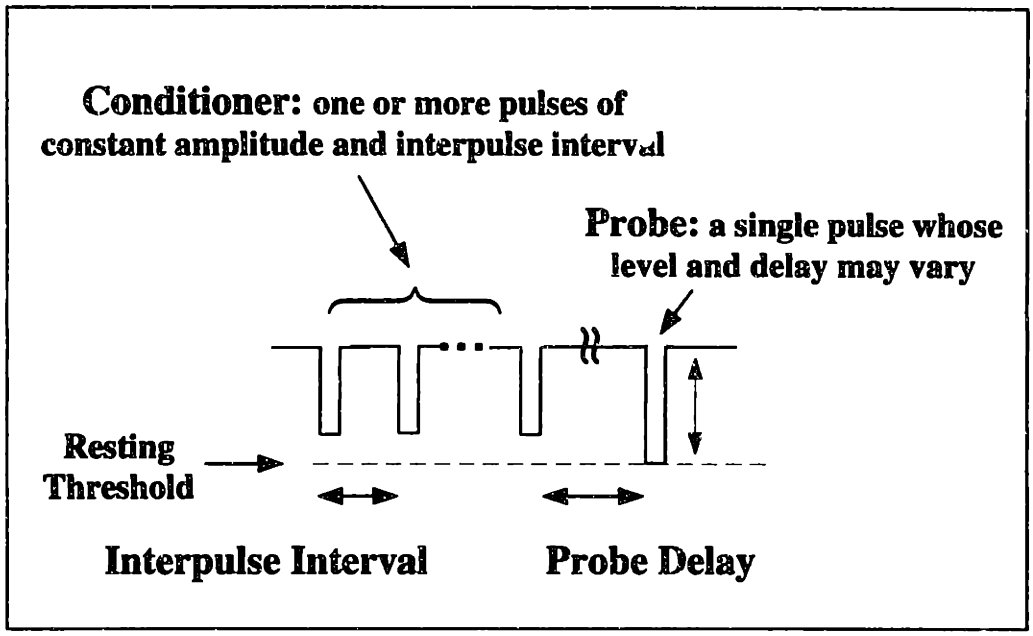

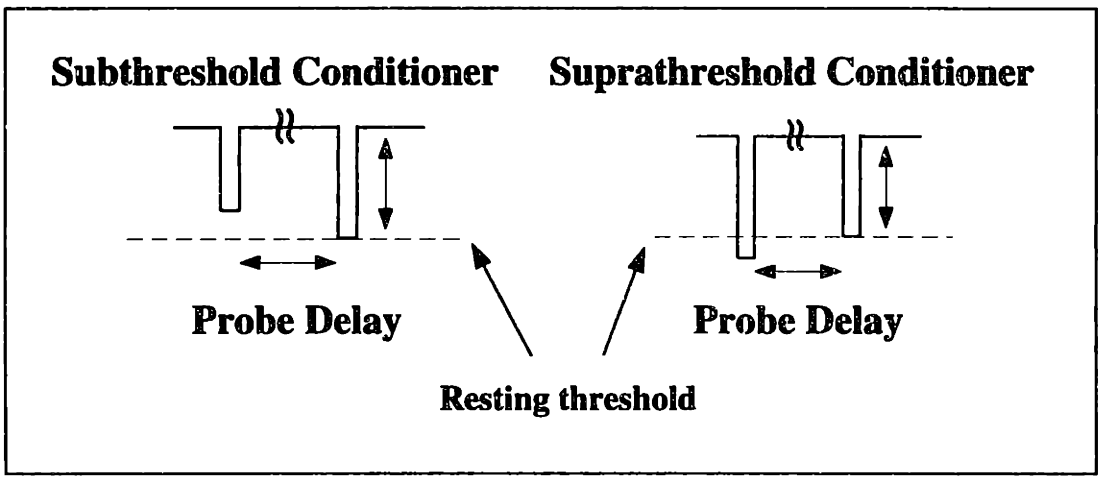

Figure 2-1: Stimuli. The top panel shows schematically the components of a stimulus. The conditioner, consisting of one or more pulses with a fixed amplitude and interpulse interval, is used to modify the state of the nerve. The probe, following the conditioner by some variable delay, is usually varied in amplitude, exploring the response properties of the modified nerve. The bottom panel explains the icons used in later figures: the dashed line represents the single-pulse resting threshold; pulses not reaching the line represent subthreshold conditioners; pulses crossing the line represent suprathreshold conditioners. The probe is represented by a pulse which is at threshold, with arrows indicating its level is varied.

This corresponds to the probe threshold without any conditioning stimuli: this value is termed the **resting threshold**. The probe threshold was then measured at various delays for different conditioners. Whenever possible, the resting threshold was re-measured to verify stability.

2.4 Neural Response Measures

The neural response was characterized by two different measures: the **neural threshold**, which is the stimulus level which results in a criterion level of neural response, and the **relative spread (RS)**, also known as the normalized dynamic range The relative spread is a measure of the the range of stimulus levels for which the probability of firing P_f (defined as the number of spikes in response to a stimulus divided by the number of stimuli) increases from 0 and 1.

Two different methods were used to determine the neural response: one for determining thresholds, the other for determining both threshold and the relative spread. The first method yields threshold determinations quickly, enabling thresholds to be determined for several probe delays. The second method provides more accurate determinations of threshold as well as providing the relative spread. Since it requires much time for each measurement, fewer probe delays can be sampled.

2.4.1 Threshold Determinations Using a Tracking Algorithm

This method determines neural thresholds by adjusting the stimulus level based on the neural response to individual stimulus presentations. The method, first described by Kiang and Moxon [42], raises the stimulus level by 0.2 dB if the preceding pulse did not cause a spike, and decreases the level by 0.1 dB if the preceding stimulus resulted in a spike. Threshold is defined to be the present level if it is the same as the level three trials previously, and the last change in level was downward. Thresholds were determined at a sequence of probe delays usually starting with the shortest delay

(100 μsec for subthreshold conditioners, 2 msec for suprathreshold conditioners). The threshold of the previous delay was used as the starting point of the threshold measure for the next delay. In this manner the threshold was tracked as a function of probe delay.

One issue with threshold determination is the stability of the unit threshold over time. With the tracking method, the stability of the resting (unconditioned) threshold could be monitored by alternating measures of the probe threshold with a conditioner with threshold measures in the absence of a conditioner. The unconditioned threshold was subtracted from the conditioned threshold, removing conditioned threshold variations due to instabilities in the resting threshold.

A set of resting and conditioned thresholds are shown as a function of delay in Figure 2-2. The probe delay for the without-conditioner case is illusory and represents only the temporal sequence of threshold measurements.

To determine the threshold-delay curve, the raw data as shown above are uncombed, yielding separate curves for the unconditioned and the conditioned threshold-delay function. To correct the threshold-delay curve for variations in resting threshold, the unconditioned threshold is subtracted from the conditioned threshold-delay curve, yielding the final threshold-delay curve. This is shown in Figure 2-3

2.4.2 Determination of Threshold and Relative Spread Using P_f-level Functions

The relative spread is a measure of the range over which the neuron responds in a stochastic manner. To determine this range, the probability of firing was determined as a function of stimulus level. This technique involved collecting neural responses for a number of stimulus presentations (50–100), and dividing the number of responses by the number of presentations to get an estimate of the probability of firing P_f. Valid responses to a stimulus pulse were defined as those spikes which occur in a window of 0.3 – 1.3 msec following the pulse. An example of a P_f-level curve is shown in Figure 2-4. Each data point shows the probability of firing for one stimulus level. An

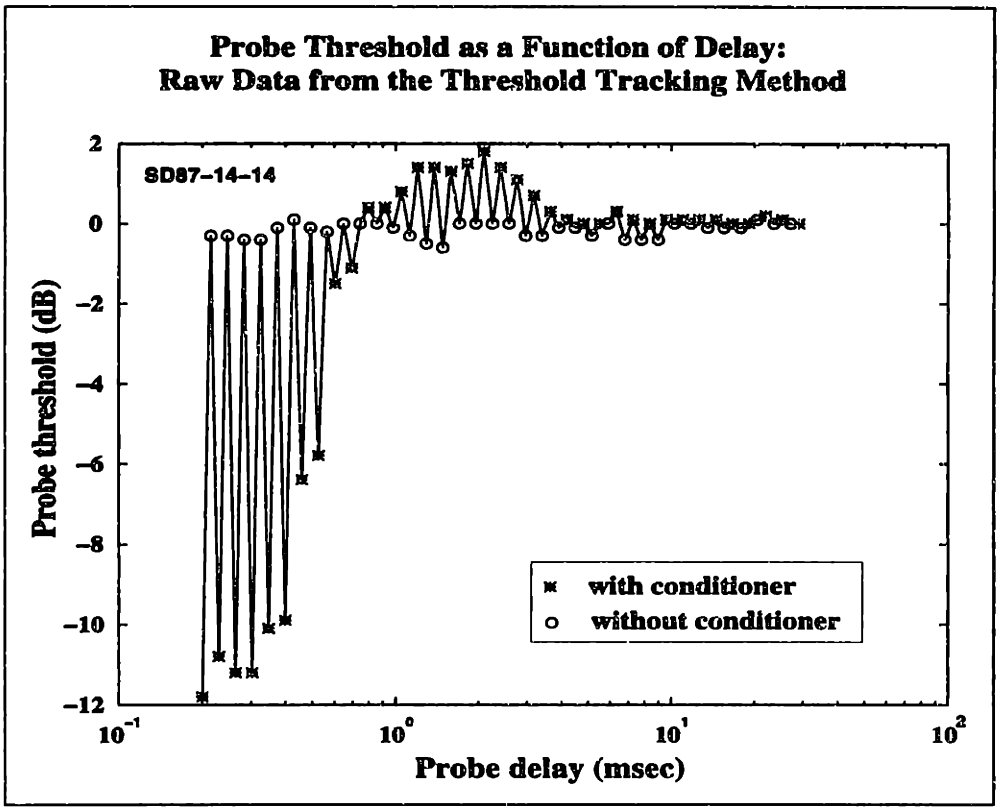

Figure 2-2: Threshold tracking method. The probe threshold is plotted as a function of probe delay for two cases: without a conditioner (o), showing how the resting threshold changes with time; and with a conditioner (×), which shows the conditioned threshold-delay curve. The with- and without-conditioner threshold measures are interleaved. The probe delay coordinate for the without-conditioner points is illusory as the probe is the only stimulus. The x-axis is in log units to better show the order of measures.

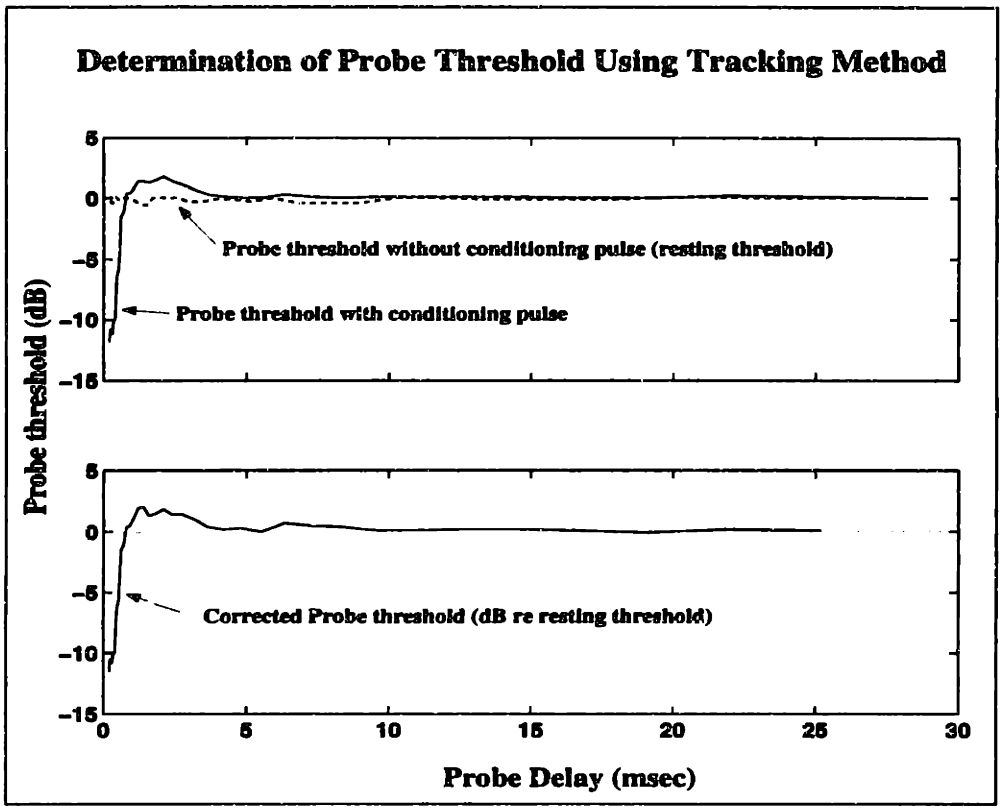

Figure 2-3: Calculation of threshold-delay curves from threshold tracking threshold data. The top panel shows the uncombed curves that were depicted in Figure 2-2: the conditioned threshold-delay curve is depicted by the solid line, the unconditioned threshold by the solid line. The bottom panel shows the difference between these two curves, which is the threshold-delay curve corrected for variations in the resting threshold.

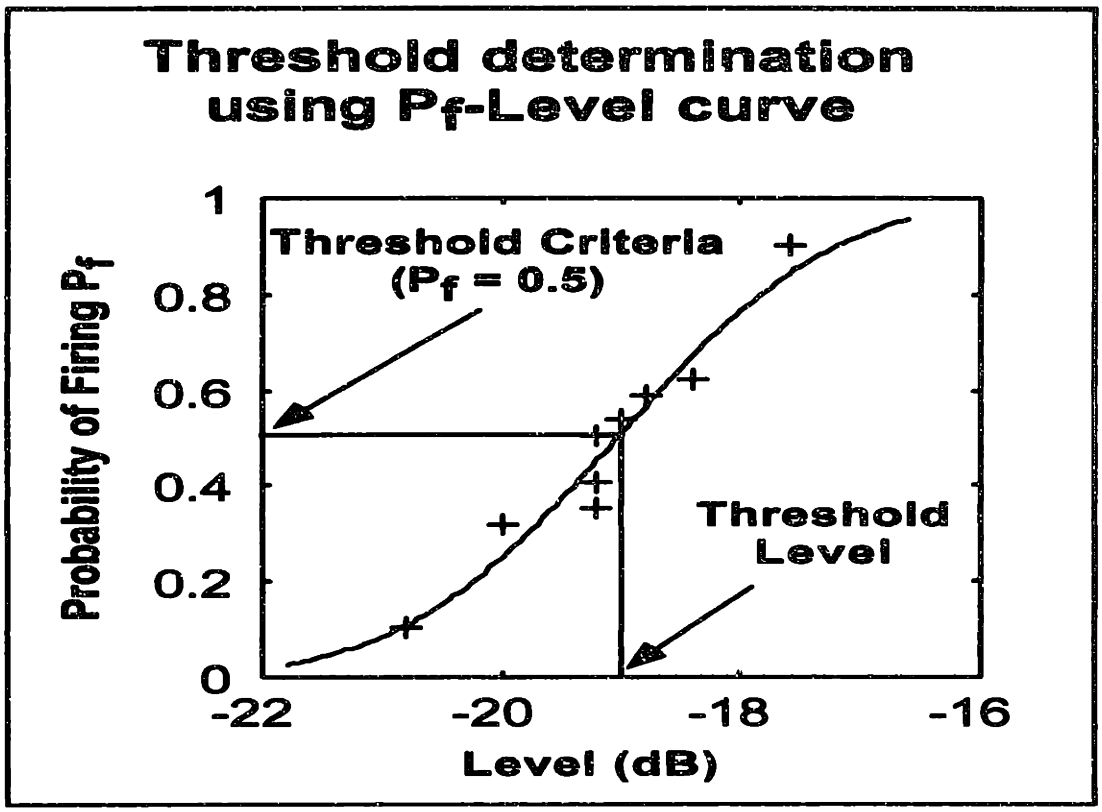

Figure 2-4: Threshold determination via P_f - level functions. The probability of firing (number of responses divided by the number of stimuli) is measured for several different stimulus levels. Using this curve as a description of the neural response, the threshold is defined as that stimulus level which would produce a P_f of the criterion level (usually P_f = 0.5). The stimulus consisted of a train of 100 100 - μsec. cathodic pulses presented at a rate of 10 pulses/sec.

error function was fit to these points using a least-squares fitting algorithm ([51]):

$$P_f(I) = \frac{1}{\sigma\sqrt{2\pi}} \int_{-\infty}^{I} \exp(-[x - \overline{I}]^2/2\sigma^2)dx$$

where I is the stimulus current, $\overline{I}$ is the threshold current, and σ is the standard deviation of the Gaussian underlying the error function. Using this fit curve as a description of the neural response as a function of stimulus level, the threshold corresponds to the stimulus level to which the unit will respond with a P_f of 0.5.

The relative spread is defined as the normalized standard deviation of the P_f-level curve:

$$RS = \frac{\sigma}{\overline{I}}$$

The relative spread is useful for two reasons: theoretically, the RS measure has its physical basis in the number of active channels present at the spike initiation site (Sigworth [81], Rubinstein [72]). From a practical point of view, the RS is a normalized measure of the dynamic range of the neuron: the range of stimuli over which the nerve responds in a probabilistic manner. It is only in this regime that the neuron can transmit information about changes in the level of the stimulus.

2.4.3 Reliability of Neural Response Measures

Both the threshold and the RS are recovered from the P_f-level curves. To gauge the reliability of these measures determined from the error-function fits to these curves, Monte-Carlo simulations were used. Each measure of a P_f-level point records the probability of an all-or-nothing event occurring (a spike in response to a current pulse). Thus, we are justified in using binomial statistics to model the distribution of P_f's measured for identical stimuli. For each Monte-Carlo trial, each data point (P_f at a particular level) was be replaced by a point randomly drawn from a binomial distribution whose mean and standard deviation were determined by the original P_f data point. An error function was fit to this synthetic distribution in the usual man-

ner and the threshold and RS calculated. To determine the statistical reliability of the originally-calculated threshold and RS, 100 trials were run, and the standard deviations of the threshold and RS distributions recorded. 95% confidence intervals for threshold based on these simulations were less than 0.3 dB wide for over 90examined. For the relative spread, 95% confidence intervals were less than 50% of the measured RS value for 90% of the data sets examined.

For thresholds determined using the tracking method, the reliability of each threshold measure can be determined by looking at the standard deviation of the unconditioned threshold measures. While this varies from measure to measure, an average value for the standard deviation of individual threshold points is 0.3 dB.

2.5 Summary Measures for Subthreshold Data

As will be shown, threshold-delay curves for subthreshold conditioners consist of an initial sensitization period during which the probe threshold is lowered, followed by a period of desensitization during which the probe threshold is increased. In order to summarize these threshold-delay curves for many units, three summary measures were developed: the minimum probe threshold for short probe delays (between 0.1 and 0.4 msec); the maximum probe threshold during the desensitization period, and the duration of the desensitization period defined as the full width of this period at half the maximum threshold (FWHM).

These summary measures are shown in Figure 2-5. The panel shows the measures which are collected from individual threshold-delay curves. In the summary figures to be presented later, one or more of these summary measures will be plotted as a function of some stimulus variable.

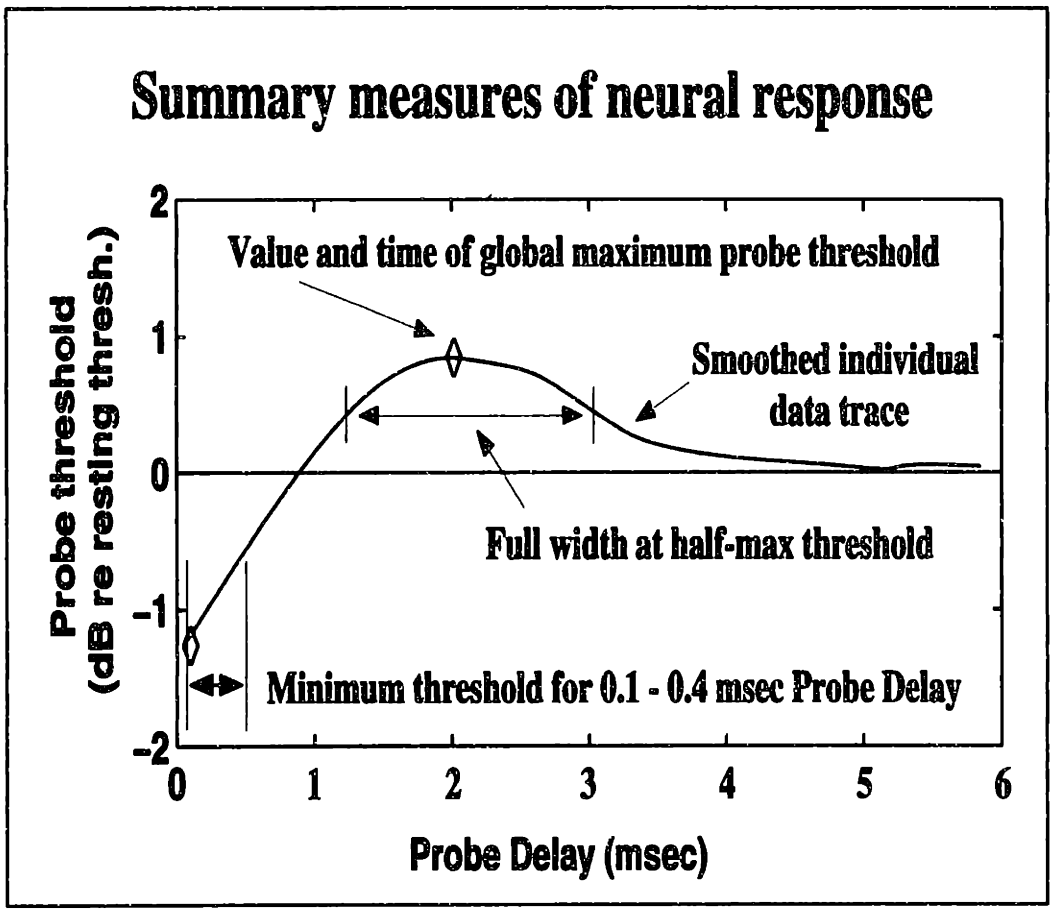

Figure 2-5: Measures and plots summarizing the threshold-delay curves for conditioned neurons. Top panel: Determination of summary measures for individual threshold-delay curves. After the curve was smoothed, the following were determined: the minimum probe relative threshold for a delay of .1 – .4 msec; the maximum relative threshold and delay of the maximum, and the delays where the relative threshold of the smoothed curve was half the maximum value.), which indicate the mean of the individual half-max measures.

Chapter 3

Effects of Single-pulse Conditioners

This chapter will present data of temporal interactions following conditioners consisting of a single pulse. These data detail the basic interaction characteristics for both threshold and relative spread measures.

3.1 Subthreshold Single-pulse Conditioners

Figure 3-1 shows probe threshold as a function of probe delay for a conditioner consisting of a single pulse. The thresholds, measured using the tracking algorithm, are plotted relative to the resting threshold. The conditioner level was 0.4 dB below the resting threshold. This figure shows the general features seen for all similar data: for short probe delays (< 1 msec), the conditioner reduces the probe threshold; here the magnitude of the sensitization exceeds 10 dB. For delays between 1 and 3 msec, the probe threshold increases above the resting threshold; the magnitude of the desensitization is much smaller than the magnitude of the sensitization. For longer delays the probe threshold approaches the resting value.

Figure 3-2 plots probe threshold following a single subthreshold cathodic conditioning pulse as a function of probe delay for 10 randomly-selected fibers from 4 cats. The conditioner level ranges from 2 to .5 dB below the resting threshold. The

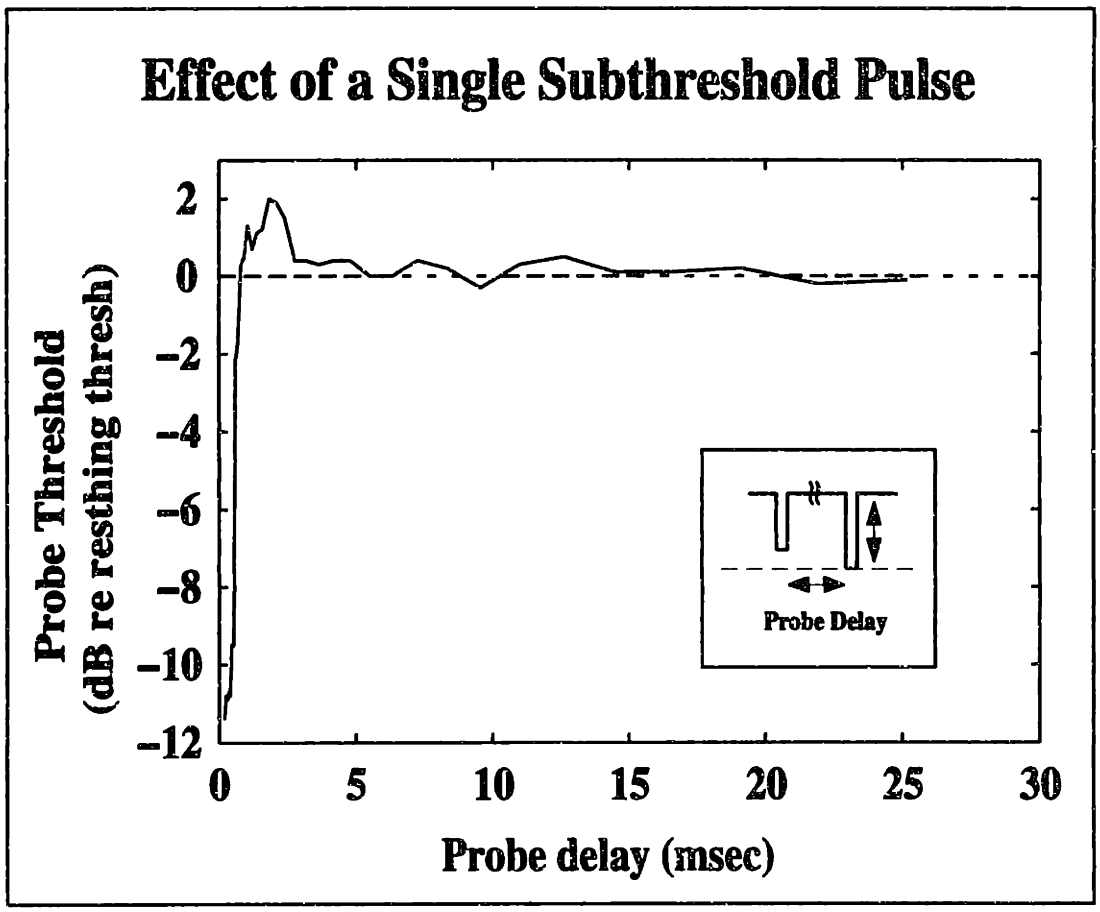

Figure 3-1: Probe threshold plotted as a function of probe delay for a single cathodic conditioner. Conditioner: a single 100-μsec pulse 0.4 dB below the threshold of a single 100 μsec cathodic pulse. Probe: a single 100-μsec cathodic pulse.

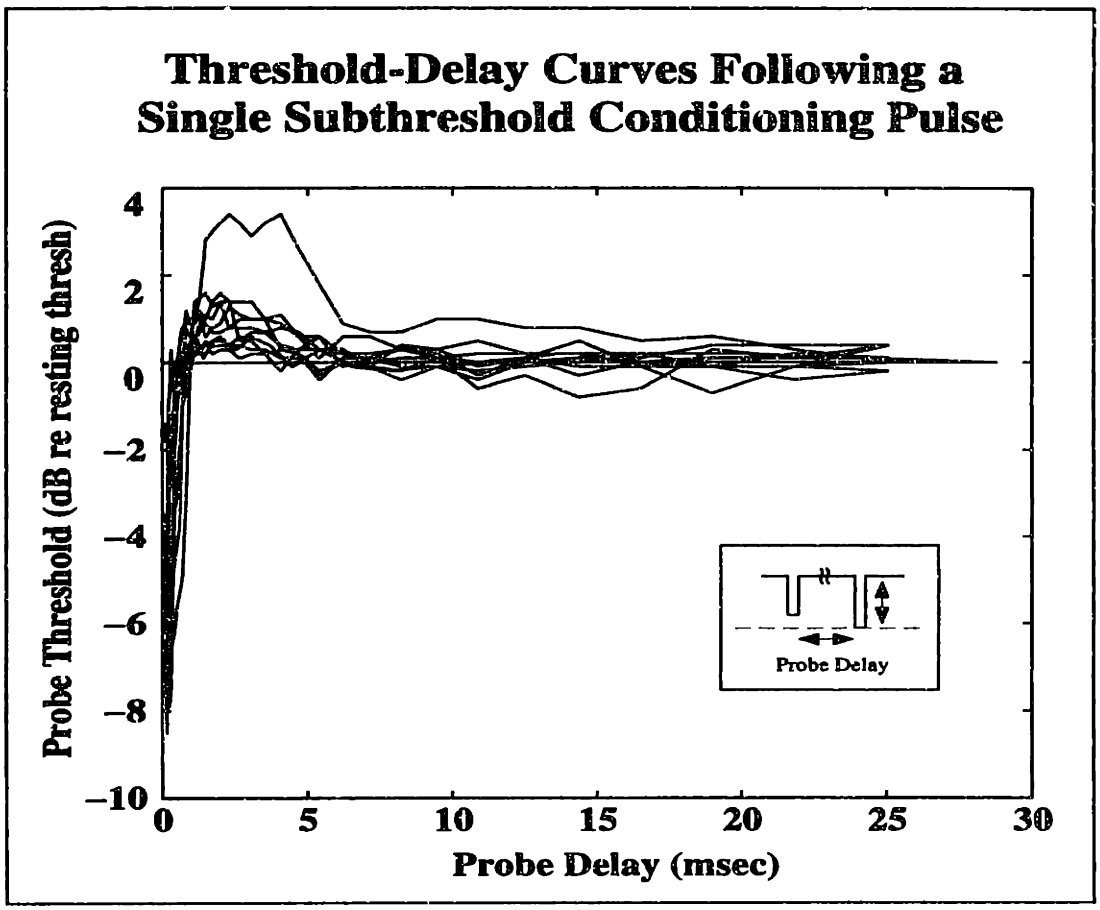

Figure 3-2: Probe threshold as a function of probe delay following a cathodic single-pulse conditioner. Data were collected using threshold tracking method. The conditioner is a single cathodic 100-μsec pulse; the probe is the same. Conditioner level: from 2 to .5 dB below the resting threshold. Data is from 10 units in four cats.

single-pulse conditioner reduces the probe threshold for short (< 500 μsec) delays, with the minimum probe threshold being 2 to 8 dB below the resting threshold for the shortest delays. This effect quickly decreases for lengthening delays. For delays between 1 and 5–10 msec, the probe threshold is above the resting threshold, with an average threshold increase of 1 dB. For delays greater than 5 msec, the probe threshold declines, with probe thresholds typically returning to the resting threshold value for delays greater than 10 msec.

One of the notable characteristics of Figure 3-2 is the variation in the magnitude of departure from the resting threshold: for the ten units shown, with the conditioner level varying only 1.5 dB, the minimum probe threshold varies from -8 to -2 dB relative to the resting threshold, and the maximum varies from a fraction of a dB to greater than three dB. Can this variation be explained by the different conditioner levels?

Figure 3-3 plots probe threshold as a function of probe delay for a single unit. Four different conditioner levels were used, ranging from 2 to 0.2 dB below the resting threshold. As might be expected, neural spikes were occasionally seen following the higher-level conditioning pulses. To avoid measuring probe thresholds following these conditioning spikes, the threshold algorithm only made use of those trials in which there were no spikes in response to the conditioner. The threshold-delay curve for the -2 dB conditioner shows an initial threshold about 8 dB below the resting threshold, and a maximum threshold during the suprathreshold period of about 0.5 dB above the resting threshold. The threshold-delay curve following the highest conditioner level, just 0.2 dB below the resting threshold, has an initial threshold of almost 12 dB below the resting threshold. The maximum threshold for this curve during the suprathreshold phase is about 2 dB above the resting threshold. The results for intermediate values of the conditioner level fall mainly between these extremes.

For this unit, there is a correlation between the conditioner level and the minimum threshold during the initial phase, and the maximum threshold during the desensitizing phase. The amount of variation seen in this unit cannot explain the variation shown in Figure 3-2, even though the range of conditioner levels is comparable (-2 –

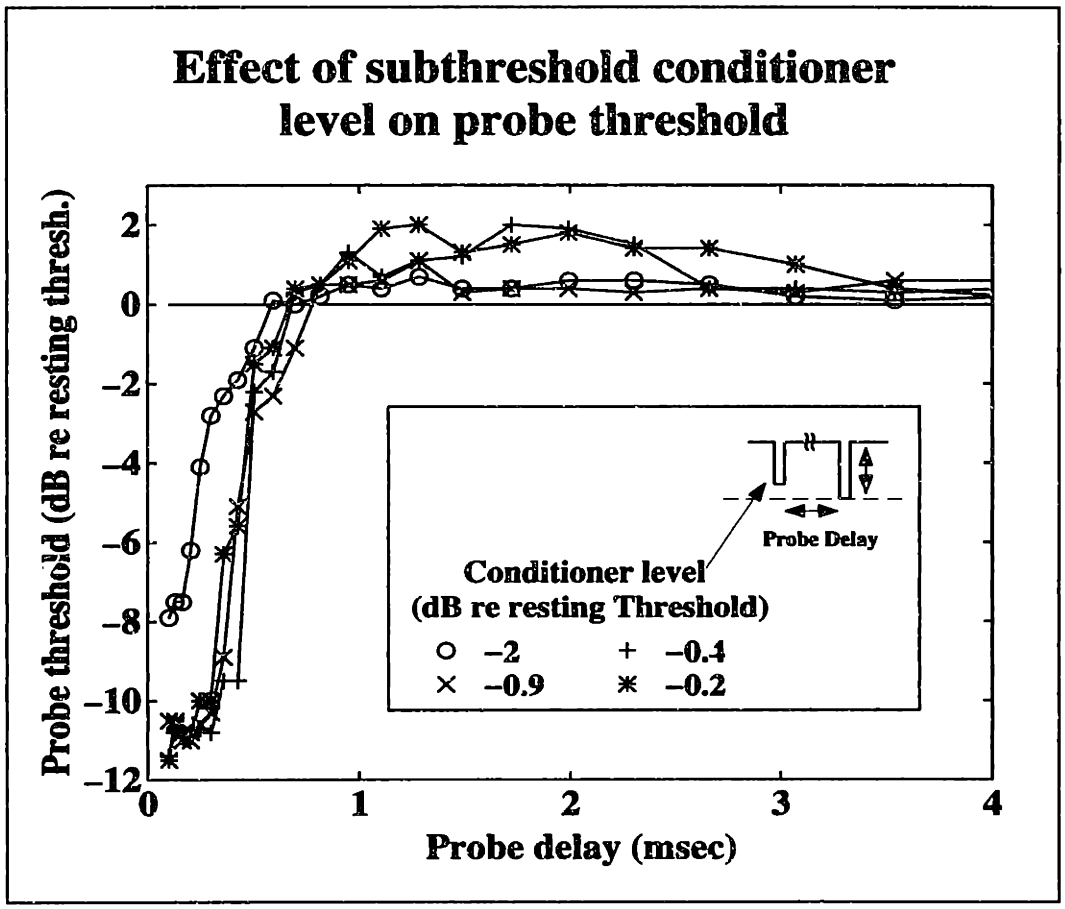

Figure 3-3: Probe threshold-delay curves for single subthreshold conditioning pulses of different levels. For a single unit, four threshold-delay curves are shown, with conditioner levels ranging from 2 to 0.2 dB below the resting threshold. The levels are denoted by the differing symbols used in the plot; the legend lists the level for each symbol. The conditioner consisted of a single 100 μsec cathodic pulse; the probe pulse was also a single 100 μsec cathodic pulse.

-0.5 for Figure 3-2, -2 – -0.2 for the present figure, units in dB relative to the resting threshold). Is there a large range for these effects as a function of conditioner level?

Figure 3-4 plots summary measures of the threshold-delay curves following a single subthreshold conditioning pulse as a function of the conditioner level. The data shown are from six units in two cats, and were chosen because they had a large number of P_f-level curves using different conditioner levels. The upper right panel shows how the minimum threshold during the initial phase depends upon the conditioner level. All six units show an overall reduction of the minimum probe threshold for the initial period as the conditioner level approaches the resting threshold. The greatest decrease in probe threshold is about 6 dB for a 1.5 dB increase in conditioner level; another unit shows a decrease of less than a dB for the same change in the conditioner level. The upper left panel shows the maximum probe threshold as a function of conditioner level during the desensitizing phase. All six units show an increase in the maximum probe threshold as the conditioner level approaches the resting threshold. The largest increase is almost 2 dB for a 1.5 dB increase in the conditioner level; two units show increases in the maximum probe threshold of a fraction of a dB for a 1.5 dB increase in the conditioner level. The bottom left panel shows how the duration of the desensitizing period (the FHWM summary measure) depends on the conditioner level; there is no apparent effect of level. From these data, it seems that the variations seen in the minimum probe threshold seen in Figure 3-2 cannot be explained by the variation in the conditioner level.

From the data shown in the above figures, the effects a single cathodic subthreshold pulse has on the neural response to a single cathodic probe pulse are:

- The **initial sensitizing period**, where there is a decrease in the probe threshold for probe delays of up to a few hundred μsec. This decrease can be as much as 12 dB, and increases as the conditioner level approaches the resting threshold.

- A **desensitizing period**, ranging from 1 to 5 msec following the conditioner, during which the probe threshold is elevated above the resting threshold of the

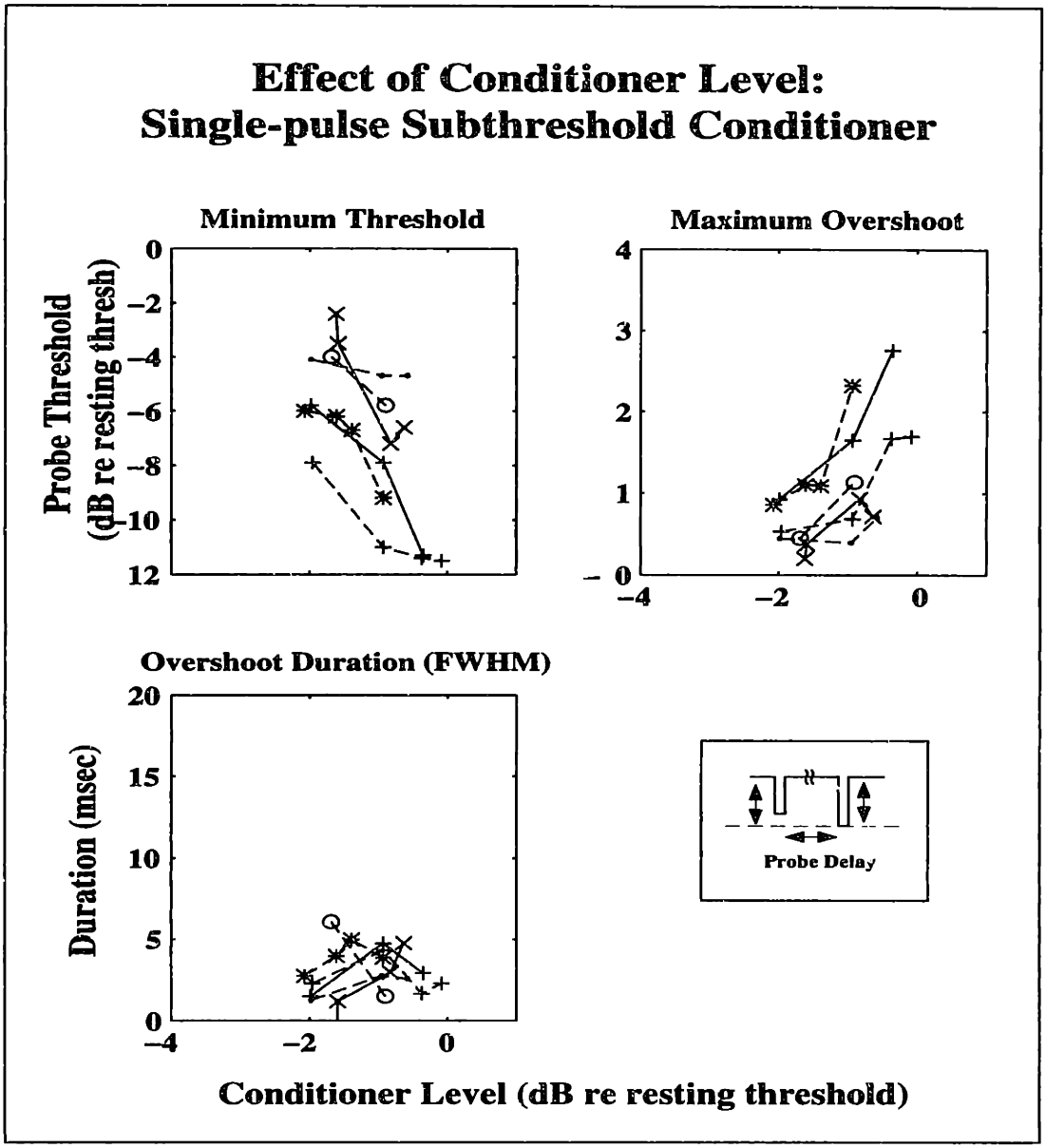

Figure 3-4: Summary measures for threshold-delay curves following single subthreshold conditioning pulses of various levels. Plotted in the three panels are different summary measures of the threshold-delay curve, as discussed in the Methods section. Within each panel, data from a single unit are connected by lines. Each unit is uniquely identified by a symbol-linetype combination that is the same for all panels. Shown are data from six units from two cats. The conditioner consisted of a single 100 μsec cathodic pulse; the probe pulse was also a single 100 μsec cathodic pulse.

neuron by roughly 1 to 2 dB. The maximum desensitization increases as the conditioner level approaches the resting threshold, but the duration remains constant.

3.2 Suprathreshold Single Pulse Conditioner

The previous section discussed the details of the neural response to a probe following a conditioning pulse which did not result in a neural discharge. This section deals with the neural response following a conditioner that causes a neural spike in response to the conditioning pulse. Much of the data was collected using conditioner levels sufficient to guarantee that each conditioner pulse resulted in a spike; that the probability of firing P_f was unity was determined by visual observation of the recorded waveform. For some of the data to be shown, the conditioner level was near threshold, resulting in a conditioner P_f being less than unity. For these measurements the threshold algorithm only made use of trials in which the conditioner did result in a neural spike.

Figure 3-5 shows how the probe threshold varies as a function of probe delay following a single suprathreshold conditioning pulse. While the probe delays for the subthreshold conditioners started at 100 μsec, the probe delays here start at 2 msec, because thresholds become very high near the absolute refractory period, which for our data shows a minimum value of about 500 μsec while a more typical value would be between 600 and 700 μsec. At a 2 msec delay, the probe threshold is elevated about 2.7 dB above the resting threshold. This elevated threshold quickly decreases in a monotonic fashion towards the resting threshold, with the time constant of a fit exponential curve being about 2 msec. This is an example of the classic relative refractory characteristics of the recently- stimulated neuron.

Figure 3-6 shows probe threshold as a function of probe delay for 8 units from 3 cats. The conditioner was a 100-μsec cathodic pulse at a level high enough to guarantee a spike for each conditioner presentation. For probe delays shorter than the absolute refractory period, a second spike could not be elicited for any probe level

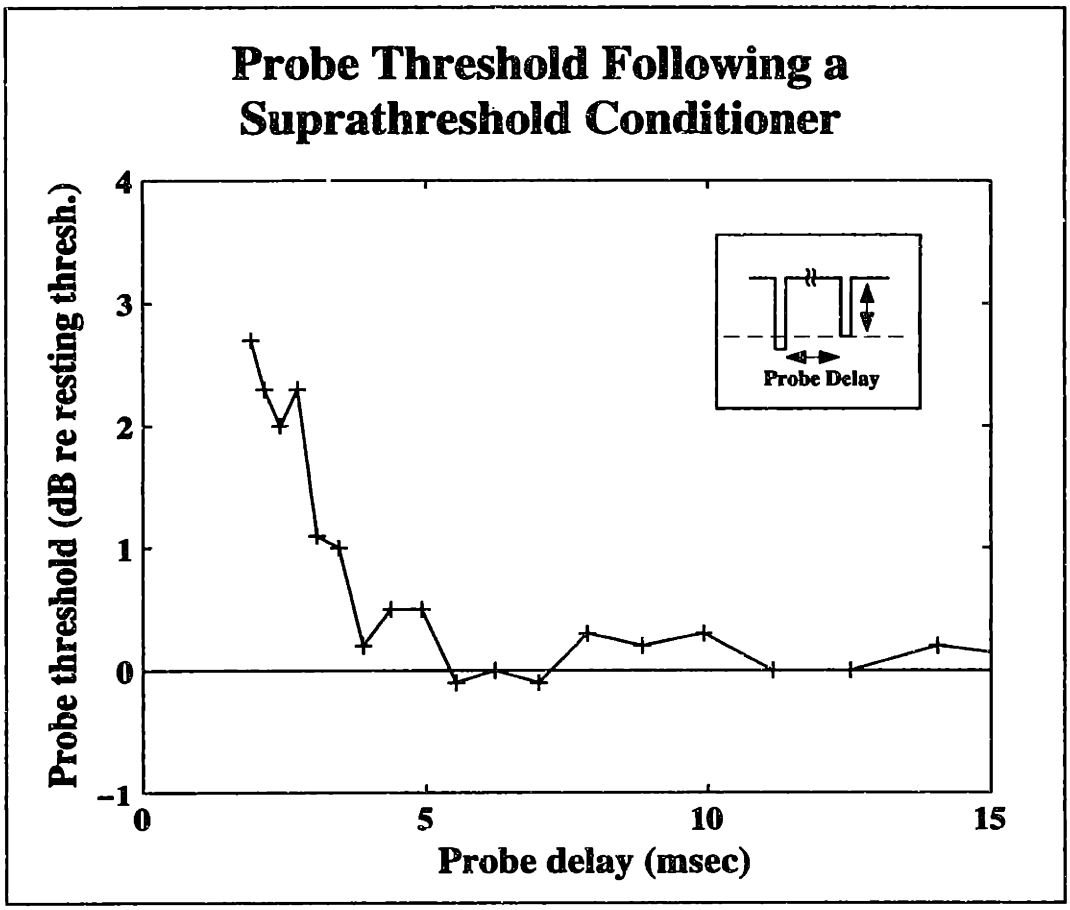

Figure 3-5: Probe threshold as a function of probe delay for a single suprathreshold conditioner. The conditioner was a single cathodic 100-μsec pulse of sufficient amplitude to guarantee a P_f of 1. The probe was a single 100-μsec pulse.

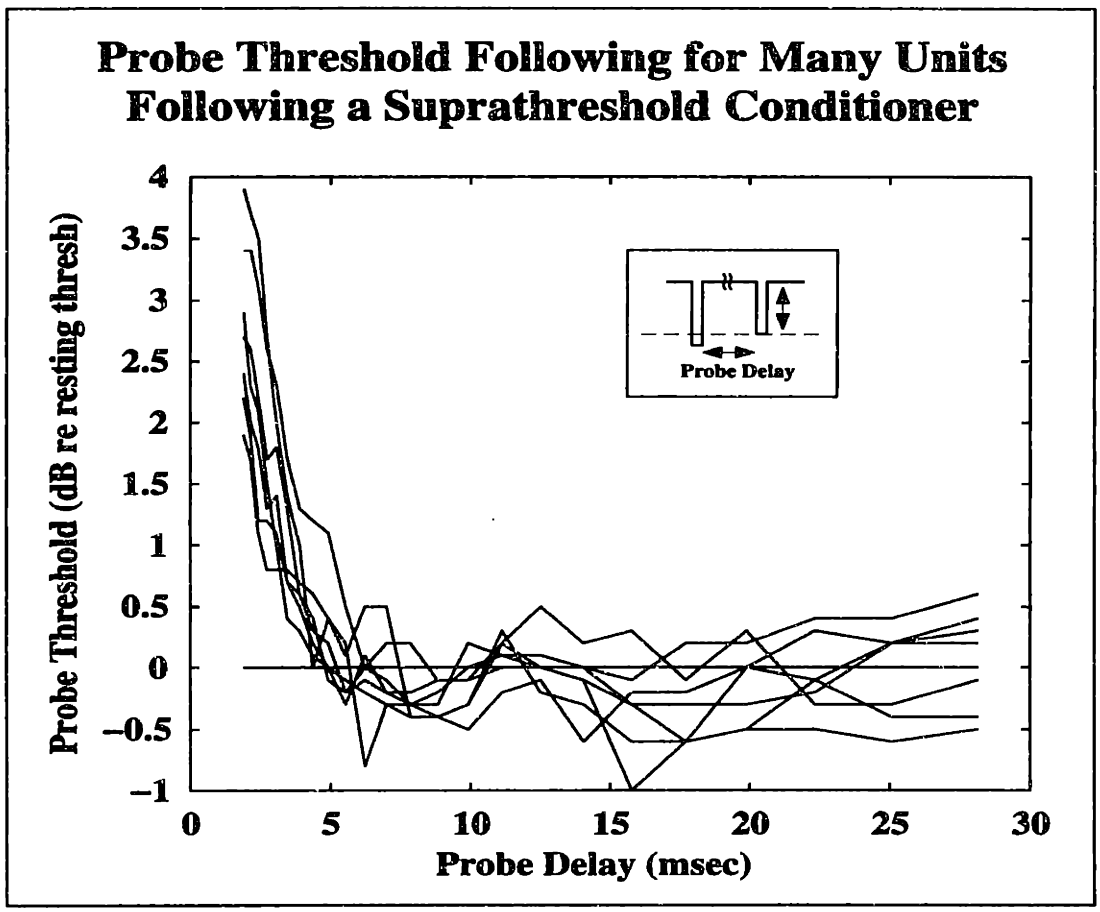

Figure 3-6: Probe threshold following a single suprathreshold conditioning pulse is plotted against the probe delay. Data from individual threshold-delay measures are individual lines; probe thresholds were determined using the threshold tracking method. The conditioning pulse consisted of a single cathodic 100 μsec pulse; the probe pulse was also a single cathodic 100 μsec pulse. Data is shown for 8 units from 3 cats

used. For probe delays longer than this, the probe threshold is elevated by a few to several dB (2–5 dB at a probe delay of 2 msec). This effect decreases quickly, the probe threshold approaching the resting threshold for delays of 5 msec. For longer delays, the probe thresholds of many units appear to remain at the resting threshold level, while a few appear to decrease below the resting threshold by up to a dB.

Again, there is a striking variability in the initial (at 2 msec delay) probe threshold. Could this variation be due to the level of the conditioner, even though all conditioner pulses resulted in a neural spike? Figure 3-7 plots for a single unit the probe threshold following a single suprathreshold conditioner as a function of probe delay for three different conditioner levels, one of which is about a dB below the resting threshold. The probability of firing P_f for this conditioning pulse is about 0.1; as mentioned above, the threshold tracking algorithm only uses trials when the conditioning pulse resulted in a spike.

The curve with the lowest conditioner level resulted in the highest initial probe threshold of about 3.6 dB above the resting threshold, which is almost a dB above the initial thresholds for conditioners of 0.1 and 2.8 dB above the resting threshold. The initial thresholds for these conditioner levels were identical at about 2.7 dB. This difference in thresholds disappeared quickly, with the thresholds being indistinguishable for probe delays greater than 3 msec. The threshold-delay pulses for the two higher-level conditioners approximated the resting threshold for delays greater than 5 msec; due to the low efficiency of data collection caused by the conditioner P_f of 0.1, the remaining curve is cut short. Based on these data, the variation in the initial thresholds seen in Figure 3-6 cannot be explained by variations in the conditioner level.

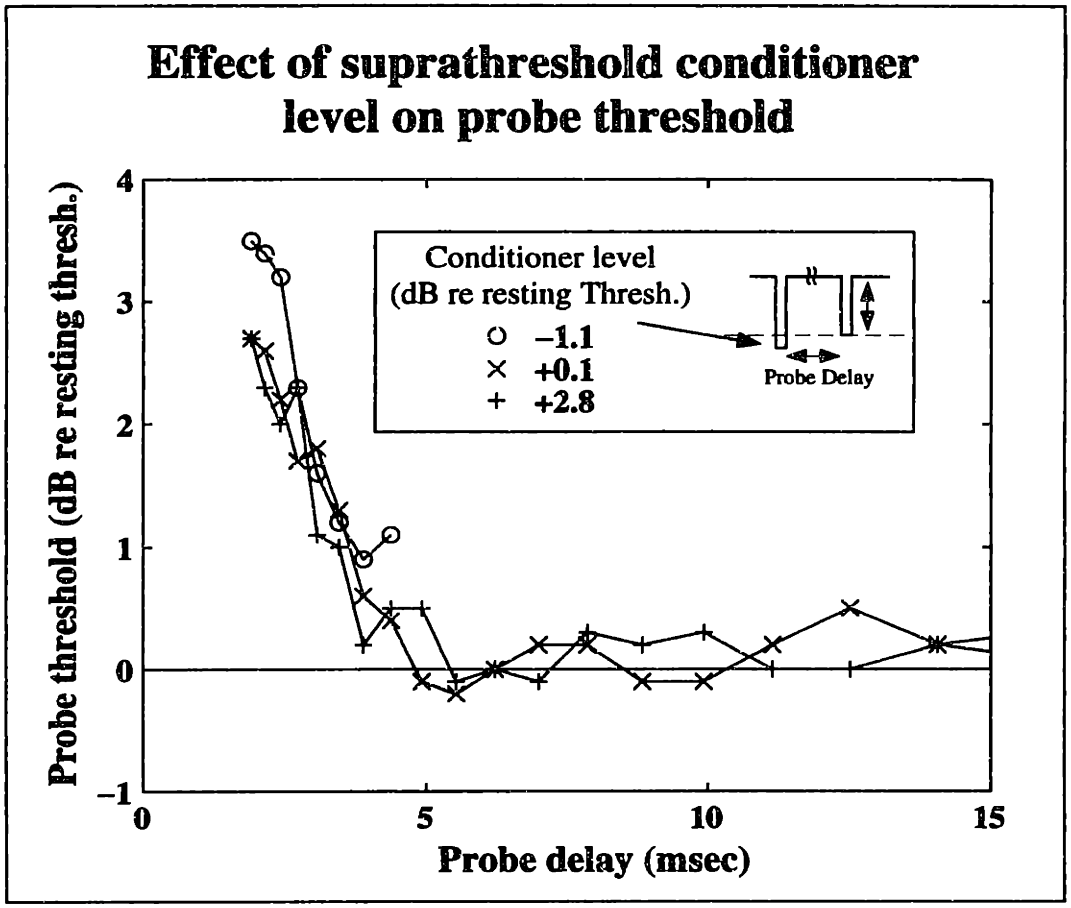

Figure 3-7: Probe threshold as a function of probe delay for suprathreshold conditioners of different levels. The three curves, all from the same unit, have conditioners whose levels are as shown in the legend. Note that the curve represented by the o symbol has a conditioner level about a dB **below** the resting threshold; the P_f of responses to the conditioner pulse was about 0.1 . As noted in the text, probe threshold measures were conducted for only those conditioners which resulted in a spike. This curve goes to a delay shorter than the others due to the time required to determine each threshold point. The conditioning pulse consisted of a single cathodic 100 μsec pulse; the probe pulse was also a single cathodic 100 μsec pulse.

3.3 Relative Spread Following Single-Pulse Conditioners

Figure 2-4 shows how the threshold and RS are calculated from the P_f-level curve of the response to a single pulse. Figure 3-8 extends this concept, showing how the RS was calculated for several delays in a given unit in the top panel. These derived RS measures were then summarized by plotting the RS value as a function of delay in the bottom panel. The plots that will now be shown are such summary plots for sub- and suprathreshold single-pulse conditioners. The bottom panel shows that the RS is significantly increased for short probe delays, with the initial value being close to 0.5, while the value for long probe delays is about 0.08.

Figure 3-9 plots RS as a function of the probe delay for 9 units from 5 cats. The subthreshold conditioner and probe were both 100 μsec cathodic pulses. The trend is for the RS to be larger for the shortest probe delays, typical values of the RS being between .1 and .25 for the shortest delay, and between .05 and .1 for delays exceeding 3 msec, which corresponds to that for single pulses. Comparing Figure 3-2 and Figure 3-9 might lead to the conclusion that the increase in RS, which is the normalized dynamic range, is due to the decrease in the probe threshold. This is not the case: plots of the non-normalized dynamic range in mA as a function of probe delay look much the same as the RS-delay plots. Thus, the dynamic range, as well as the RS, is increased for short probe delays.

Figure 3-10 plots the relative spread following a single suprathreshold conditioning pulse as a function of the probe delay for a sample of 7 units. For the initial (1 msec) probe delays, the measured RS values are between 0 and 0.05. The trend is for the RS to increase with increasing probe delay, with RS reaching 0.05 to 0.1 for delays longer than 5 msec.

Summarizing the effects of a single cathodic conditioning pulse on the relative spread of the following neural responses, subthreshold conditioning pulses tend to increase the relative spread for probe delays of less than 1 msec. In contrast, for single cathodic suprathreshold conditioning pulses, the RS value is decreased for delays of

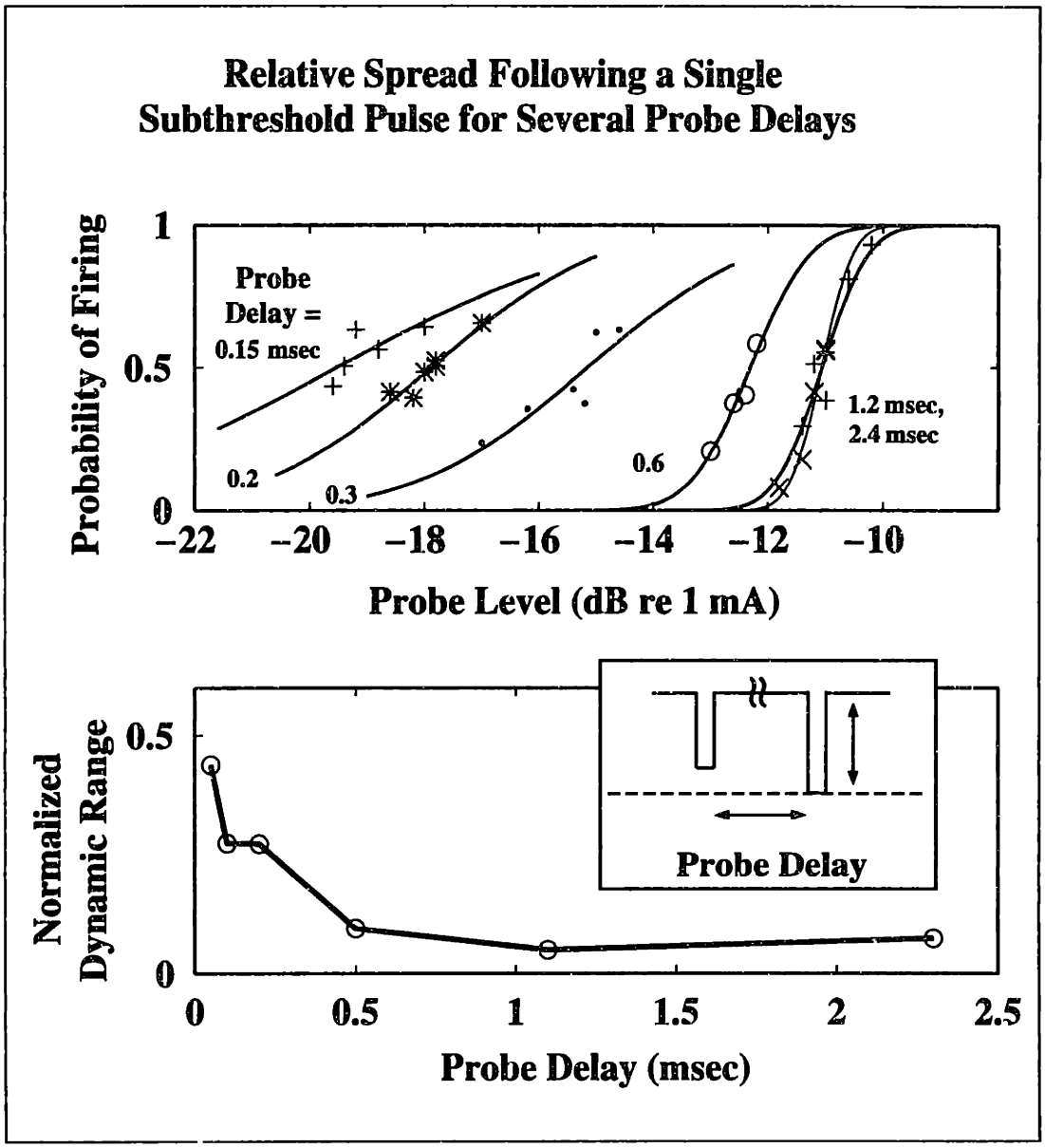

Figure 3-8: Basic Measures and Summary Plots. The top panel plots the probability of firing P_f as a function of probe level for several probe delays, the delay (in msec) being shown close to each P_f-level curve. The bottom panel plots the relative spread as a function of the probe delay. The conditioner is a single subthreshold 100-μsec cathodic pulse, the probe is also a single 100-μsec cathodic pulse.

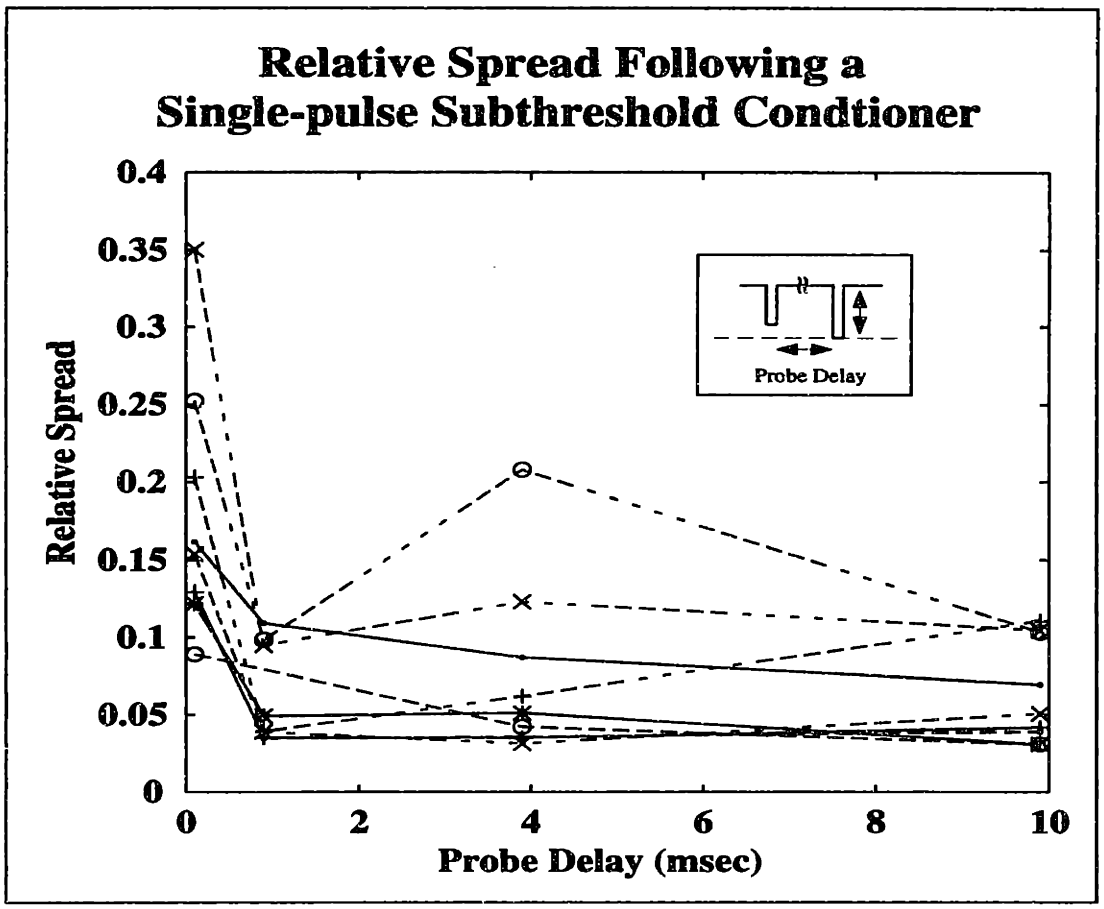

Figure 3-9: Relative Spread in response to a single subthreshold conditioning pulse plotted as a function of probe delay. Data is from 9 units in 5 cats. The conditioner and probe are single cathodic 100-μsec pulses.

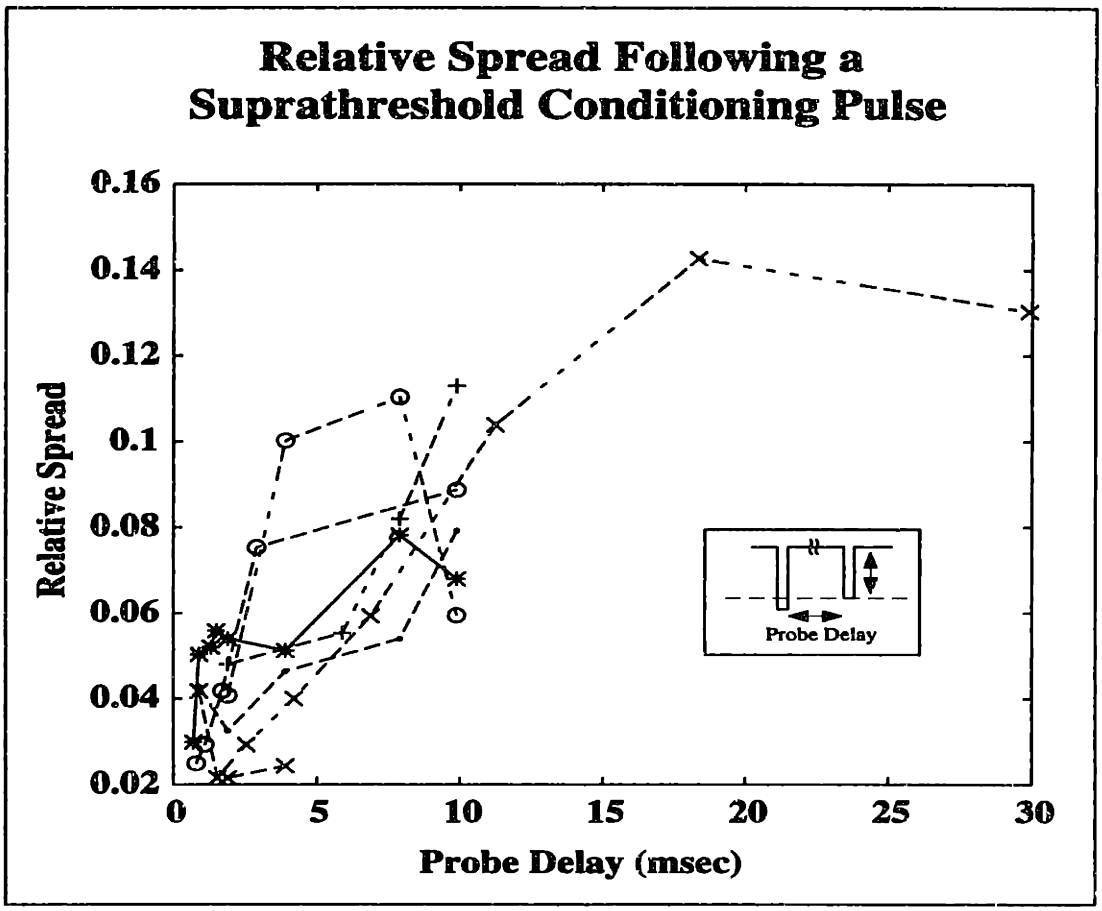

Figure 3-10: Relative Spread in response to a single suprathreshold conditioning pulse plotted as a function of probe delay. Data is from 7 units in 4 cats. The conditioner and probe are single cathodic 100-μsec pulses.

less than 2 msec.

3.4 Discussion

3.4.1 Relative Spread

The relative spread (**RS**) was first introduced by Verveen and Derksen [89] in their study of the fluctuation of neural excitability. From his study of many frog sciatic nerve fibers Verveen concluded that curves of neural response vs. stimulus level (our P_f-level curves) could be adequately fit with an integrated Gaussian. Verveen further concluded that while a fiber's threshold could depend upon the stimulus parameters (such as stimulus duration), the relative spread did not, and seemed to be an inherent property of the nerve. Verveen found a strong correlation between the RS and the fiber diameter. Finally, he postulated that the observed fluctuations could be accounted for by a noise source inherent to the neuron.

Sigworth [81], building on the work of Verveen and others (Hille [23], Lecar and Nossal [46]), showed that the probabilistic opening and closing of the sodium ion channels in the neural membrane could be this inherent noise source.

Rubinstein [72] developed a computer model incorporating many independent sodium channels. The channel dynamics were governed by equations analogous to the Hodgkin-Huxley equations, and the number of open and closed channels were calculated as a function of time. Modeling a peripheral node of the frog, he showed the observed threshold noise characteristics (the RS) could indeed be explained using the number of sodium channels thought to exist in this particular node. Whether the noise inherent to the open/closed characteristics of membrane ionic channels can give rise to the observed changes in RS is further examined in Section 5.2.4.

While RS is a characteristic grounded in the noisiness of the trans-membrane potential, its practical aspect derives from the relation of the RS measure to the dynamic range of the neural response, the range of currents which leads to a response whose P_f is between zero and one.

The RS values that are calculated from our data are larger than those seen by Verveen and Derksen [89], which show typical values for the frog sciatic nerve of 0.01. The RS values of 0.05 – 0.10 in cat auditory nerve fibers in response to single pulses suggests that the number of sodium channels at the site of excitation is lower than for the frog, as fewer channels results in more channel noise. A quantitative estimate will be made in Section 5.5.2.

3.4.2 Effects of Subthreshold Conditioners

The effects of subthreshold pulses on the neural response to subsequent pulses have been studied previously in various preparations (Erlanger and Blair [15], Katz [37] [38]). These preparations have not recorded single unit potentials as a measure of the neural response, relying instead on the compound action potential (Erlanger and Blair) or muscle twitches (Katz) as a measure of the neural response. The threshold vs. probe delay curves shown by Katz [38] shows a monotonically-decreasing change in the probe threshold as referred to the resting threshold.

Further describing Katz's data: for a cathodic conditioner followed by a cathodic probe, the probe threshold is decreased for shorter probe delays. For the case where the conditioner level is well below the resting threshold, the shape of the curve is adequately described by a single exponential (Katz [38]). As the conditioner level is increased towards the resting threshold, there is a pronounced departure from this exponential shape, with the probe threshold remaining depressed for a period of time, and then decaying exponentially to the resting threshold.

The data of Katz are in qualitative agreement with those presented in Figure 3-1 in that the gross sense of the changes in the probe threshold with probe delay are the same. We do not see a flattening of the probe threshold/probe delay curve as indicated by Katz; looking across the data we have for which the conditioner level differed from -2 dB re resting threshold, there is no obvious change in the shape or time constant of the effect for the cathodic-cathodic case. Katz's interpretation of the change in the shape of the threshold/delay curve was that above a certain level the nerve exhibits an active 'local response' to the depolarization of the neural membrane which causes

a continued reduction in the probe threshold. For smaller values of the conditioner level, the change in the probe threshold is due to a 'local potential' corresponding to the charge remaining on the capacitive membrane. The data we show do not exhibit any pronounced departure from an exponential decay to the resting threshold for the first 500 – 700 μsec of probe delay. While this is consistent with this phase of the effect being dominated by capacitive effects, we will show that this cannot be the case. Additionally, Katz does not see a desensitization period following subthreshold pulses; this may be the result of his studying a population response rather than a single-unit response as is the case with the present study.

For a cathodic conditioner followed by a cathodic probe, Katz shows that the magnitude of the probe threshold change depends monotonically on the conditioner level, with the probe threshold being displaced the most by conditioner levels nearest to the resting threshold. This is consistent with the data shown in the upper right panel of Figure 3-4, where for individual units the probe threshold at a delay of 100 μsec decreases in a monotonic fashion as the conditioner level increases towards the resting threshold level. This behavior is also seen in the dependence in the maximum probe threshold during the suprathreshold phase in the conditioner level.

3.4.3 Effect of Suprathreshold Conditioners

Suprathreshold effects on the neural threshold have been studied for many years. The conventional technique is as used here: a conditioning pulse is used to elicit a spike from the nerve, and a probe pulse used to determine the threshold characteristics as a function of probe delay.

Figure 3-11 shows in an abstract form the results from others of the neural threshold as a function of probe delay for a nerve stimulated with a suprathreshold conditioning pulse. The figure is after a similar figure in Raymond [66], and summarizes neural thresholds following a spike as seen in frog sciatic nerve ([66], [55], [65]), cat saphenous and phrenic nerves [19], cat cerebellar fibers [18], and rat spinal root axons [4]. Following a single suprathreshold conditioning pulse, the response seen in these studies consists of an absolute refractory period, where the nerve fiber will not sup-

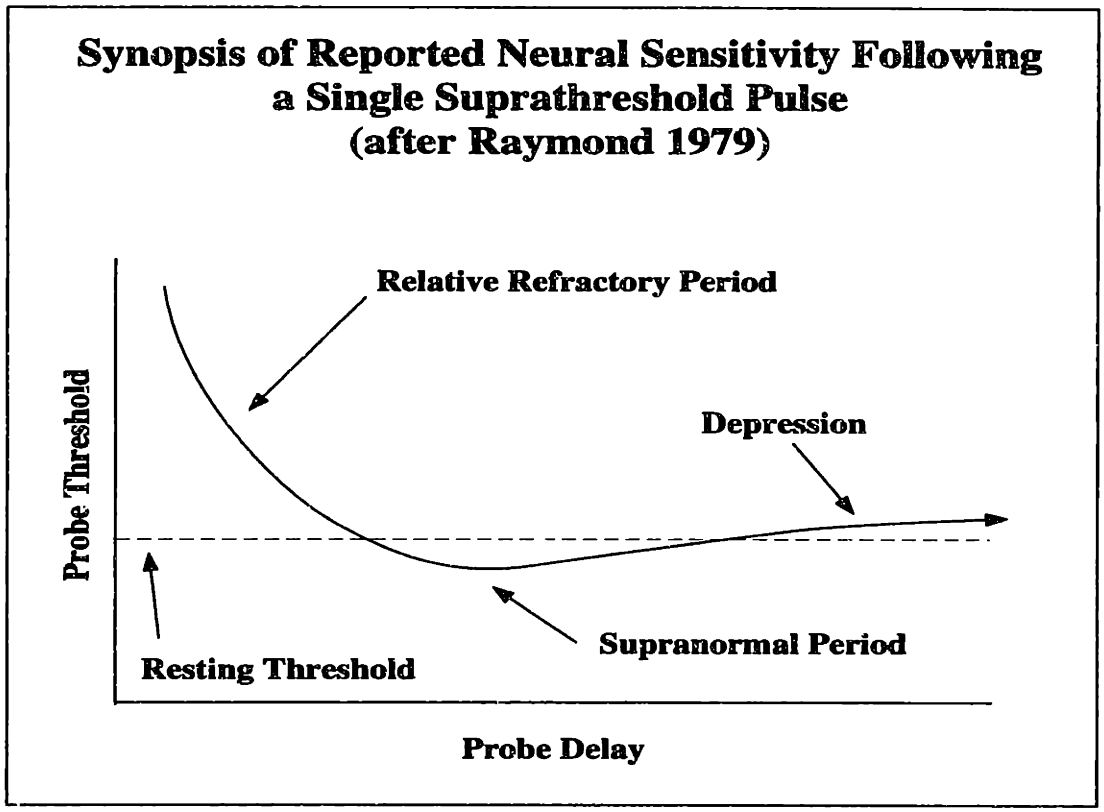

Figure 3-11: A summary of threshold variations of the stimulated nerve observed by others. The threshold of a nerve is plotted as a function of the time following a single suprathreshold pulse. The relative refractory period lasts from the time a second propagating spike can be produced for any stimulus level to the time the threshold reaches the initial threshold value. Here, there is a period (the supernormal period) following the relative refractory period where the threshold is lower than the resting threshold. This is followed by a period of depression, where the neural threshold is higher than the resting threshold. Ordinate: Probe delay in logarithmic units. Absicca: threshold in arbitrary units. After Raymond [66].

port a propagating spike at any probe level, followed by a relative refractory period, where neural spike propagation is possible for probe levels higher than the resting threshold level. After the relative refractory period, the probe threshold drops below the resting threshold for a period of time (the supernormal period), followed lastly by the subnormal period, where the probe threshold is elevated above the resting threshold. This subnormal period can last for a substantial length of time which depends on the preparation [66].

Gasser and Grundfest ([19]) studied the saphenous and phrenic nerves in cat using the compound action potential as a measure of the neural response. Their data show the relative refractory period lasting from 2.5 to 5 msec following the conditioner; the supernormal period reaching a maximum at a delay of 5 to 10 msec, and the transition from supernormal to the depressed stage occurring at delays of 12 to 18 msec. The average increase in the size of the compound action potential (CAP) during the supernormal period was 7%, ranging from 0% to 20%.

Data from cerebellar parallel fibers shown by Gardner-Medwin ([18]) indicate a larger (increase in the CAP by 40% over resting CAP level), longer-lasting supernormal period for parallel fibers in the cerebellar cortex in cat. In spinal root axons of rat, Bostock and Grafe [4] show a supernormal period with a maximum threshold decrease of 10% at a probe delay of 6 msec.

In the study most comparable to the present study, looking at single unit responses of the sciatic nerve of frog , Raymond and Lettvin [65] state that the maximal supernormal effect occurs 7–20 msec following the conditioning pulse, and results in a threshold decrease of 18%, which would correspond to a decrease in level of greater than 1.5 dB.

These studies show that across a large range of preparations and species, a supernormal period occurs following the relative refractory period during which the neuron is sensitized to following pulses. Our data in Figure 3-6 show, with a single exception, no indications of a supernormal period. The time course of the threshold is a monotonically-decreasing function of probe delay for delays greater than 2 msec, and for no delay is the average probe threshold significantly less than the resting

threshold.

It is not clear why the cat auditory nerve lacks a period of sensitization following the relative refractory period. A sensitization period would lead to preferred interspike intervals, because near-threshold stimuli would tend to trigger the neuron at a specific time following the preceeding spike. A preferred interspike interval would distort neural phase-locking and degrade information about the stimulus frequency. Thus, the lack of a sensitization period in the auditory nerve is consistent with the hypothesis that the auditory nerve is specialized for precise encoding of temporal information.

Chapter 4

Effect of Multi-Pulse Conditioners

This chapter is an extension of the inquiries of the last chapter using more complex stimuli. In chapter 3, the aims of the research were to characterize the modification of the neural response caused by a single-pulse conditioning stimulus, and to explore the causes and consequences of these effects. The aim of the present chapter is to describe how the response characteristics of the conditioned nerve change as the number and level of the conditioning pulses changes. As before, the two response characteristics that will be examined are the neural threshold, and the relative spread.

There are many reasons to look at how multiple-pulse conditioners affect the subsequent neural response. First, it provides information that will constrain the possible physical mechanisms responsible for these behaviors. From a more practical point of view, the case of multiple pulses more realistically mimic the stimuli used with cochlear implant subjects. It will be shown that for subthreshold stimuli, the neural response to a single pulse differ from the neural response following several pulses. In contrast, the neural threshold following one suprathreshold pulse is nearly indistinguishable from that following two or three-pulse conditioners.

4.1 Subthreshold conditioners

4.1.1 Effect on threshold

While basic response characteristics of neural thresholds for single and multipulse conditioners are similar, the details differ. The decrease in the probe threshold at short delays is significantly less for multipulse conditioners compared to the single-pulse case. This is demonstrated in Figure 4-1, which shows the probe threshold at

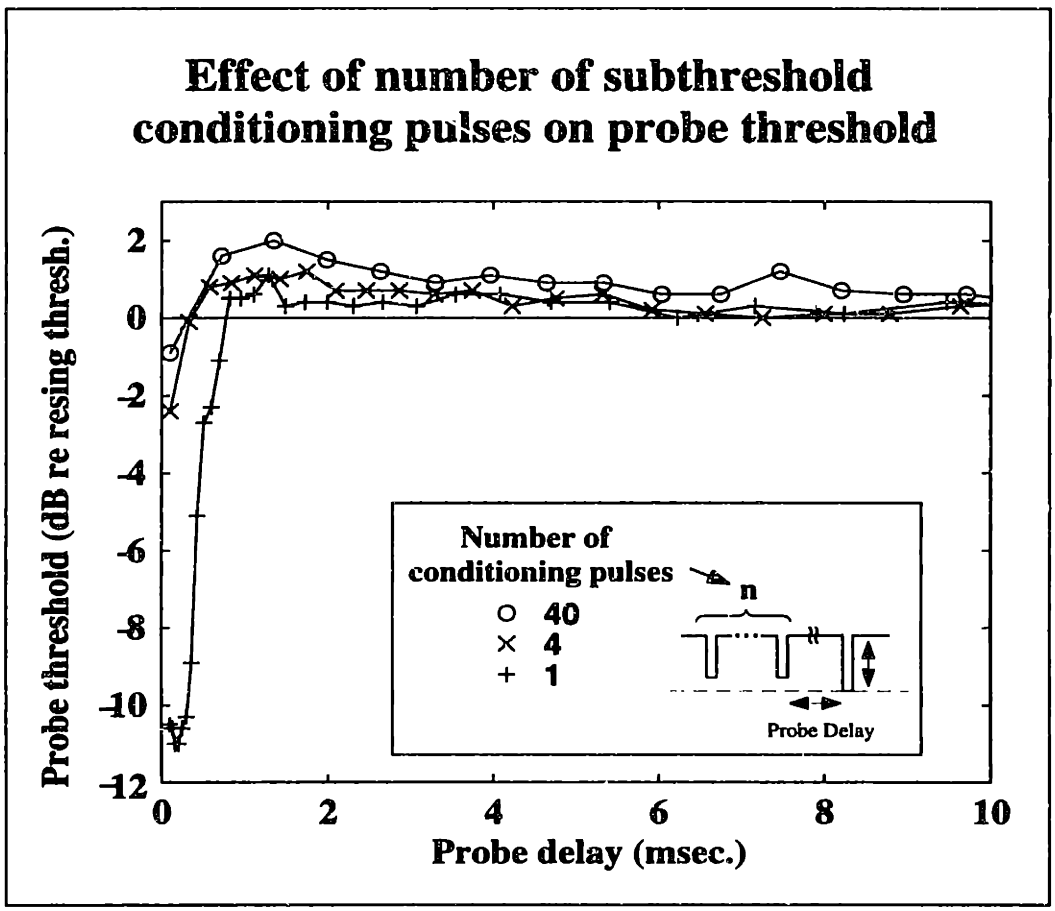

Figure 4-1: Probe threshold at various delays for three different conditioners. The number of pulses in each conditioner is different: Probe thresholds for a single conditioning pulse are represented by a ○ symbol; four pulses by ×, and forty pulses by the +. The individual conditioner pulses are 100 μsec cathodic pulses 1 msec apart, the probe pulse is a single cathodic 100 μsec pulse. All data are from a single neuron. Conditioner level: -1 dB re the resting threshold.

several delays for conditioners consisting of one, four, and forty pulses. All the data

shown are from a single neuron. The conditioner level is one dB below the resting threshold. For single-pulse conditioners there is a large ($\sim$ 11 dB) decrease in the probe threshold for short delays. The desensitizing period lasts from delays of 0.8 to approximately 6 msec, with a maximum threshold of roughly 1 dB above the resting threshold. The four-pulse conditioner reduces the probe threshold no more than 3 dB, and the start of the desensitizing period occurs at a delay about half of that for the single-pulse case. The maximum probe threshold increase is about the same as in the single-pulse case for this neuron, although the suprathreshold period lasts longer for the four-pulse conditioner. Finally, the forty-pulse conditioner threshold measures show a minimum threshold for short probe delays that is around 1 dB below the resting threshold. The suprathreshold period begins at a delay of $\sim$ 0.5 msec, the same delay as for the four-pulse conditioner. The maximum threshold during this phase is almost 2 dB above the resting threshold and remains elevated for more than 10 msec.

Thus, in addition to the changes in the threshold-delay curves due to changes in the conditioner level, which we saw in Chapter 3, there is another variable which changes the threshold-delay curve: the number of pulses in the conditioner. In order to most fully investigate the threshold-delay curve as a function of these two variables, we studied multi-pulse conditioners consisting of either four or forty pulses. These numbers were chosen to provide a wide range of conditioners.

Figure 4-2 plots three summary measures of the threshold-delay curve as a function of the number of subthreshold pulses in the conditioner. The conditioner levels in the data shown here are between -0.7 and -1.7 dB relative to the resting threshold. Data from individual units are connected by lines.

The upper left panel plots the minimum probe threshold for short (01. - 0.4 msec) probe delays for different numbers of conditioning pulses. Here there is a convincing change in the behavior from a single pulse and four pulses. Three of the five units plotted show a large ($>$ 3 dB) decrease in the sensitization going from one to four conditioning pulses. The probe thresholds decrease about 1 dB on the average going from four to forty conditioning pulses. The magnitude of the sensitization is much

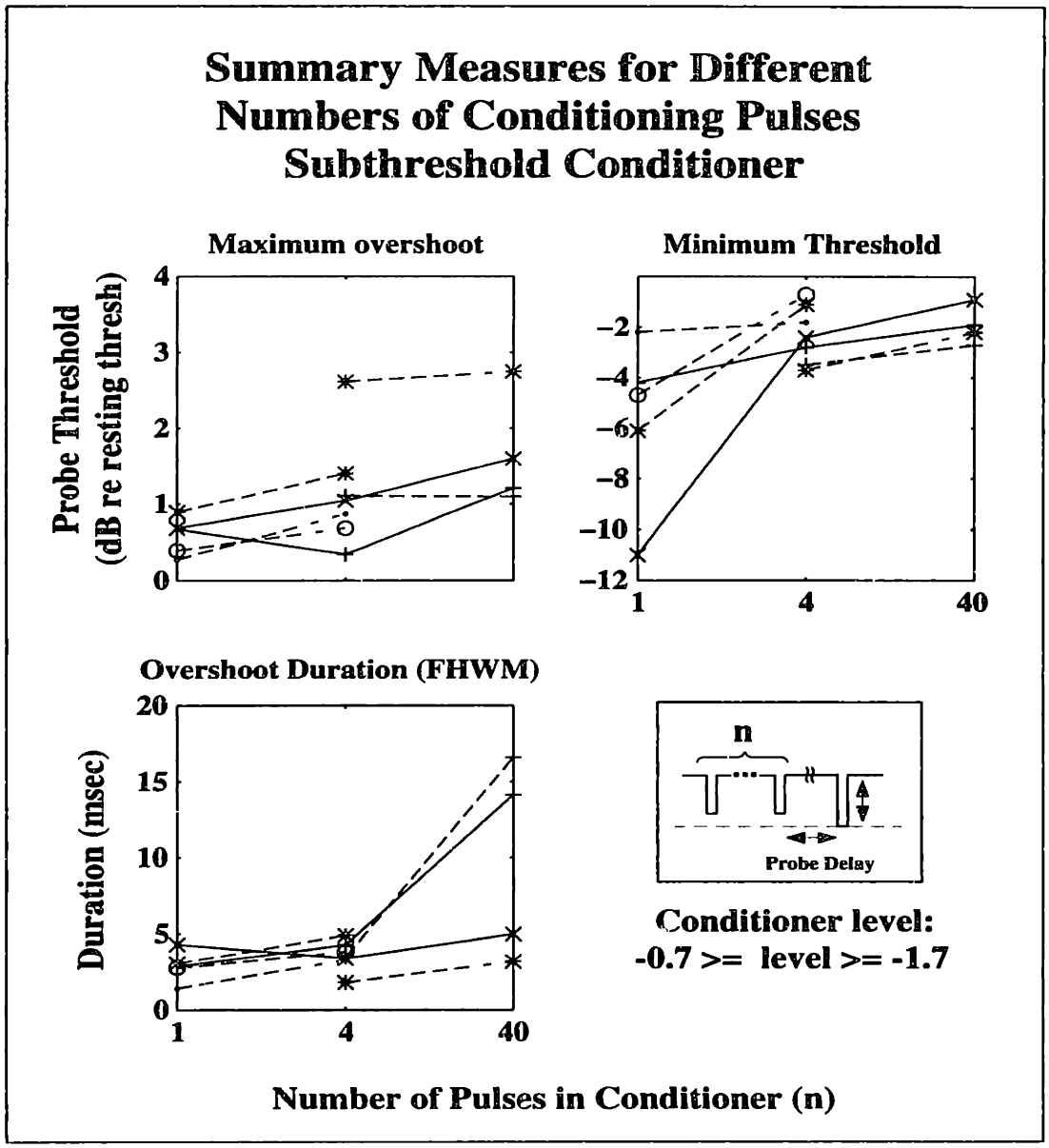

Figure 4-2: Summary measures for subthreshold conditioners containing differing numbers of pulses. Three different summary measures of threshold-delay curves(upper left panel: maximum probe threshold during the suprathreshold phase; upper right panel: minimum threshold for short delays; lower right panel: duration of the suprathreshold phase) are plotted as a function of the number of pulses in the conditioner. The conditioner levels were between -0.7 and -1.7 dB below the resting threshold of the included neurons, as indicated beneath the stimulus panel in the lower right corner. Lines connect data from the same unit. The summary measures are calculated as depicted in Figure 2-5. Seven units from three cats are plotted.

greater for a single conditioning pulse.

With one exception, the maximum threshold (upper right panel) during the desensitization period are higher for a four-pulse conditioner than for a single-pulse conditioner, as is depicted in the upper left panel. The magnitude of the increase is variable, but is less than a factor of two. Three of the four units [plotted show a higher maximum threshold following a forty-pulse conditioner than a four-pulse conditioner.

The lower left panel displays how the duration of the desensitizing phase of the threshold-delay curve depends on the number of conditioning pulses. Four of five units show a small ($\approx$ 2 msec) increase in the duration of the desensitization period going from one to four pulses.

Increasing the number of pulses from 1 to 4 to 40 has the following effects: the greatest decrease in the probe threshold for short delays occurs following a single-pulse conditioner and drops rapidly for four or more pulses. The minimum probe threshold for 4 and 40 pulse conditioners is rarely more than 3 dB below the resting threshold. The maximum probe threshold during the desensitization period increases somewhat with the number of pulses for the majority of units. Finally, the duration of the suprathreshold effect is longest following the forty-pulse conditioner, with little difference in the duration seen between the one and four-pulse conditioners.

These conclusions are reinforced by Figure 4-3, which plots for an average over all data the minimum probe threshold for short delays, the maximum probe threshold, and the desensitization period duration for 1, 2, 3, 4, 8, 16 and 40-pulse conditioners. The minimum threshold is clearly greatest for a single-pulse conditioner, and the maximum threshold and suprathreshold period duration don't vary appreciably except for the forty-pulse conditioner.

4.1.2 Relative Spread

Figure 4-4 plots RS-delay curves from six units in three cats following a four-pulse subthreshold conditioner. The conditioner levels range from 1.6 to 2.3 dB below the resting threshold. Four of the six units show a near- monotonic decrease in the RS as the probe delay increases. The initial RS value can be twice the value for long

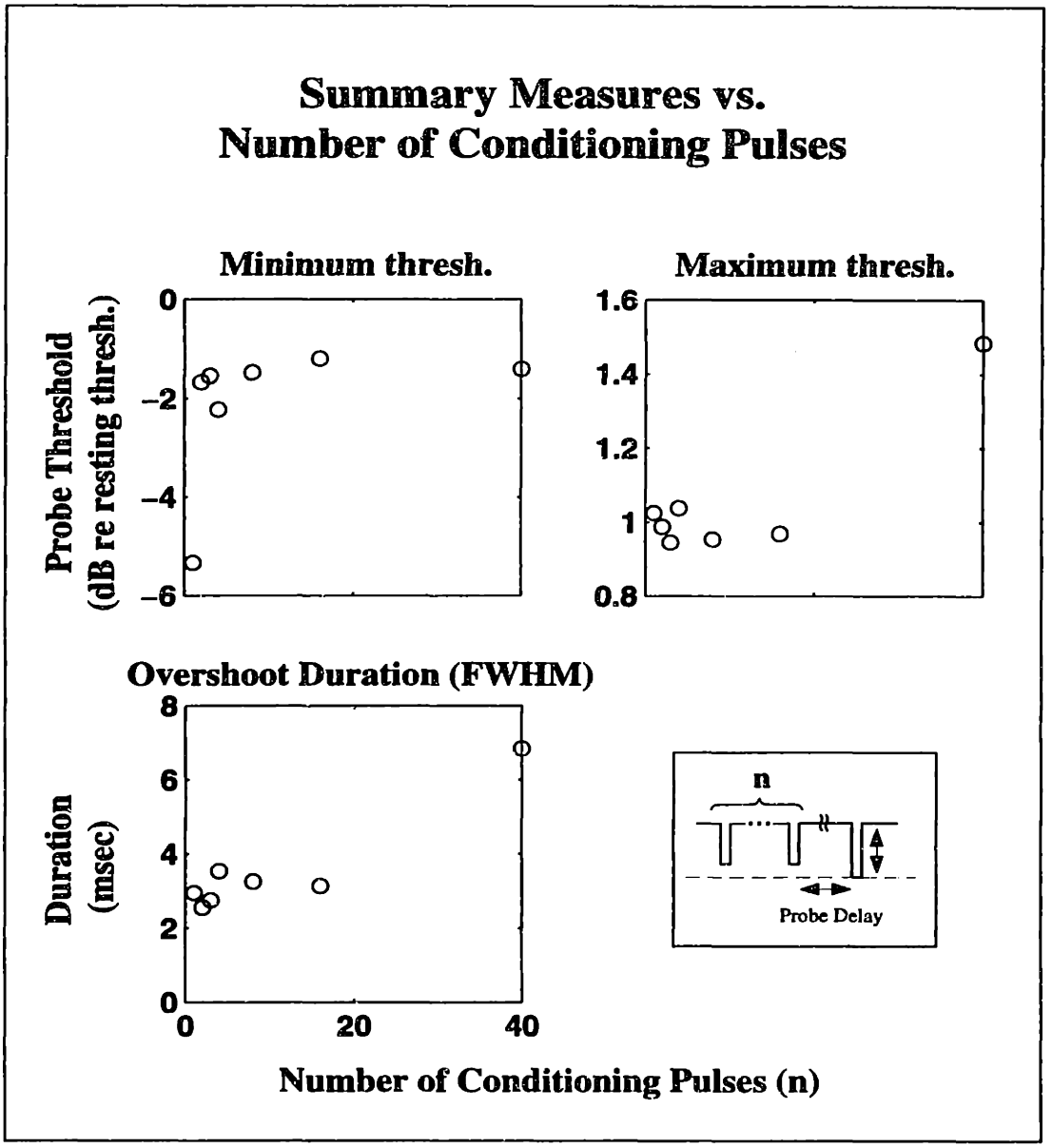

Figure 4-3: Summary measures plotted against number of pulses in subthreshold conditioners. Minimum probe threshold for short delays (upper left), maximum probe threshold (upper right), and desensitization period duration (lower left) are plotted for conditioners of 1, 2, 3, 4, 8, 16 and 40-pulse subthreshold conditioners. The majority of data for any given conditioner are from units not present for other conditioners; data are from all conditioner levels. Data are from 35 units in 4 cats.

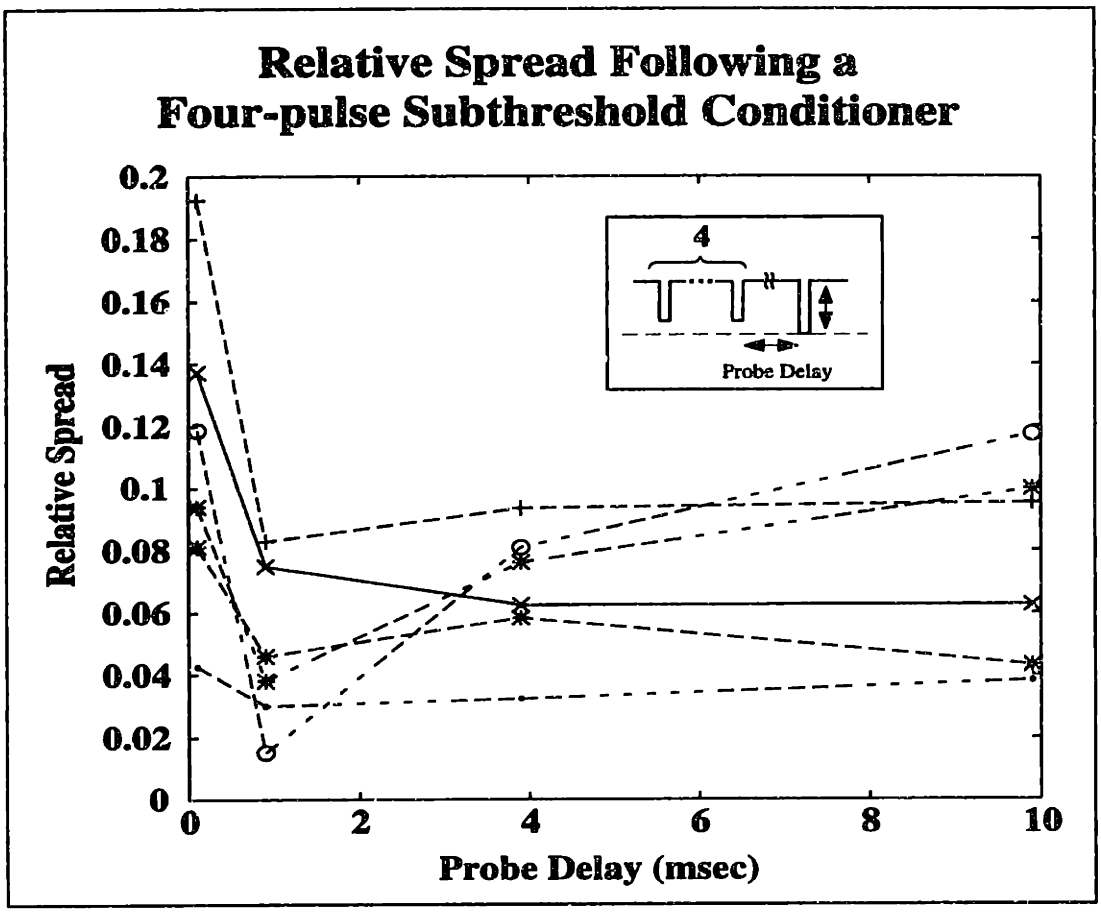

Figure 4-4: Relative spread plotted as a function of probe delay for a conditioner consisting of four subthreshold pulses. The conditioner levels range from 1.6 to 2.3 dB below the resting threshold. Each pulse in the conditioner is a 100 μsec cathodic pulse; 1 msec separates the conditioning pulses. The probe is a single 100μsec cathodic pulse. Six units are shown from three cats.

delays. The remaining two units exhibit a sharp decrease in RS from the initial delay of 100 μsec to 1 msec, followed by a marked increase at 4 msec. At a probe delay of 10 msec, the probe RS is near the resting value.

Comparing the multipulse results with the results using a single-pulse conditioner is difficult, since there is only one unit where RS data was taken using different numbers of conditioning pulses. This unit showed a decrease in RS at the initial probe delay of 100 μsec as the number of conditioning pulses increased. Comparing Figure 4-4 with Figure 3-9 indicates that the increase in RS is smaller for the four-pulse conditioner than for the single-pulse case although making quantitative comparisons is risky because of the large range in RS values for both cases. The value of the relative spread is similar for the two cases for delays of 10 msec.

4.2 Suprathreshold conditioners

Multiple-pulse suprathreshold conditioners differ from their subthreshold counterparts in that the interpulse interval is the major parameter, not the number of pulses. While it is realistic to assume there can be many closely-spaced pulses to which the nerve will not respond, it is unrealistic to assume that the nerve will respond to every such pulse of such a stimulus. Instead, the interpulse interval is varied between 2 and 10 msec, corresponding to spike discharge rates of 100 – 500 spikes/sec. The number of pulses is varied from 1 to 3 to investigate how suprathreshold temporal interactions vary with the number of preceding pulses.

Figure 4-5 plots threshold-delay curves following a suprathreshold conditioner consisting of two pulses with five different interpulse intervals. For each interpulse interval (IPI), the gross character of each curve is the same: an elevated threshold for the initial probe delay of 2 msec, followed by a monotonic decrease to the resting threshold. The threshold-delay curve following a 2 msec IPI conditioner has an initial probe threshold of 3.5 dB above the resting threshold. The threshold declines for larger delays, approaching a value about 1 dB above the resting threshold at a delay of 10 msec. The threshold-delay curves for conditioners of 3, 4, 6, and 10 msec IPIs

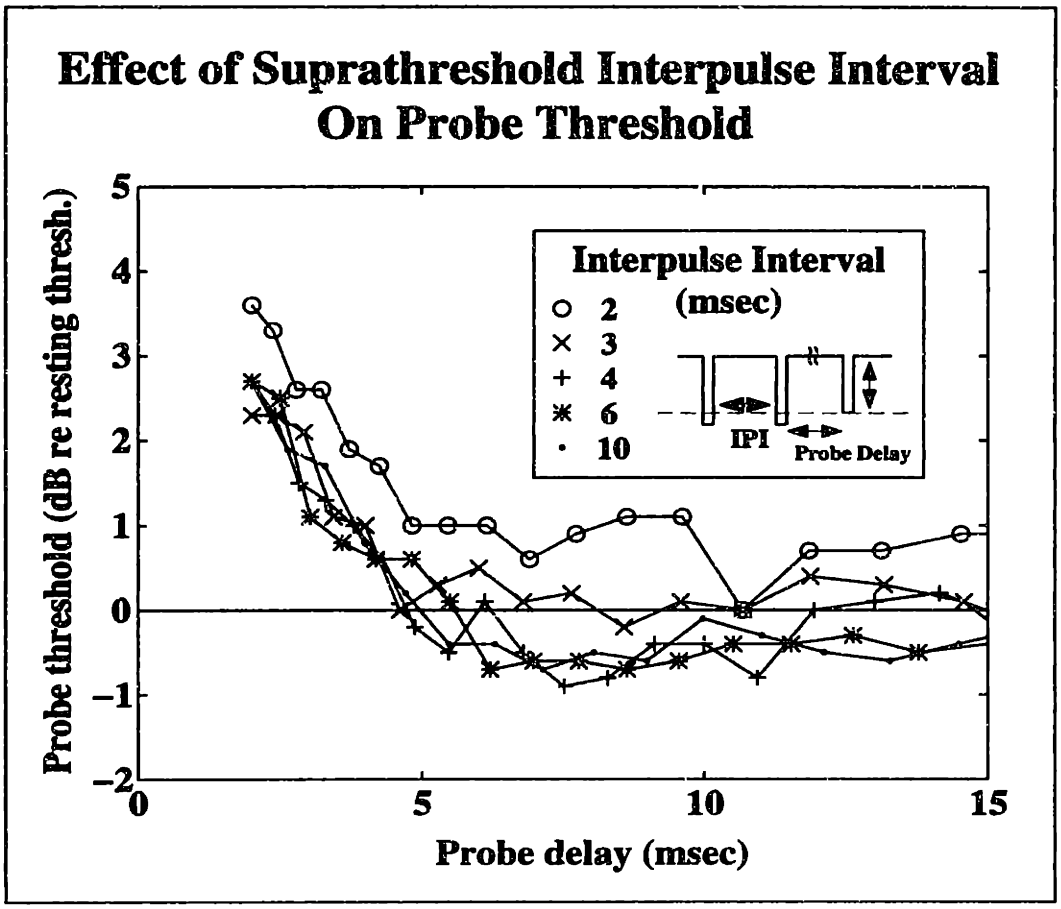

Figure 4-5: Effects of increasing the interpulse interval for a multipulse suprathreshold conditioner. Plotted is the probe threshold in dB relative to the resting threshold as a function of probe delay for five different interpulse intervals. The conditioner consists of two cathodic 100 μsec pulses with an interpulse interval indicated by the symbols. The conditioner stimulus level was sufficient to guarantee that each conditioner pulse resulted in a neural discharge. The probe was a single cathodic 100 μsec pulse.

overlay each other for delays between 2 and 5 msec; for longer delays the threshold-delay curve following the 3 msec IPI conditioner approaches the resting threshold, while the 4, 6, and 10 msec conditioner curves end about 0.5 dB below the resting threshold. Similar results were seen in another unit for which probe threshold-delay curves were obtained using a two-pulse conditioner and many different interpulse intervals, except there was no elevation of the curve for an IPI of 3 msec. All the threshold-delay curves were nearly identical.

Figure 4-6 shows recovery curves for several units from several cats following a two-pulse suprathreshold conditioner with IPIs of 2, 3, 4, 6 and 10 msec. For each panel there is a range of curves, with initial thresholds (at 2 msec delay) ranging from less than one dB to greater than 5 dB. Following this initial increase, every threshold-delay curve decreases in a monotonic fashion towards the resting threshold. Time constants for these decays, derived from exponential fits, range from 1.3 to 2 msec, with no significant correlation with IPI.

Figure 4-7 shows probe threshold-delay curves following a three-pulse conditioner; as previously, the IPI for each panel is shown in the upper right corner. Again each curve reflects the refractory properties of the neuron: an initially high threshold which decays to the resting threshold value over a period of 5 to 10 msec. The time course of the curves is indistinguishable from the two-pulse conditioner case; the range of initial probe thresholds is also similar.

From the above data, it appears that neither the number of suprathreshold conditioning pulses nor the interpulse interval has much effect on the shape of threshold-duration curves. To first order, a spike appears to reset the neural state.

4.3 Discussion

The effects exhibited above extend the results on the response of the neuron following single-pulse stimuli to the case of more complex and, from the point of view of cochlear implants, more realistic stimuli. A single conditioning pulse can have a much greater effect than multiple pulses on the subsequent neural behavior, not just for threshold

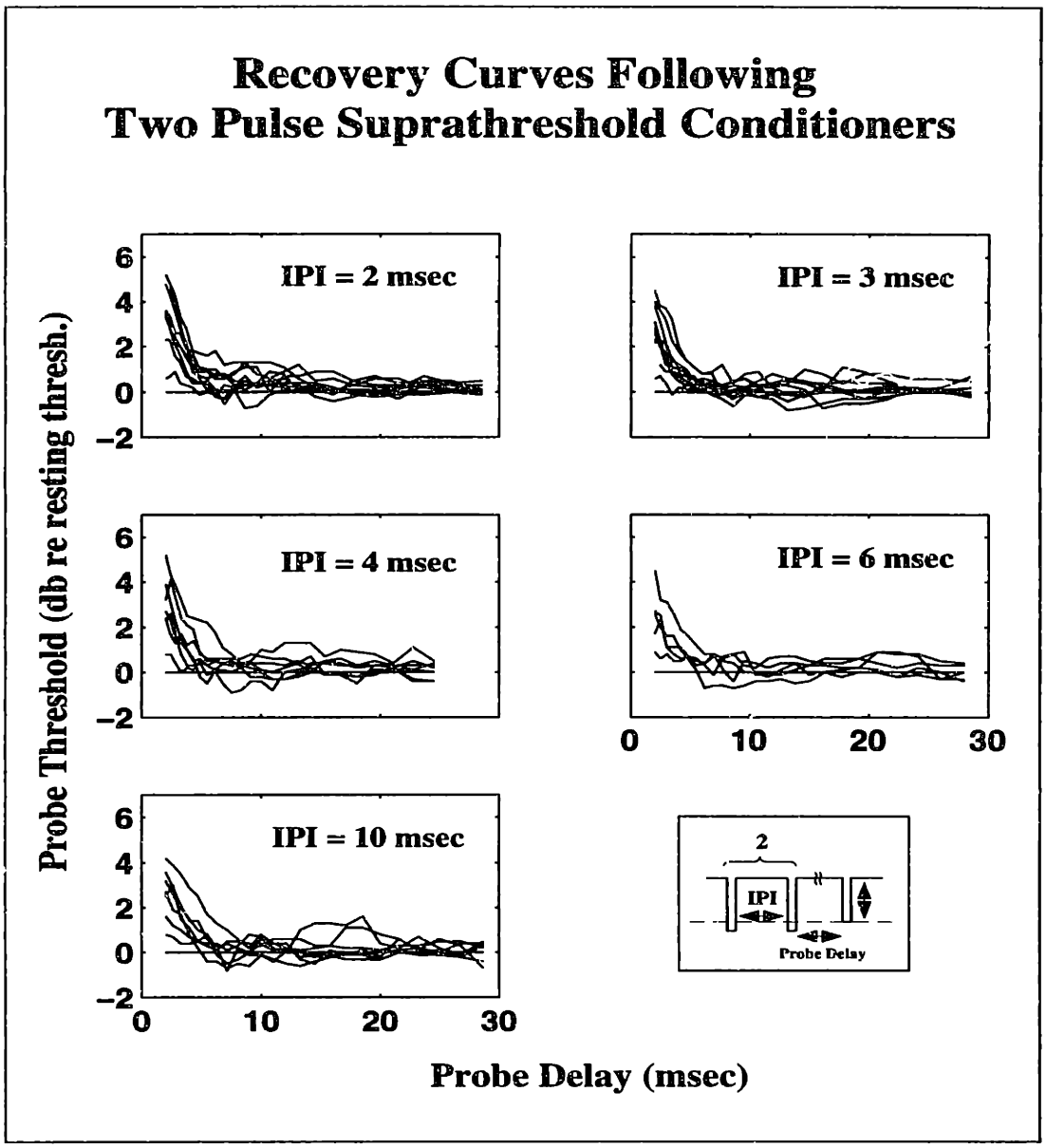

Figure 4-6: Probe threshold is plotted as a function of probe delay for suprathreshold conditioners. Each panel shows the threshold-delay curves for many units. The conditioners consist of two cathodic 100 μsec pulses with an interpulse interval indicated in each panel. The conditioner level was such that a neural spike was elicited by each conditioner pulse. The probe was a single cathodic 100 μsec pulse whose level is adjusted using the PEST algorithm as described in the methods section.

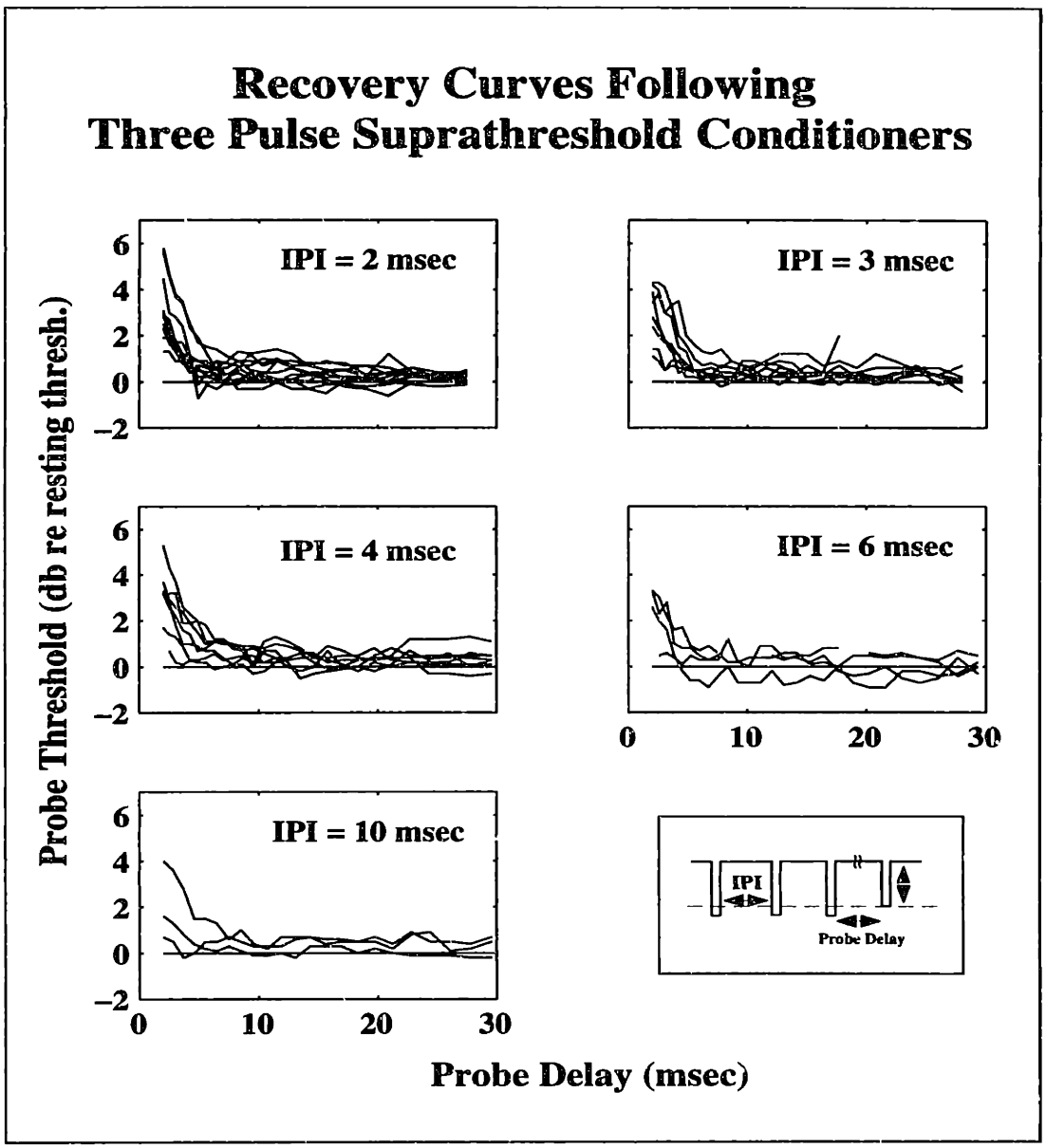

Figure 4-7: Effects of increasing the interpulse interval for a multipulse suprathreshold conditioner. Plotted is the probe threshold in dB relative to the resting threshold as a function of probe delay for five different conditioner levels. The conditioner consists of three cathodic 100 μsec pulses with an interpulse interval indicated by the symbols. The conditioner stimulus level was sufficient to guarantee that each conditioner pulse resulted in a neural discharge. The probe was a single cathodic 100 μsec pulse.

measures but also for the relative spread. While this has implications for cochlear implants, the discussion of these implications will be deferred until Chapter 6, where elements from both the experimental and modeling studies can be integrated.

4.3.1 Comparison with previous results

As far as we can determine, there is only one set of studies that has examined the issues concerning the neural response following multiple electric pulses: the studies by Raymond and others ([55], [65], [66]). The stimuli in Raymond's work were suprathreshold monophasic rectangular pulses; the pulse width was varied to increase the magnitude of the charge per pulse. The amplitude was adjusted so that the resting threshold duration was 100 μsec. Raymond's conditioning pulses were 10 msec apart, and their level was characterized as being well above threshold. Measurements were conducted in frog sciatic nerve.

In Chapter 3 it was noted that one basic characteristic of the neural response as seen by Raymond were not seen in our results: namely, the existence of a supernormal period following a single suprathreshold conditioning pulse (see Figure 3-11 for a summary of Raymond's results). When Raymond studied the neural response following several conditioning pulses, he noted that increasing the number of conditioning pulses increased the magnitude of the superexcitable and depressed phases of the neural response up to about 8 conditioning pulses ([66]). The probe delay of the maximum superexcitability was between 7 and 15 msec in Raymond's preparation. This maximum of superexcitability is within the range of delays that the present study includes.

As noted previously, no such superexcitability period is seen in our data; additionally, our data shows that increasing the number of conditioning pulses results in no discernible change in the neural response following the conditioner. The differences between our results and those of Raymond are likely not due to the experimental techniques, but are likely due to the different experimental systems (toad sciatic nerve versus cat auditory nerve). As will be seen in Chapter 5, the neural membrane models of some systems do predict that there is a period of superexcitability.

4.3.2 Comparison with Single-pulse Results

The substantial decrease in the initial sensitization resulting from increasing the number of subthreshold conditioning pulses from one to many is counterintuitive. Naively, one would expect that, if one pulse produces a certain result, more pulses would produce a bigger effect. A very simple model of the sensitization views the neural membrane as an RC circuit. The conditioner charges the membrane capacitance, lowering the probe threshold. In this model, additional conditioner pulses will never result in an increase in the probe threshold. The experimental data refute such a linear model. As will be shown in Chapter 5, nonlinear models of the neural membrane can correctly predict this trend in the probe threshold with increasing conditioner pulses.

In contrast, for the suprathreshold conditioner case, the results with many conditioning pulses are much like the single-pulse case: an initial probe threshold elevated by a few dB, and returning in a monotonic fashion to the resting threshold at a delay of about 5 msec. Conditioner levels near the resting threshold yielded initial thresholds that were higher than for stronger conditioners. Both of these effects are qualitatively simulated by nonlinear models.

Chapter 5

Model Simulations

The data presented in the previous chapters describes the neural response to one or more electrical conditioning pulses. As discussed before, the stimuli have been chosen to maximize the chances that the neural state is always measured at the same site. This was done so that the modeling work presented in this chapter could approximate this single site as a space-clamped neuron like that supposed by the HH-like models, rather than resorting to more sophisticated cable models of the complete neuron with the attendant increase in parameters and uncertainties. The line of inquiry that was followed was to see how well the simplest system could simulate the observed experimental behaviors.

Following a detailed presentation of simulations using the standard Hodgkin-Huxley model, the abilities of four additional HH-like models to simulate the experimental data are presented. Comparisons are made between models in an attempt to understand why some models provide better simulations than other models.

5.1 Models

Five different active membrane models were used: the Hodgkin-Huxley (HH) [30] of the giant squid axon, the Frankenhaeuser-Huxley (FH) [16] model of the frog sciatic nerve, the Schwarz and Eikhof (SE) [76] model of the rat sciatic nerve, the Chiu, Ritchie, Rogart and Stagg (CRRS) [7] of the rabbit sciatic nerve, and the Rothman,

Young and Manis (RYM) [69] model of the cochlear nucleus bushy cell. Except where explicitly stated, these models used the parameters set forth as compiled by Rattay and Aberham [64], with the exception of RYM, which were taken from the original work. The model parameters were adjusted to a temperature of 37 Celsius using the temperature corrections suggested by Rattay and Aberham when necessary.

The models were implemented using an explicit integration method in which the values of the state variables at the next time step were determined by calculating the change in each variable with time from the rate equations using parameter values for the current time step. The timestep used was 5 μsec in all cases; comparisons of runs with this timestep and a timestep of 1 μsec showed no detectable difference.

The response of the five models to a single suprathreshold 100-μsec pulse is shown in Figure 5-1. For each model, the three panels show the transmembrane potential (top panels), ionic currents (middle panels) and state variables (bottom panels) plotted as a function of time. Note that while all models have a sodium channel, the HH, FH, and SE models have one potassium channel, the CRRSS model has no potassium channels, and the RYM model has two: a fast and a slow potassium channel.

Model stimulus threshold levels were determined using a bisection method that would vary the stimulus level to achieve a maximum depolarization of some threshold amount. For those models which exhibited sharp threshold characteristics on the scale of the level steps that were used (0.1 dB) this threshold depolarization was determined visually. Some models exhibited a graded response where the maximum depolarization changed more gradually with stimulus level: in these cases, the threshold depolarization was taken to be the stimulus level where the maximum depolarization vs. stimulus level curve was steepest.

5.1.1 Stochastic Extension of the Hodgkin-Huxley Model

Because the deterministic nature of the studied models precludes their direct use in modeling the relative spread, a stochastic model was developed based upon the binomial statistics associated with the open/closed states of the sodium channels in the Hodgkin-Huxley model. The work of Lecar and Nossal [46], Clay and DeFe-

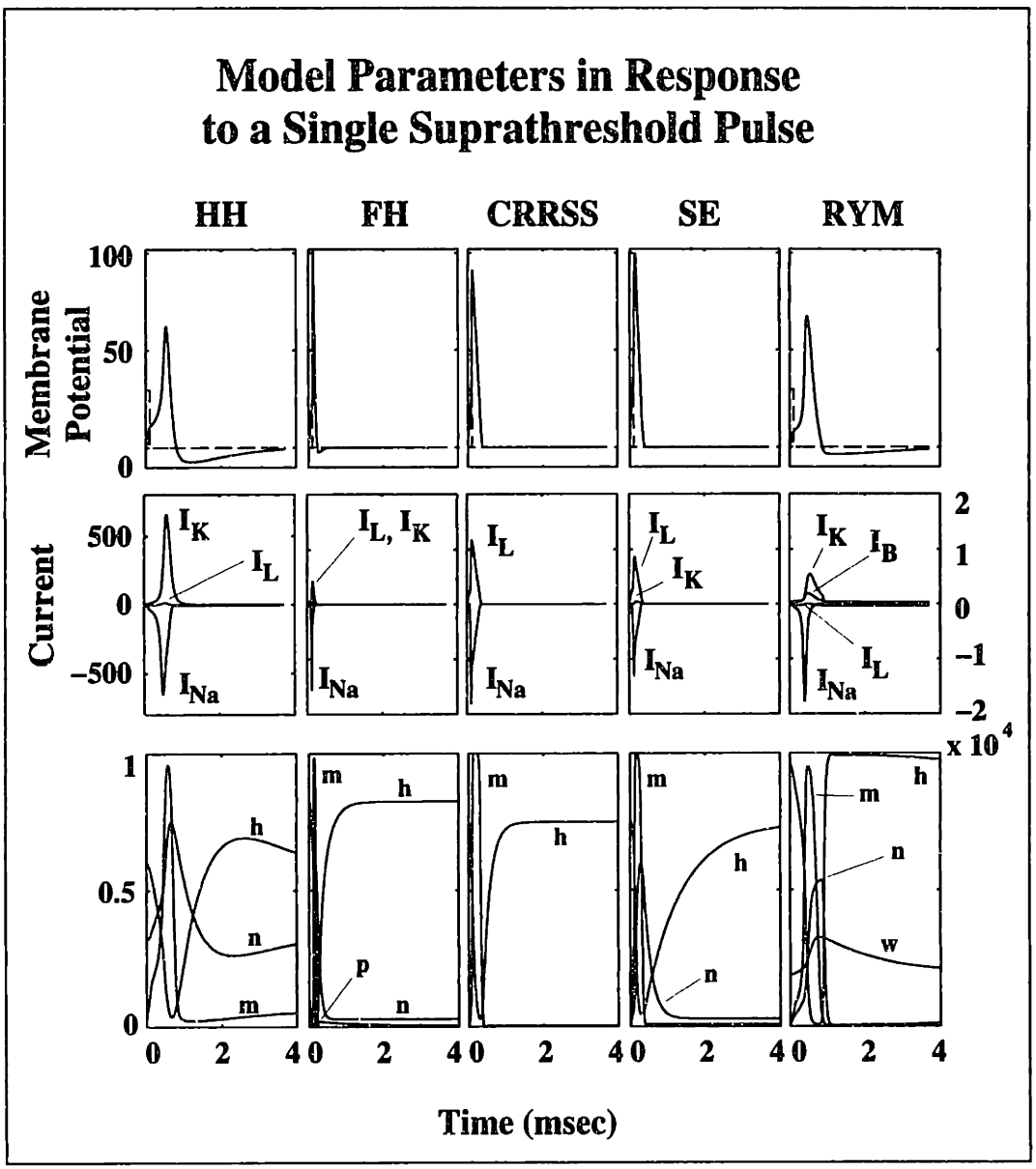

Figure 5-1: Response of models to a single suprathreshold pulse. For each of the five models examined, the transmembrane potential (top panels), ionic currents (middle panels) and state variables (bottom panels) are plotted as a function of time. The stimulus was a single 100-μsec pulse 1 dB above the resting threshold.

lice [9] and Rubinstein [72] shows that this channel noise is sufficient to explain the experimentally-observed relative spread of the neural response to a single pulse. It was reasoned that changes in the sodium channel noise following a conditioning pulse could lead to the changes seen in the relative spread. While the model of Rubinstein is explicit in the modeling of the relative spread from the underlying sodium channel noise, it is currently unable to predict the changes in the relative spread with probe delay seen experimentally (Rubinstein, pers. comm.). A much simpler model was developed using the standard deviation of the sodium channel open/close probability to estimate the relative spread.

The standard deviation of the probability that a sodium channel is open is given by the formula for the standard deviation of a binomial distribution with a probability of m^3h:

$$\sigma_{m^3h} = \sqrt{m^3h(1 - m^3h)}$$

We define the model relative spread RS_{model} to be proportional to this quantity:

$$RS_{model} \propto \sigma_{m^3h} \tag{5.1}$$

A more quantitative model would require relating the channel noise to a membrane current noise. While this is not difficult analytically, relating the noise in the transmembrane current to the noise in the threshold stimulus current, which determines the RS [illegible] more difficult, since the relationship depends critically on the exact characteristics of the sodium conductance noise. The work of Rubinstein explicitly accounts for the noise characteristics. The model described above was used instead of Rubinstein's model in keeping with the line of inquiry of seeing how well the simplest system recreates the experimental results.

To actually calculate RS_{model}, the state variables m and h controlling the sodium channel open/close probability were stored as a function of delay following a conditioning pulse. These values were used to calculate σ_{m^3h}, and RS_{model}.

5.2 Hodgkin-Huxley Model Simulations

In order to determine to what extent models employing the Hodgkin-Huxley framework can simulate the experimental results on temporal interactions, stimuli identical to those used experimentally were used to "stimulate" the classical Hodgkin-Huxley model. The only modification was to use the temperature-dependent rate coefficient corrections suggested by Rattay and Aberham [64]. As the model is used in a space-clamped manner, a stimulus pulse results in a short transmembrane current.

5.2.1 HH Subthreshold Characteristics

Figure 5-2 shows the HH model response to a single subthreshold pulse for two different levels. The top panel shows the calculated probe threshold as a function of probe delay; the conditioner level is indicated in the legend. From top to bottom, the remaining three panels plot, as a function of time, the transmembrane potential V_m, along with a representation of the stimulus; the calculated ionic currents; and the model state variables m, h, and n.

Concentrating on the -1 dB conditioner level (shown by the dotted line), the probe threshold at the initial delay of 100 μsec is about 18 dB below the resting threshold. At this delay, V_m is elevated from its resting value as a result of the conditioner pulse. The state variables m, h and n have started to react to the increase in V_m; m and n increasing, h decreasing.

This increase in m is the first step in the spike initiation process, as more sodium channels become open, leading to further depolarization. This depolarization process will continue as long as the sodium inactivation variable h does not decrease too much or the inward potassium current, controlled by the n variable, does not become too large. In Figure 5-2, the depolarization ceases at a post-stimulus time of about 0.5 msec, as is indicated by the zero slope of the V_m-time curve. At this point, the inward sodium current is balanced by outward potassium and leak currents. The peak sodium current occurs slightly earlier than the peak depolarization, while the peak potassium current occurs later as the neuron is repolarized.

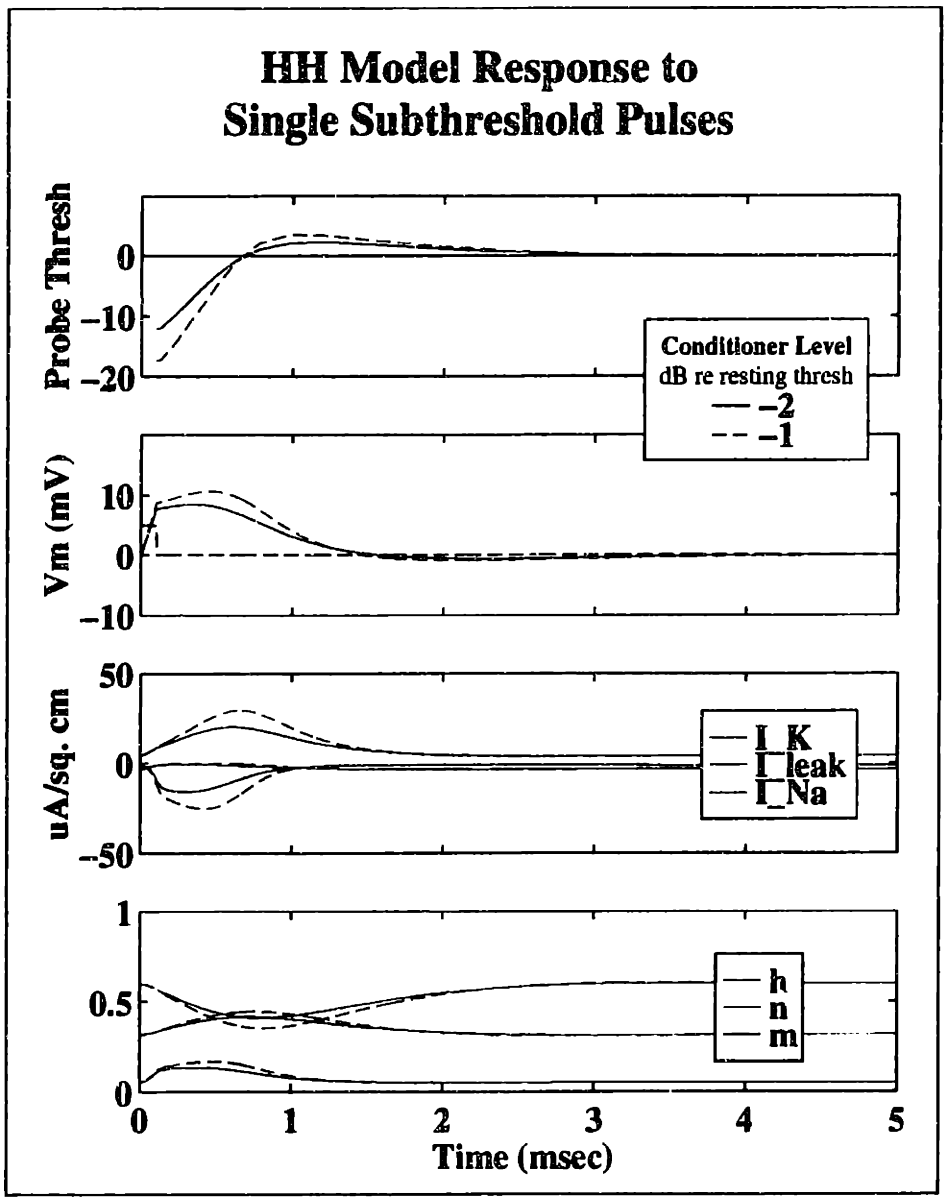

Figure 5-2: HH model response to a single conditioning pulse of two subthreshold levels. Four measures of the response of the HH model to a single subthreshold 100-μsec cathodic pulse: the threshold-delay curve (top panel), the transmembrane potential (upper middle panel), the ionic currents (lower middle panel), and the state variables m, n, and h. The conditioner level is either -1 or -2 dB below the resting threshold as is indicated in the legend in the top panel. The conditioner is indicated by the dashed line in the second panel. The probe pulse used to determine the threshold-delay curve was a single 100-μsec cathodic pulse. If the color labels are missing, refer to Figure 5-1 for the identities of the individual curves.

Even though the nerve is being repolarized, the probe threshold is still lower than the resting threshold: this is a consequence of V_m and m being above their resting values. When the probe threshold is equal to the resting value at a delay of roughly 0.7 msec, the state variables are far from their resting values. The following desensitizing effect is due to the increased value of the n variable, resulting in an outward flow of current, and the decreased value of the h variable, resulting in a greater inactivation of sodium channels.

The effects of increasing the conditioner level are seen by comparing the dotted and solid lines in Figure 5-2: as the conditioner level goes from -1 to -2 dB below the resting threshold, the initial threshold goes from -18 to -12 dB below the resting threshold. This is due mainly to a smaller increase in m and V_m. The desensitization effect is smaller also: this is due to smaller changes in h and n from their resting values.

Both the sensitizing and desensitizing phases seen experimentally are present in this simulation. Additionally, trends in the initial probe threshold with changes in the conditioner level are the same for the model and experimental data.

5.2.2 Multiple Subthreshold Pulses

There are distinct changes in both the model simulations and the experimental data as the number of conditioning pulses increases from one to four — most notably the initial sensitizing effect is much weaker for multiple conditioning pulses. Figure 5-3 displays the membrane potential, the ionic currents and the state variables for the HH model following a subthreshold four-pulse conditioner. The values of the state variables m, h, n, and V_m following the first pulse are markedly different from their values following the fourth pulse; the amplitudes of the variables show a complex pattern as a function of the pulse number.

Examining the effects these different initial conditions have on the threshold-delay curves of the HH model, Figure 5-4 plots HH model responses for both a single and a four-pulse subthreshold conditioner. The change in the initial threshold of the threshold-delay curve is about 8 dB; the higher threshold for the multiple pulses

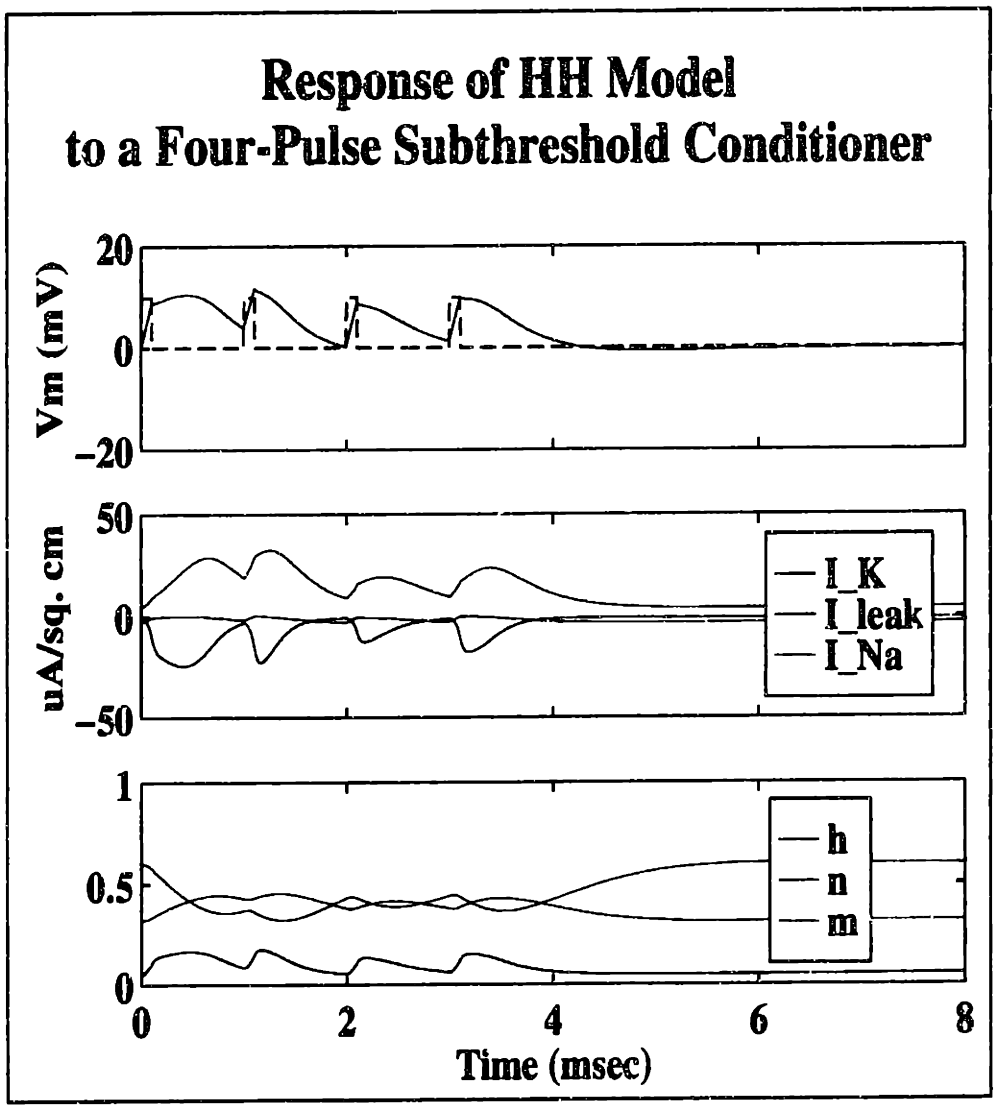

Figure 5-3: Response of the HH model to a four-pulse subthreshold conditioner. The three panels show the change in the transmembrane potential V_m; the ionic currents, and the state variables m, h, and n as a function of time. Comparison of this figure with Figure 1-8 reveals that the state variables (m, h, n, and V_m) after the fourth pulse are much different than after a single pulse. The conditioner consisted of four 100-μsec cathodic pulses 1 dB below the resting threshold presented 1 msec apart, represented by the dashed line in the top panel. If the color labels are missing, refer to Figure 5-1 for the identities of the individual curves.

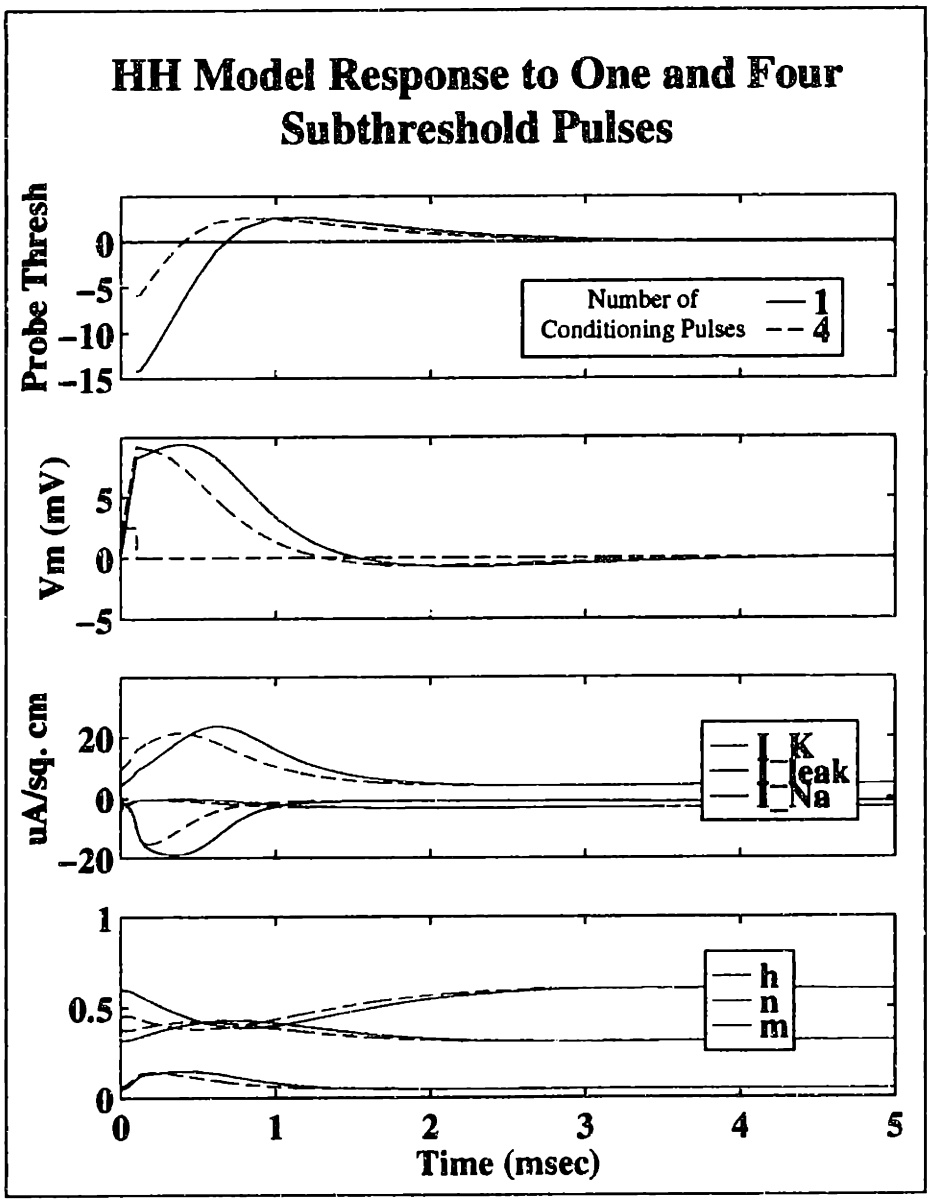

Figure 5-4: Response of the HH model to a one- and four-pulse subthreshold conditioner. The four panels display the threshold-delay curves, V_m, the ionic currents, and the state variables as a function of time since the onset of the last conditioning pulse, which is represented by the dashed line in the second panel. The conditioner consisted of either one or four 100-μsec cathodic pulses 1.5 dB below the resting threshold presented 1 msec apart. The probe was a single 100-μsec cathodic pulse. If the color labels are missing, refer to Figure 5-1 for the identities of the individual curves.

result from a decrease in the initial h and an increase in the initial n values following the fourth conditioner as compared to those following the first conditioner.

The decrease in the sensitization of the model simulation following a four-pulse subthreshold conditioner is consistent with that seen in the experimental data.

5.2.3 HH Suprathreshold Characteristics

Figure 5-5 plots the response of the HH model to a single suprathreshold conditioning pulse at two different levels: 1 and 3 dB above the resting threshold. To facilitate comparison with the experimental data, the threshold-delay curve shown in the top panel starts at a probe delay of 2 msec. At this initial delay, the probe threshold is about 2 dB above the resting threshold. This threshold elevation is due entirely to the decrease in the sodium activation variable m; the h variable is higher than the resting value and the n variable is lower that its resting value, both of which tend to lower the probe threshold, the opposite of what is observed.

As the transmembrane potential V_m returns to its resting value, the sodium activation variable m increases. As the inactivation variable h changes more slowly than the m variable, there is a short period of sensitization. This is the same mechanism that is responsible for anodic break excitation described by Rattay and Aberham [64].

Comparing the two conditioner levels plotted in the top figure of Figure 5-5 shows that increasing the conditioner level results in a slight decrease of the probe threshold at a delay of 2 msec. This is a result of the earlier initiation of the spike due to the increased stimulus level, which results in the value of the h variable being greater at the 2 msec delay for the higher stimulus level. As the m and n variables are virtually identical for both stimuli, the initial probe threshold is lower for the higher conditioner.

The model results are consistent with those seen experimentally.

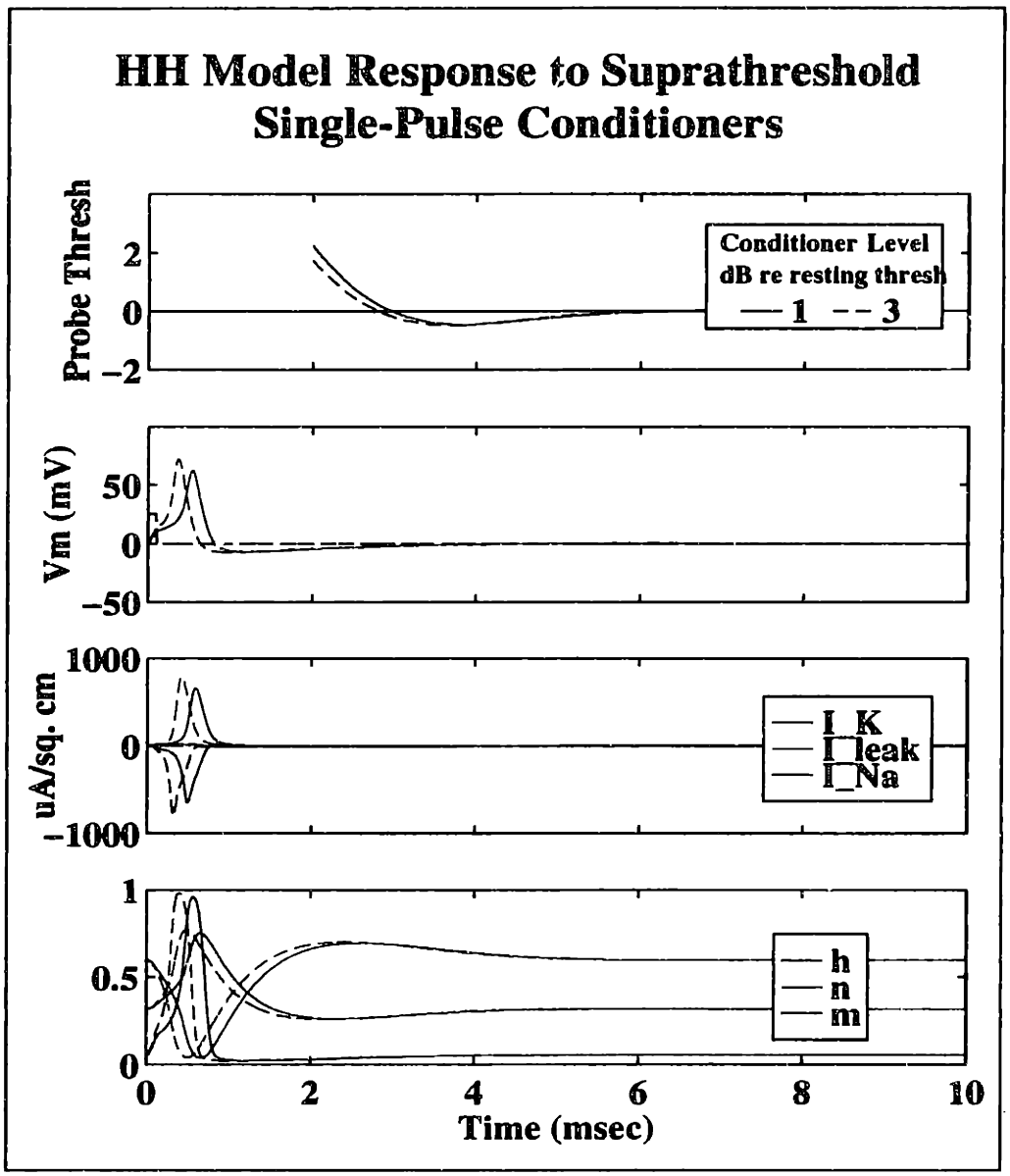

Figure 5-5: HH model simulation of a single suprathreshold conditioning pulse of two levels. The top panels plots the probe threshold as a function of probe delay The remaining panels show, as a function of post-stimulus time, the transmembrane potential, the ionic currents, and the state variables h, n, and m. The conditioner was a single 100-μsec cathodic pulse 1 or 3 dB above the resting threshold, and is represented by the dashed line in the second panel. The probe used in the top panel was a single 100-μsec cathodic pulse. If the color labels are missing, refer to Figure 5-1 for the identities of the individual curves.

Multiple Suprathreshold Pulses

In contrast to the subthreshold case, increasing the number of suprathreshold conditioning pulses has no significant effect on the experimental or model probe threshold-delay curves. Figure 5-6 shows the response of the HH model to a suprathreshold

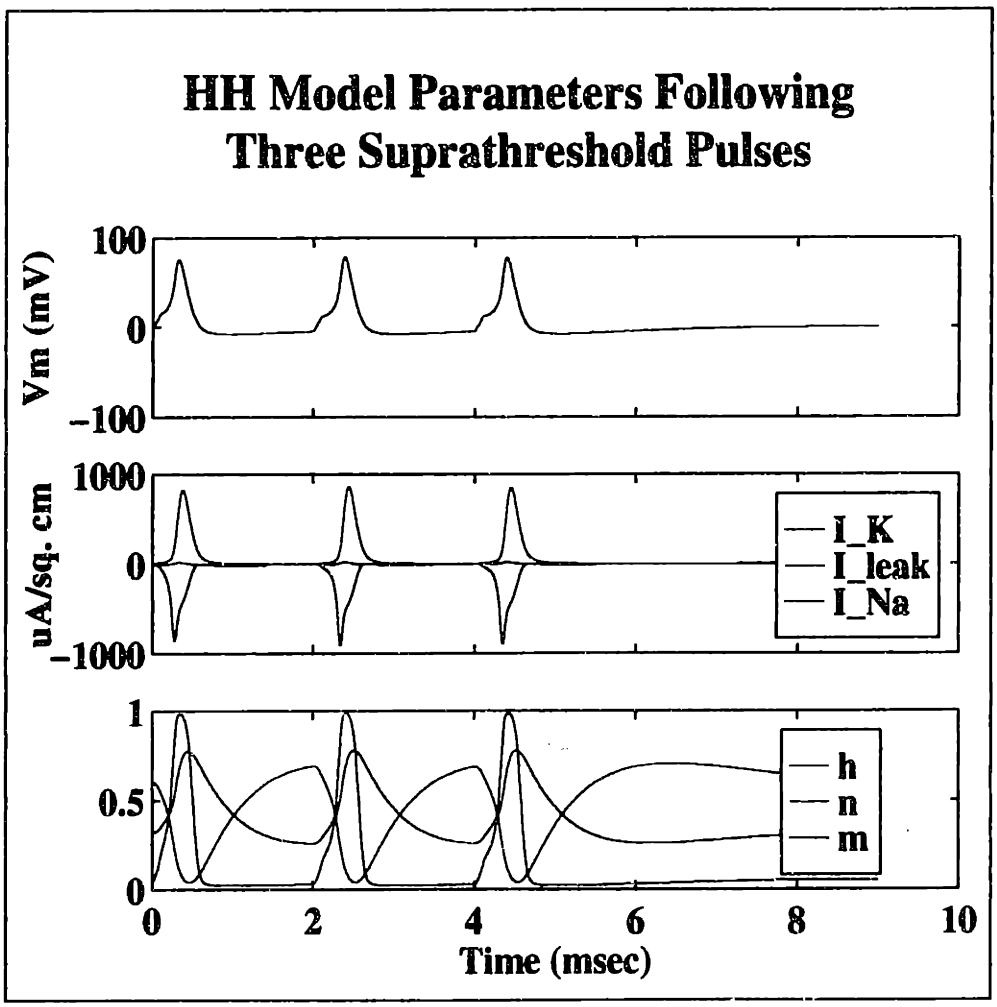

Figure 5-6: HH model response to three suprathreshold pulses of two msec interpulse interval. From the top, the panels show plotted as a function of time the transmembrane potential and stimulus (dotted lines); the ionic currents; and the state variables m, h, and n. The stimulus pulses were 100 μsec cathodic pulses 4 dB above the resting threshold. If the color labels are missing, refer to Figure 5-1 for the identities of the individual curves.

stimulus consisting of 3 pulses 2 msec apart. The course of the state variables m, h, and n are almost identical following each of the neural spikes — this would result in the observed invariance of threshold-delay curves following one and three suprathresh-

old conditioning pulses. It is common to regard a neural spike as 'resetting' the neural membrane, erasing all memory of previous stimuli and responses.

5.2.4 Relative Spread

The stochastic version of the Hodgkin-Huxley model described on page 78 was used to simulate the change in RS for sub- and suprathreshold conditioners. The results of this model are shown in Figure 5-7, which plots the model RS as a function of time following sub- and suprathreshold pulses. The model RS is normalized so that the model and experimental RS are the same for the longest delay. The experimental RS from a single unit for the given conditioner is plotted underneath.

For the subthreshold conditioner (top panels) the model RS for short delays is much larger than the model RS value at longer delays, as is the case with the experimental data shown in the panel underneath. The time course for the experimental and model RS differ in that the model RS remains elevated to longer probe delays than the experimental RS.

The suprathreshold conditioner gives rise to a model RS that is lower than the resting value for short delays, as is seen in the experimental data. There is again a discrepancy in the delay at which the model and experimental RS depart from their resting values; the model RS shows a change at a later probe delay than the model RS. For the shortest delays, the model RS increases very rapidly with decreasing delay.

Overall, the model RS qualitatively predicts the change in the relative spread with probe delay seen experimentally following both sub- and suprathreshold conditioners.

5.2.5 Summary of Hodgkin-Huxley Simulations

The Hodgkin-Huxley model was used to simulate the neural response to the stimuli used experimentally. For both sub- and suprathreshold conditioners, the model qualitatively predicts the threshold-duration curves seen experimentally. Additionally, the trend of probe threshold with changes in conditioner level and number of conditioning

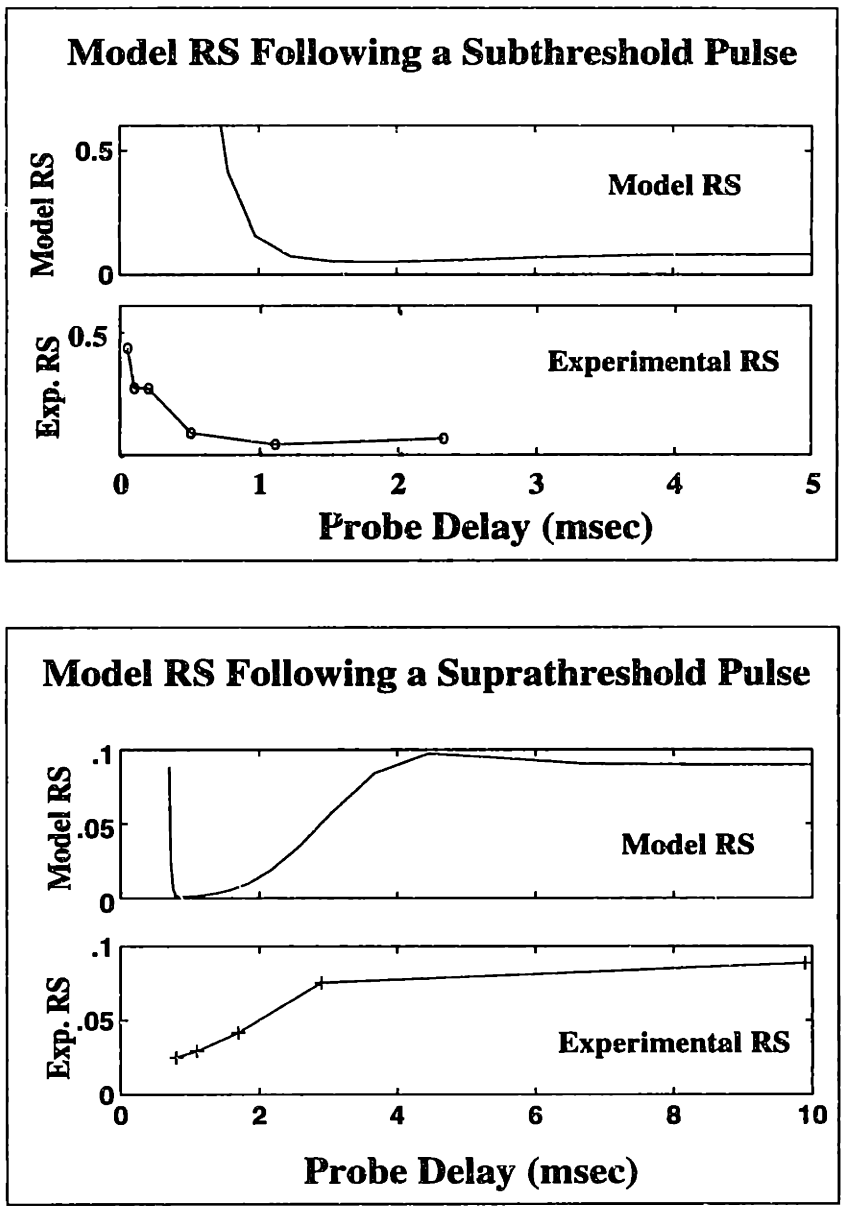

Figure 5-7: Results of a model for the relative spread using the noise of the sodium channel open/close states. The top panel plots the calculated standard deviation in the open probability m^3h as a function of time following a single subthreshold conditioning pulse. The experimental RS is plotted underneath. The model RS values are normalized so the model and experimental RS are the same at the longest delay. The bottom panels show similar results following a single suprathreshold pulse. Conditioner and probe were 100-μsec cathodic pulses, and the conditioner level was 1.5 dB above or below the resting threshold.

pulses are successfully simulated by the HH model. With stochastic extensions, the HH model also qualitatively predicts the changes in relative spread with probe delay for both sub- and suprathreshold conditioners. We conclude that existing models of the neural membrane are capable of simulating the temporal interactions observed experimentally.

5 Comparison of Model and Experimental Data

In the previous section it was shown that the Hodgkin-Huxley model of the squid giant axon can qualitatively predict the temporal interactions seen in auditory nerve fibers. There are models of other systems that might be expected to provide more accurate simulations, since the HH model applies to an unmyelinated fiber in an invertebrate, while our experimental system is a mammalian myelinated fiber, and models exist for such a system. To determine which of the five models provides the best simulation of the experimental data, comparisons were made between the model data and the experimental data.

5.3.1 Subthreshold Simulations

Figure 5-8 shows threshold-delay curves as calculated by the five models with a conditioner level 1.5 dB below the resting threshold as well as an average of experimental threshold-delay curves taken from data whose conditioner levels range from -1 to -2 dB. At this particular level, the mean data curves show a minimum initial threshold for short delays almost 5 dB below the resting threshold. The desensitization period lasts from about 0.75 msec to roughly 5 msec; the maximum threshold is about 0.7 dB above the resting threshold.

The HH model shows a sensitization period with a minimum threshold almost 15 dB below the resting threshold, followed by a maximum threshold of greater than 2 dB during the following period of desensitization, which lasts from 0.5 msec to 3 msec. The RYM model shows a similar threshold-delay curve, except the duration of the desensitization is shorter, lasting from 0.5 to 1 msec.

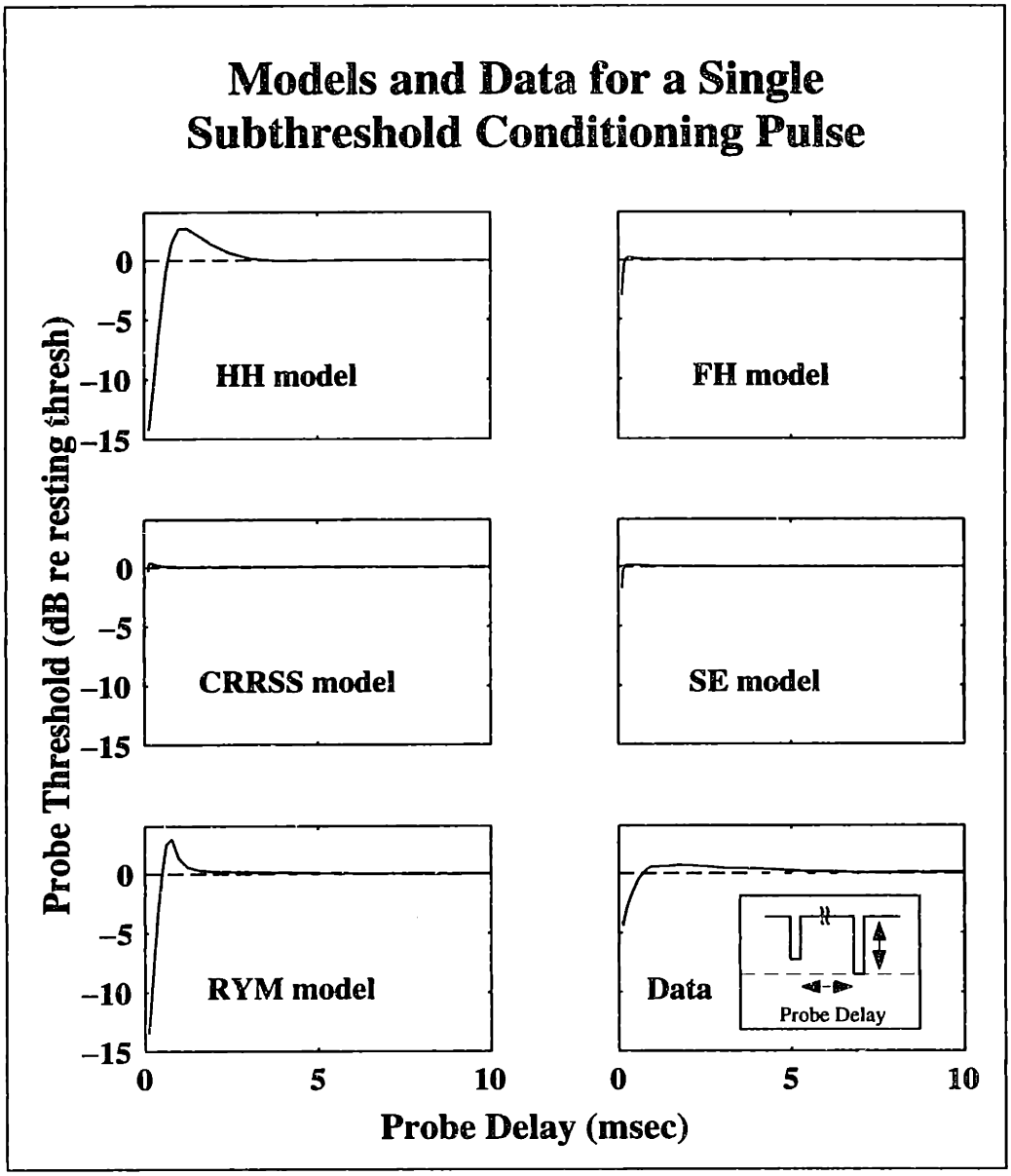

Figure 5-8: Model simulations and data for a single subthreshold conditioning pulse. Plotted as a function of delay is the probe threshold-delay curve as calculated by five models and as determined experimentally (lower right panel). The conditioner level for the models is 1.5 B below the model resting threshold; the curve given for the data represents an average of all data with conditioner levels 1 – 2 dB below resting threshold (18 units from 4 cats). Both conditioner and probe pulses were single cathodic 100 μsec pulses.

The FH model shows a minimum threshold for short delays of 3 dB below the resting threshold. The desensitization period is small and short, with a maximum threshold of 0.25 dB, and lasting from 0.3 to 0.7 msec. Similarly, the CRRSS model shows almost no decrease in the probe threshold (< 0.7 dB), and a small (0.4 dB), short (0.1 – 0.7 msec) desensitization period. Last, the SE model shows a modest minimum threshold (about -2 dB), but almost no desensitization (< .2 dB) and lasting from 0.2 to 1.5 msec.

Of the five models, only the HH and RYM models show magnitudes and time course which are similar to the experimental data. The SE and CRRSS models show very small, fast effects, while the FH model falls in between.

Dependence on Conditioner Level

Figure 5-9 plots the minimum probe threshold for short delays as a function of conditioner level as calculated by the five models as well as determined from experimental cat data. The data (lower right panel) show a decrease of 1 to 5 dB for this measure as the conditioner level increases from 2 to 1 dB below the resting threshold. Of the six units shown, four exhibit sharp decreases (3–6 dB) in the minimum threshold for a 1–1.5 dB increase in the conditioner level. The average value for the minimum threshold measure during the sensitization period is roughly 5 dB below the resting threshold for a conditioner level of -2 dB re the resting threshold.

Both the HH and RYM models give minimum thresholds that are at least 12 dB below the resting threshold for conditioner levels of -2 dB re the resting threshold; the slope of these curves indicate that an increase in the conditioner level from -4 to -2 dB results in a 5 dB decrease in the minimum threshold. The FH and SE models calculate a minimum threshold of -2.5 dB for a conditioner level of -2 dB; as the conditioner level increases towards the resting threshold, the minimum threshold decreases to about 6 dB below the resting threshold. The CRRSS model shows a slight decline in the minimum threshold, going from near resting threshold for a conditioner of -2 dB to -2 dB at a conditioner level of -0.5 dB.

Figure 5-10 plots the maximum probe threshold during the desensitization period

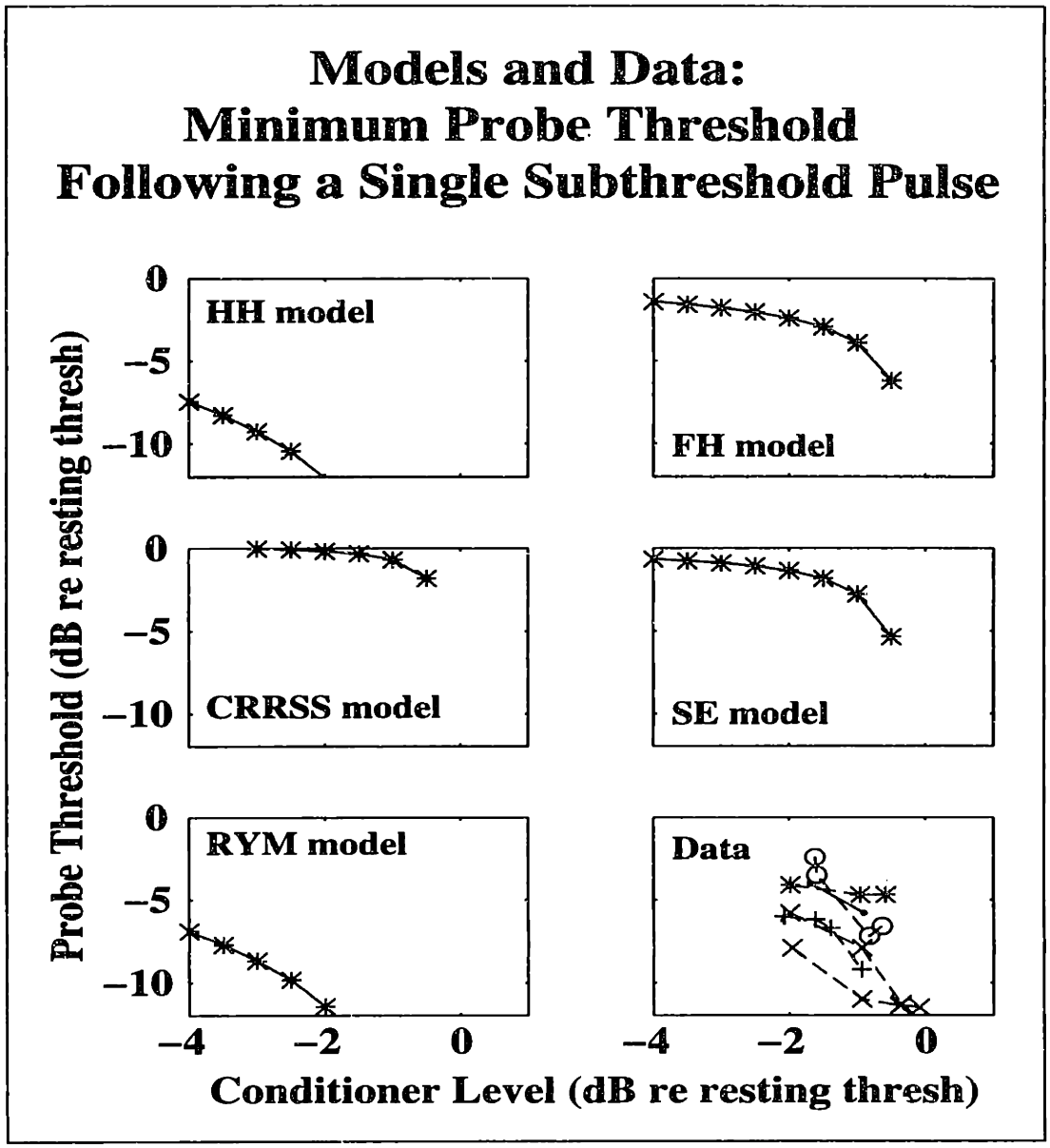

Figure 5-9: Model and data minimum initial thresholds following a single subthreshold pulse of different levels. Five models were used to calculate threshold-delay curves for several subthreshold conditioner levels; the minimum probe threshold for those curves is plotted as a function of the conditioner level. The same plot showing data from cat is in the lower right panel. Both conditioner and probe stimuli were single 100-μsec cathodic pulses.

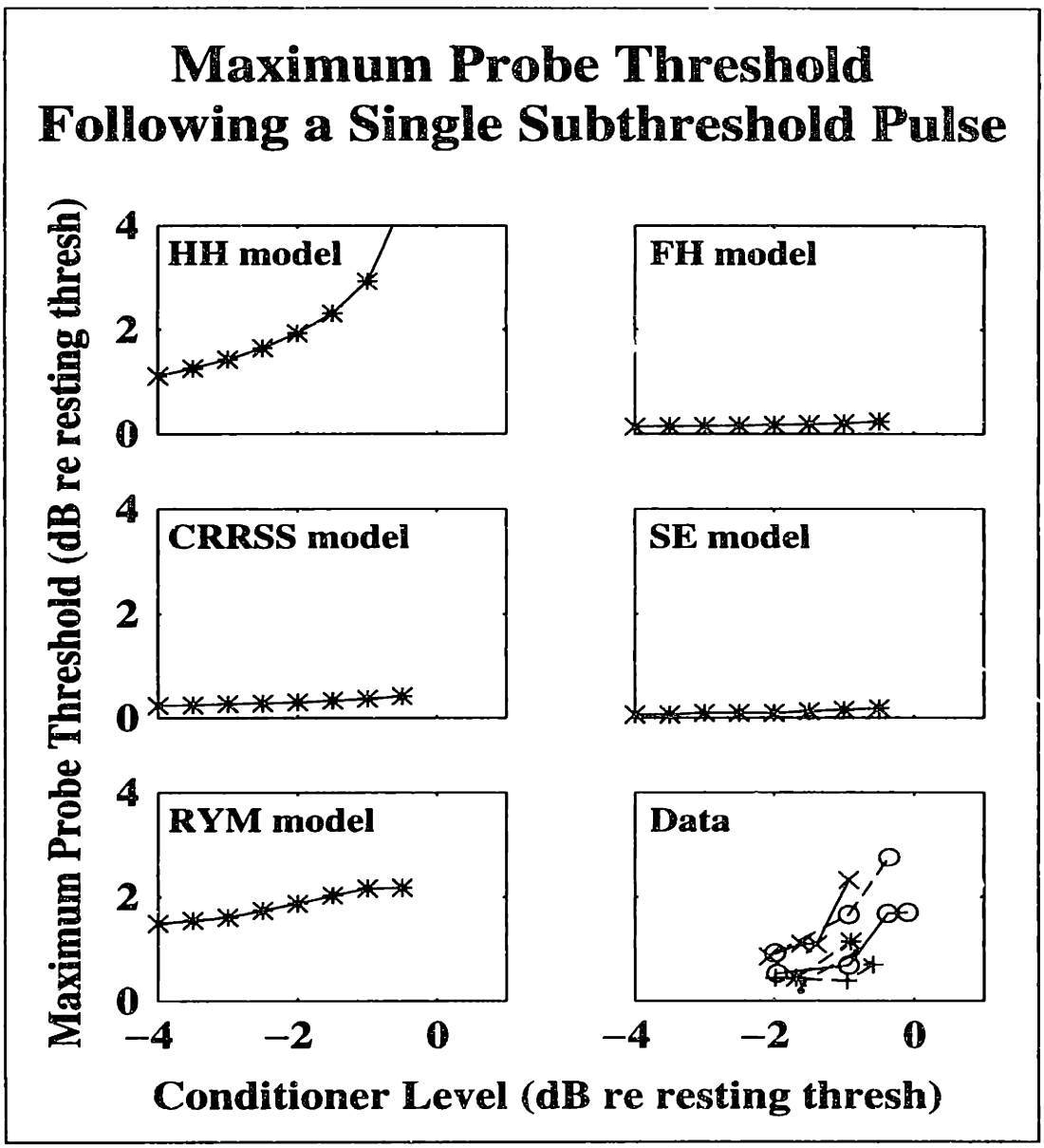

Figure 5-10: Model and data maximum probe thresholds following a single subthreshold conditioning pulse. The maximum threshold during the desensitization period as calculated using five models and determined experimentally is plotted as a function of conditioner level. The cat data, shown in the lower right panel, is the same shown in Figure 3-4. In all cases, the conditioner and probe were single 100 μsec cathodic pulses.

for a single subthreshold conditioner as a function of probe level. The calculated thresholds from five models are shown as well as experimental data (lower right panel).

The experimental data shows maximum probe threshold values of 0.5–1 dB above resting threshold for a conditioner level of -2 dB. As the conditioner level increases, there is a sharp increase in the maximum threshold, with an average value of about 1 dB for a conditioner level of -1 dB, and increasing an additional dB for conditioner levels 0.5 dB below the resting threshold.

Only the HH and RYM models show a significant change in the maximum probe threshold with increasing conditioner levels. For a conditioner level of -2 dB, both the HH and RYM models show a maximum threshold of about 2 dB. As the conditioner level increases to 1 dB below the resting threshold, the HH model shows an increase in the maximum threshold to about 3 dB, while the RYM model shows an increase of roughly a quarter dB. As the conditioner level increases towards threshold, the HH model shows a strong increase in the maximum threshold, while the RYM model seems to saturate at the level of the -1 dB conditioner level.

The FH, CRRSS, and SE models show maximum probe threshold values lower than most of the experimental data, and almost no increase in the maximum threshold value as the conditioner level increases towards threshold.

To summarize the modeling results for a single subthreshold pulse: the HH and RYM models show sensitization and desensitization periods which most closely resemble the experimental data; the dependence of the the magnitude of these effects on the conditioner level is best simulated by the HH and RYM models for the sensitization period, and the HH model for the desensitization period.

Model Simulations of Multi-Pulse Subthreshold Conditioners

The experimental data shows that the magnitude of the sensitization decreases for multi-pulse conditioners. Is this reflected in the model simulations?

Figure 5-11 plots model and experimental threshold-delay curves following a four-pulse subthreshold conditioner. The experimental data, shown in the lower right panel, resembles that of the single-pulse conditioner case, except the minimum initial

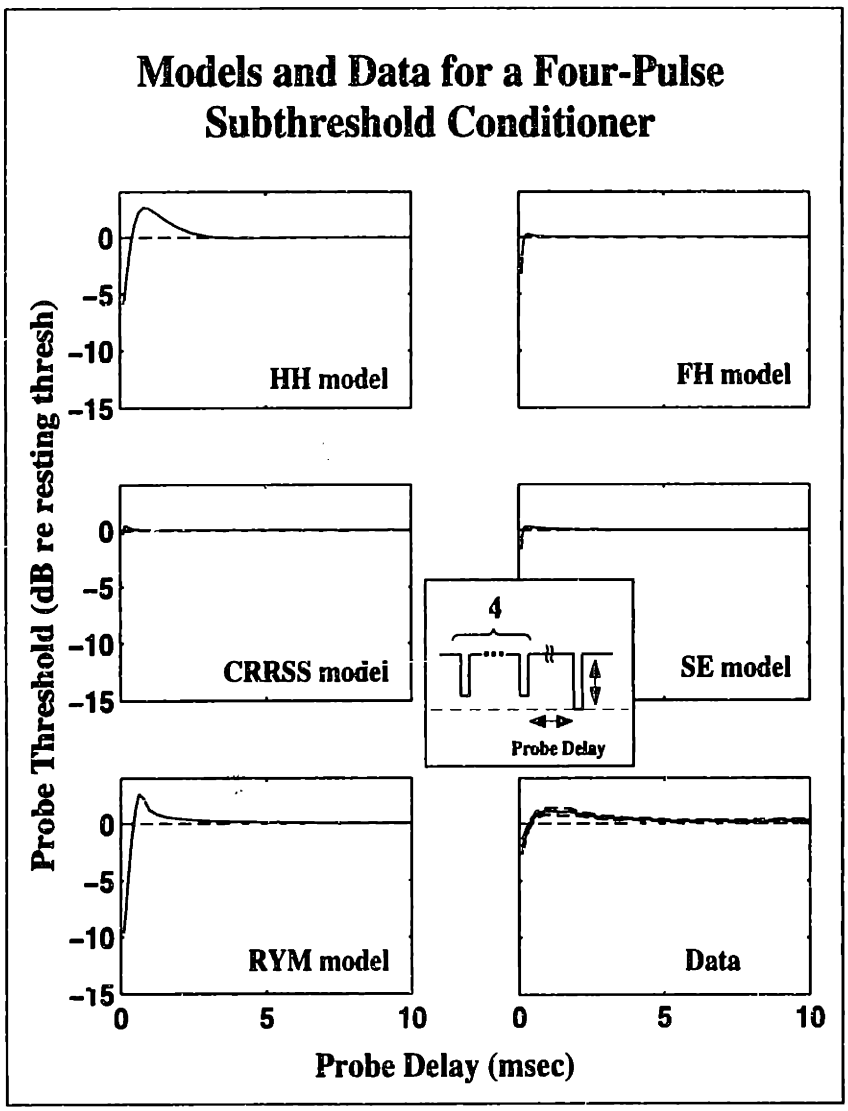

Figure 5-11: Model simulations and data for a single four-pulse subthreshold conditioner. Plotted as a function of delay is the probe threshold-delay curve as calculated by five models and as determined experimentally (lower right panel). The conditioner level for the models is 1.5 dB below the model resting threshold; the curve given for the data represents an average of all data with conditioner levels 1 – 2 dB below resting threshold (12 units from 4 cats). Both conditioner and probe pulses were single cathodic 100 μsec pulses.

threshold is only 2 dB below the resting threshold, compared to 5 dB with the single-pulse conditioner. Also, the average curves show that the magnitude of the maximum threshold during the desensitization period is slightly elevated.

Only the HH and RYM models show a large decrease in the sensitization effect going from the one- to four-pulse case, with the HH model minimum threshold increasing from -14 dB to -6 dB, and the RYM model showing an increase from -13 to -9 dB relative to the resting threshold. During the desensitization period the maximum thresholds for these models remains constant or decreases slightly.

Both the CRRSS and the FH models show a decrease in the minimum threshold and an increase in the maximum threshold as the number of conditioning pulses increases from 1 to 4, the opposite of the trend seen in the experimental data. The magnitude of these effects is a small fraction of a dB. The SE model shows the same threshold-delay curve for both conditioners.

On the basis of how the models track the changes associated with increasing the number of conditioning pulses, only the HH and RYM models offer plausible simulations of the effects seen in the data.

Based on the changes in the model simulations going from one to a four-pulse subthreshold conditioner, the HH model simulation comes closest to matching the changes seen in the experimental data, with the sign of the change in the maximum and minimum probe threshold changes being consistent with the data, and the ratio of the change in these measures being more like the experimental data than the RYM model, which also shows changes in the same direction as the experimental data. The CRRSS and FH models show changes in the magnitudes of these measures with increasing conditioner level that are opposite those seen experimentally; the SE model seems insensitive to the number of conditioning pulses for the probe delays and conditioner levels examined.

5.3.2 Suprathreshold Simulations

One of the more intriguing features of the experimental data was the lack of variation of threshold-delay curves for suprathreshold stimuli. As was shown in Figure 4-6

and Figure 4-7, the shape of the threshold-delay curves varies little as the number of suprathreshold conditioning pulses and the interpulse interval is varied. Do the models show this same insensitivity?

Figure 5-12 plots threshold-delay curves resulting from simulations using the five models as well as experimental data following a conditioner consisting of a single suprathreshold pulse. The conditioner level used for the models was 1.5 dB above the resting threshold; the lower right panel shows the average of experimental data for conditioners 1–2 dB above the resting threshold. The experimental data, shown in the lower right panel, have an initial probe threshold, taken at a delay of 2 msec, of about 3 dB above the resting threshold. The probe threshold then decreases monotonically to a value which is about two standard errors below the resting threshold, with the probe threshold approximating the resting threshold at a delay of roughly 5 msec.

Both the HH and RYM model show a probe threshold increase comparable to that of the experimental data; the initial threshold for the HH model is about 2 dB. For the HH model, this initial desensitization is followed by a short period of sensitization lasting from 3 to 6 msec; the probe threshold decreases to a level of about 0.5 dB below the resting threshold. The RYM model shows a desensitization period that matches the experimental data quite closely; there is no following sensitization period.

While the SE model shows a very small ($\approx$ 0.5 dB) increase in the probe threshold at the initial probe delay, the FH and CRRSS models show no period of desensitization for the delays studied.

While modeling studies were conducted for each suprathreshold stimuli used in collecting experimental data (2 and 3 pulses with interpulse intervals of 2, 3, 4, 6 and 10 msec), the changes in the threshold-delay curves were very slight, and only the most extreme case, three pulses with an interpulse interval of 2 msec, will be shown.

Figure 5-13 plots threshold-delay functions for the five models as well as an average of experimental data following a conditioner consisting of 3 pulses 2 msec apart. The conditioner level for the models was 4 dB above the resting threshold; the lower right panel shows the average of experimental data for which the conditioner level was 3–5 dB above the resting threshold. Comparing the experimental data with the single-

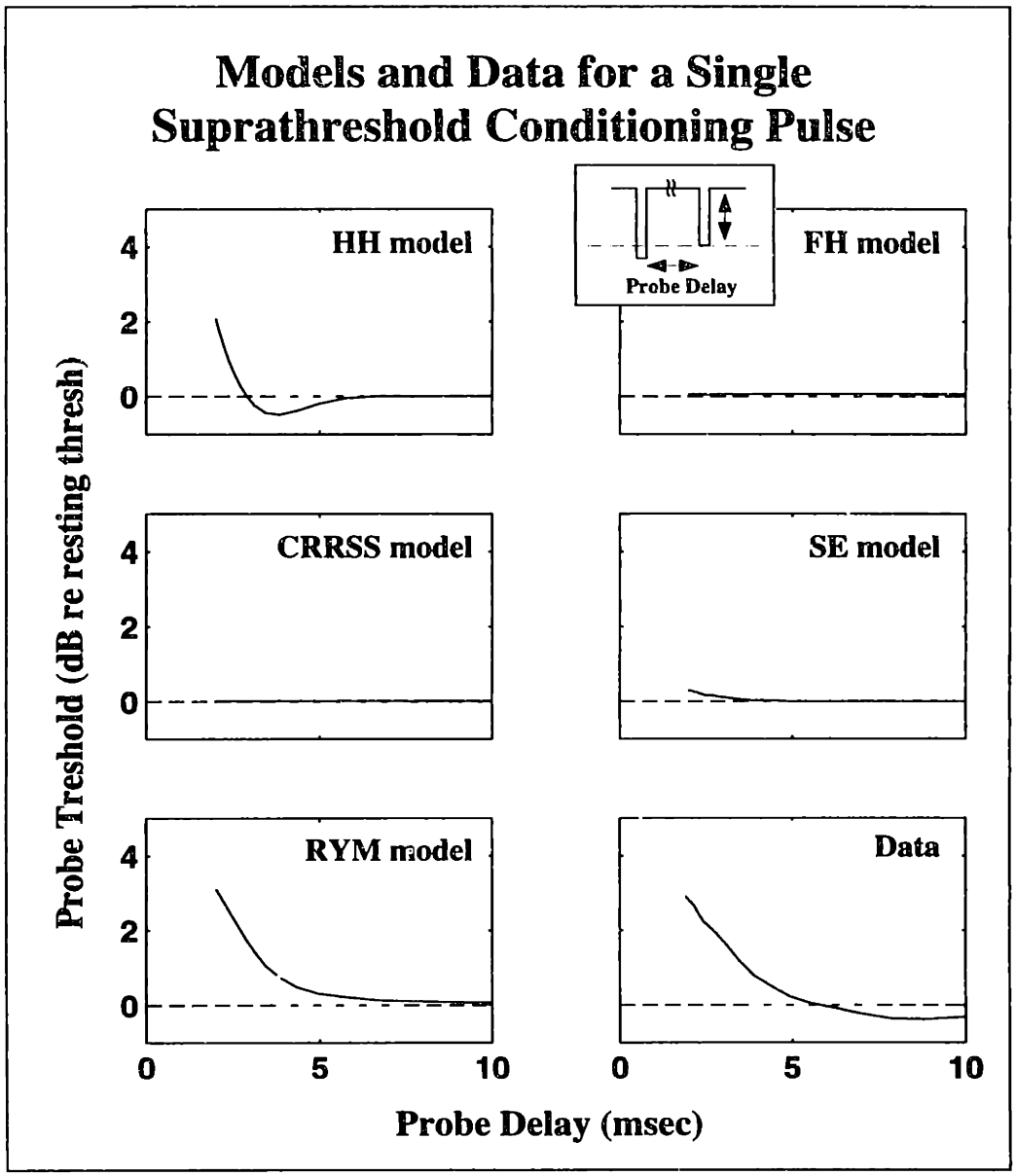

Figure 5-12: Model and data threshold-delay functions following a single suprathreshold conditioner. Plotted as a function of delay is the probe threshold-delay curve as calculated by five models and as determined experimentally (lower right panel). The conditioner level for the models is 1.5 dB above the model resting threshold; the curve given for the data represents an average of all data with conditioner levels 1 – 2 dB above resting threshold (12 units from 4 cats). Both conditioner and probe pulses were single cathodic 100 μsec pulses.

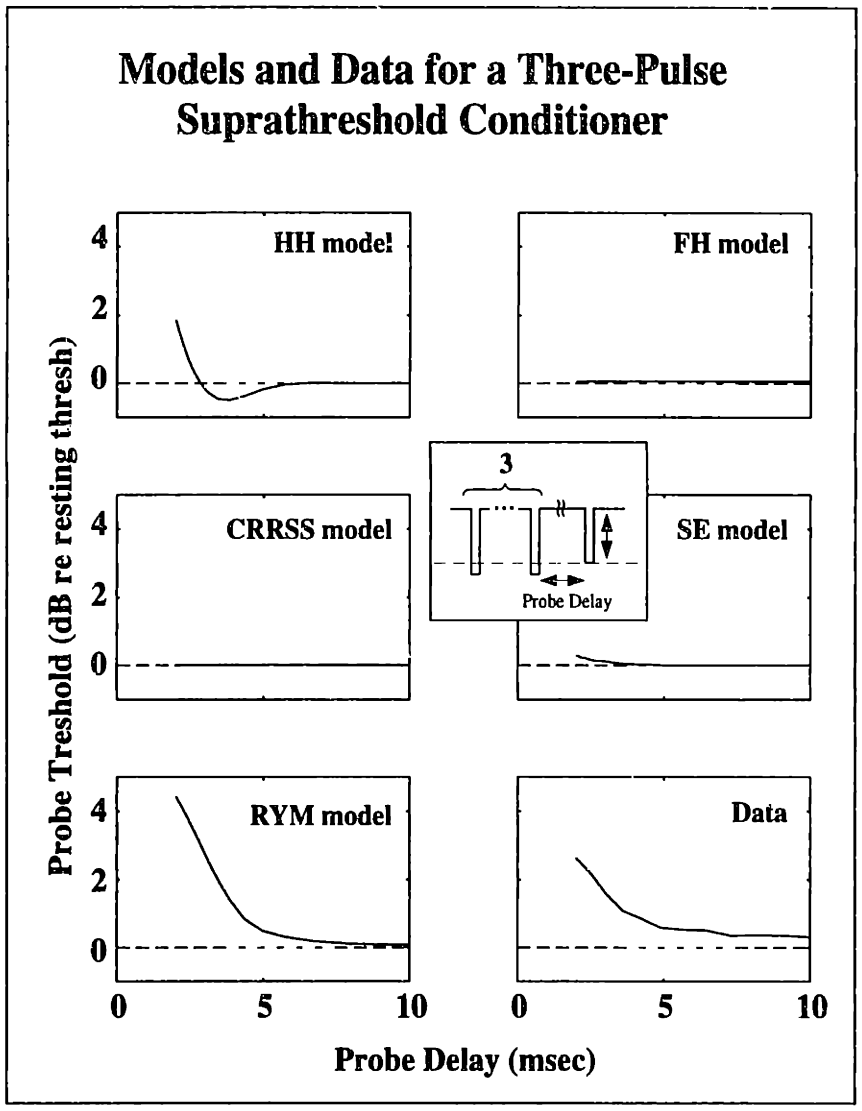

Figure 5-13: Probe threshold as a function of delay for models and data following a three-pulse suprathreshold conditioner. Threshold-delay curves were calculated from simulations using the five models as well as from experimental data and plotted as a function of the probe delay. The conditioner consisted of three cathodic 100-μsec pulses 2 msec apart; the probe was a single 100-μsec cathodic pulse. The conditioner level was 4 dB above the resting threshold for the models; the experimental data shown in the lower right panel is an average of 7 units in 4 cats for which the conditioner level was 3–5 dB above the resting threshold.

pulse case, the initial threshold is fractionally lower for the multipulse conditioner, and there is no drop in the probe threshold below the resting threshold. The probe threshold remains elevated above the resting threshold by about 0.5 dB from a delay of roughly 5 msec, this increase being about two standard errors above the resting threshold.

Going from one to three conditioner pulses, the HH model shows a slight increase in the initial threshold from slightly below to slightly above 2 dB above the resting threshold; there is no change during the sensitizing period of the threshold-delay curve. The RYM model also shows a change in the initial threshold; an increase of about a dB from slightly above 3 dB for the single pulse to above 4 dB for the multiple-pulse conditioner. While the small change in initial threshold calculated by the HH model is consistent with the experimental data, the RYM model, due to its large change in the initial threshold, is not. The remaining models show virtually identical threshold-delay curves for the single and multiple-pulse conditioners.

With the exception of the RYM model, model simulations of suprathreshold threshold-delay curves show little change as the number of conditioning pulses is increased from one to four. This is consistent with the experimental data.

5.4 Summary of model simulations

Of the five models examined, the HH and RYM models most closely simulate the behaviors of the experimental data: for subthreshold pulses, they predict large decreases in probe thresholds for short delays, as is the case with the experimental data. In these two models, this initial sensitization is followed by a period of desensitization, also seen in the experimental data. The HH and RYM model threshold values, while somewhat larger than the average experimental data, agree well with the most extreme cat data. The HH and RYM models also exhibit a decrease in the strength of the sensitization following a multiple-pulse conditioner, similar to the experimental data. The remaining models do not show these characteristics; the two mammalian models (SE and CRRSS) show very small, very short periods of sensitization and

desensitization.

For suprathreshold conditioners again the HH and RYM models offer the closest simulations; the other models do not show substantial relative refractory periods for the probe delays examined. While the RYM simulation is closer to the average cat data than the HH model, the HH model exhibits a sensitization phase not seen in the experimental data. While both models show the same trends as the experimental data going from the single-pulse conditioner to the 3 pulse, 2 msec IPI conditioner, the HH model shows a small change in the initial threshold, as opposed to the RYM model, which shows larger changes not consistent with the experimental data.

5.5 Discussion

5.5.1 Explanation of Model Behaviors

The previous section compared five different models; the HH and RYM models were found to have characteristics that more closely resemble the experimental data than the remaining models. This section will study why these models produce more realistic simulations than other models by examining how the dynamics of the underlying state variables differ. The explanation of the observed behaviors for the HH and RYM models are very similar. For comparison, the HH model of the invertebrate squid giant axon and the SE model of the mammalian rat sciatic nerve are used as they are structurally similar, having only one sodium and one potassium conductance.

Figure 5-14 shows four measures of the response of the HH and SE models to a single subthreshold pulse 1.5 dB below the resting threshold. The top panel shows the calculated probe threshold as a function of probe delay. The remaining three panels plot, as a function of time, the transmembrane potential V_m, along with a representation of the stimulus; the calculated ionic currents; and the model state variables m, h, and n.

As shown previously, the SE model shows a much smaller, shorter sensitization when compared to the HH model. This is due in large part to the much shorter time

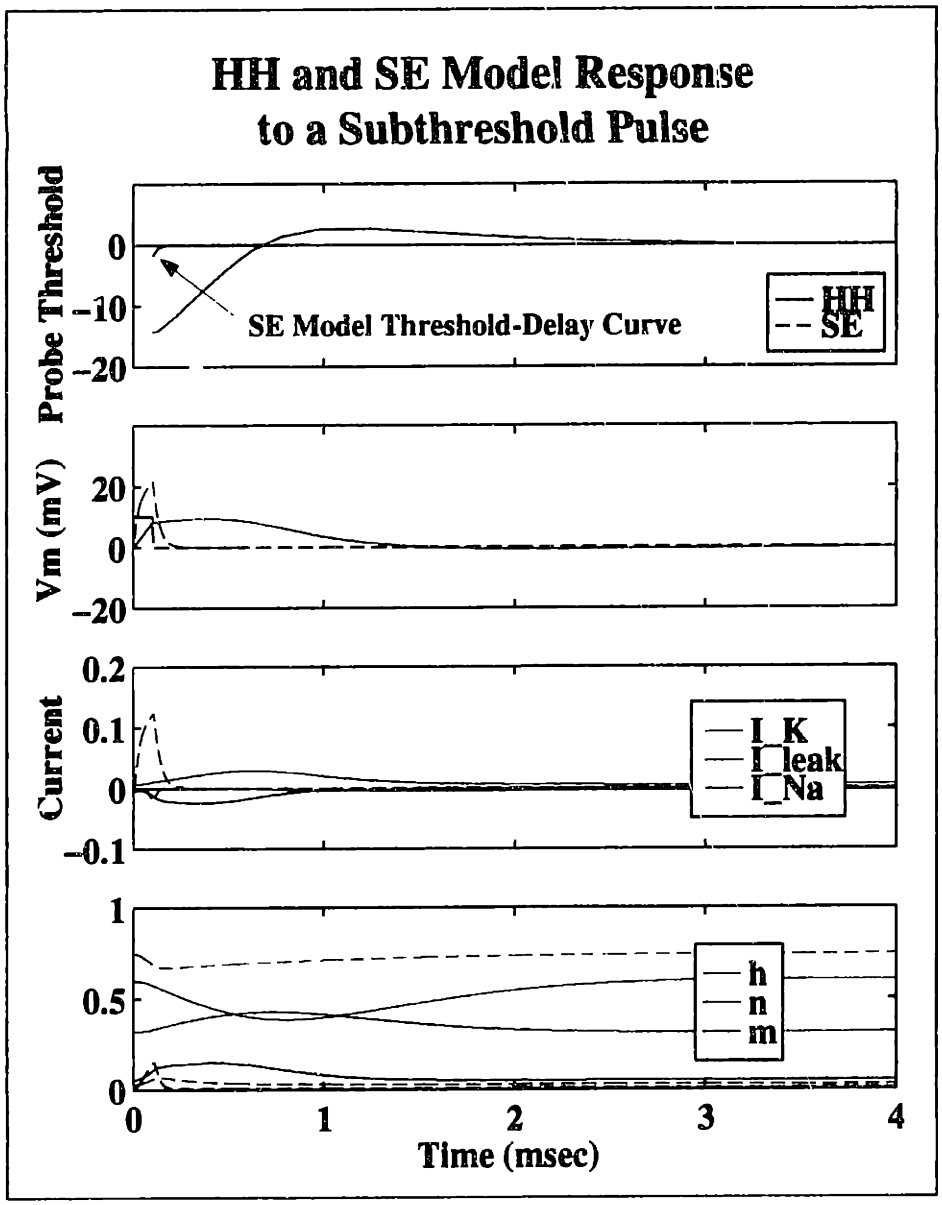

Figure 5-14: HH and SE model response to a subthreshold conditioning pulse. Four measures of the response of the two models are shown: the threshold-delay curve (top panel), the transmembrane potential (upper middle panel), the ionic currents (lower middle panel), and the state variables m, n, and h (bottom panel). The conditioner level is 1-.5 dB dB below the resting threshold. The conditioner, denoted by the dashed line in the second panel, and the probe were single 100-μsec cathodic pulses. If the color labels are missing, refer to Figure 5-1 for the identities of the individual curves.

constants associated with the state variables of the SE model, as can be seen in the bottom panel. Consequently, the transmembrane potential V_m recovers its resting value very quickly; this coupled with the speedy state variables leads to a very quick return of the probe threshold to the resting value. The excursions of all the SE variables from their resting value appears passive for this subthreshold conditioner level in that the variables start to return to their resting value at the end of the stimulus pulse. There is no increasing deviation from their resting value, as is readily apparent for the HH model variables. This may explain the small sensitization effects of the SE model.

For the suprathreshold case, we refer to Figure 5-1, which shows the response of each model to a suprathreshold pulse. The SE model again exhibits much faster time constants than the HH model; the m and n variables are at or near their resting values at a delay of 1 msec. The h variable is increasing towards its resting value, which it achieves around a delay of 4 msec. It is this decrease in the h variable accounts for the small relative refractory period shown in Figure 5-1.

We conclude that the main cause of the difference between the temporal interactions between the HH and the SE models is the speed with which their state variables m, h, and n respond to changes in the transmembrane potential V_m.

Does this explanation hold for the results of other models? The other mammalian model, the CRRSS model, shows a very narrow spike in response to a suprathreshold stimulus (top panel of Figure 5-1), with V_m returning to its resting value after about 0.5 msec. The state variables m, h, and n for the CRRSS model are at their resting state 1 msec following the stimulus onset. This explains why there is no relative refractory period for the CRRSS model as shown in Figure 5-12 and Figure 5-13: the initial delay that is used for the suprathreshold simulations is 2 msec, by which time all the effects of the previous pulse are gone for the CRRSS model.

The short response times of the state variables for the two mammalian models explains the surprisingly poor simulations these models produce of the experimental data. These models, which are based on recordings from myelinated sciatic nerve fibers in rat and rabbit at a temperature of 37 Celsius, are anatomically much more

like the experimental system of the cat auditory nerve could be expected to provide a better fit to our experimental data than the HH model of the unmyelinated squid giant axon.

One reason that the HH model may perform so well is that the temperature corrections to the model rate constants (to account for the difference between the squid temperature of 3 Celsius and the cat temperature of 37 Celsius) were explicitly chosen by Rattay and Aberham to model the maximum discharge rate of auditory nerve fibers responding to electrical stimulation. Thus it is not surprising that the HH and RYM models provide the best fits to the experimental data, as each was optimized in some manner to fit experimental data from the cat auditory system.

5.5.2 Relative Spread and Implications of the Stochastic Model

The classical membrane models are deterministic in the sense that they always produce the same output given the same input. For a particular conditioning stimulus, the calculated probe thresholds are constant, in sharp contrast to the experimental case where the variations in the neural response to identical stimuli gave rise to the P_f-level curves and the study of the relative spread. This is due to these models treating the ionic channels as being a single channel that, rather than being either open or closed, can be continuously varied between those states in a continuous manner. The stochastic extensions to the Hodgkin-Huxley model were made to enable this model to be used to simulate the probabilistic neural responses.

These extensions treat the standard deviation of the binomial open/close probability m^3h of a sodium ion channel as being proportional to the relative spread. The results of this model were shown in Figure 5-7, and overall qualitatively simulate the experimental RS-delay curves. Following a subthreshold stimulus, the model RS is increased above the resting value for short probe delays, although the magnitude of the model RS is much greater than the experimental RS at these short delays. The model and experimental RS curves appear offset along the time axis, with similar

effects in the model RS occurring about 0.75 msec later than the experimental RS.

The suprathreshold case, shown in the lower panel of Figure 5-7, also finds that the model RS qualitatively simulates the experimental data: the RS is decreased from the resting value for shorter probe delays. Again, there appears to be both a magnitude difference and a time shift between the two RS curves. At short delays, the model RS decreases much more then the experimental RS, and for the shortest delays rises dramatically, an effect not seen in the experimental data. The model RS effects again appear delayed by a little less than 1 msec. This offset in the model effects may account for the sharply increased RS at the shortest probe delays following a suprathreshold pulse — this delay corresponds to the falling phase of the model spike following the suprathreshold pulse, while the shortest experimental delay is after the neural spike.

For both sub- and suprathreshold conditioners, the magnitude of the model RS is markedly different than that of the experimental RS for short probe delays. This is likely a result of the model RS not accounting for the spike initiation mechanism, as well as differences in the time course of the HH and experimental sodium kinetics. The nonlinearities associated with spike initiation may cause a saturation in the experimental RS not seen in the model RS. Differences in the time course of the rate constants could cause the membrane conductance noise being different in the model and the cat at identical post-conditioner times, also resulting in RS magnitude differences.

Differences in the time course of the HH and experimental sodium kinetics may also account for the model and experimental RS curves appearing offset along the time axis. By speeding up the rate constants of the HH model, a better fit to the experimental RS may be achieved. As noted above, the temperature correction for the HH rate constants was chosen by Rattay and Aberham to set an upper limit on the maximal discharge rate due to electrical stimulation. It seems that changing the rate constants to obtain a better fit of the RS model to the experimental data would be a more reasonable criteria.

From these results it appears that the trend of the RS for both sub- and

suprathreshold conditioners can be explained using the noise statistics of the HH model sodium channels.

The Results of Rubinstein

J.T. Rubinstein [72] has also modeled the stochastic response of nerve fibers, developing a model incorporating thousands of independent sodium ion channels whose kinetics are based upon a modification of the Schwartz-Eikhof model. Each ion channel is either open or closed, with the probability of a given ion channel being open being determined using the m^3h formalism. The independence of the ion channels gives rise to a neural response that is stochastic in nature, allowing Rubinstein to study the RS in response to arbitrary pulses. Rubinstein kindly ran simulations using single conditioning pulse stimuli as inputs to his stochastic model. He reports that his simulations show no change in RS following subthreshold conditioning pulses (pers. comm.), in contrast to both our experimental and stochastic model studies. The Rubinstein model with a large number of channels and the extended HH model should produce similar results, since the variance of the noise associated with the independent channels in the Rubinstein model will approach the variance of the continuous binomial distribution used in the extended HH model.

It is likely that the reason why Rubinstein's results differ from the experimental and model RS results is his use of the sodium channel from the Schwartz-Eikhof model. As noted above, the state variables of the SE model act very quickly, resulting in very small departures of m, h, and n from their resting values over the range of probe delays investigated experimentally. This would likely be the case with his stochastic model, leading to his model results of no change in the RS following a subthreshold conditioning pulse.

Estimating of the Number of Sodium Channels

A related result of the investigations into the RS and threshold noise is the ability to estimate the number of sodium channels at the site of neural excitation. Assuming a large population of independent sodium channels, the membrane noise, and pre-

sumably the RS, will depend on the square root of the number of sodium channels. Rubinstein examined the stochastic threshold characteristics of nodes containing between 60 to 32000 sodium channels. He shows that the RS is inversely related to the square root of the number of sodium channels, and provides a plot of the correspondence between the two. Thus, knowing the RS resulting from a single pulse, an estimate of the number of sodium channels at the spike initiation site can be made.

Above it is argued that the reason why Rubinstein's RS simulations do not successfully predict the experimental results is due to the time constants of the SE sodium channel being different than those in the cat auditory nerve. Those differences cause the state variables to quickly resume their resting values, resulting in short temporal interactions. This argument does not hold for calculating the RS following a single pulse. At threshold, the neural membrane response is dominated by the conductance noise which leads to the probabilistic response, not by the details of the membrane model. Thus we would expect the Rubinstein model to predict the experimental results for a single pulse. A study of how the computed RS changes with variations in the model parameters support this conclusion.

For a single 100-μsec cathodic pulse, typical RS values for the cat auditory nerve fiber are between .05 and .10 . Using Rubinstein's results, this translates to 600 – 1000 sodium channels at the spike initiation point. For comparison, the rat sciatic nerve fiber that Sigworth [81] used in his studies had a diameter of 14.5 μm and 32000 sodium channels. If the channel density remains constant, based on the rat fiber a 1.2 μm peripheral auditory nerve fiber [48] would have a channel count of roughly 2600.

The RS-based estimate of 600 – 1000 sodium channels at the spike initiation point in an auditory nerve fiber is within the same order of magnitude of the number estimated from scaling a rat sciatic neuron to the size of an auditory neuron. This seems reasonable, given the uncertainty in how sodium channel density differs among various neural systems.

5.6 Summary

It was shown that models based on the Hodgkin-Huxley framework can qualitatively simulate the temporal interactions seen experimentally. Models of five different systems were examined for their ability to simulate the experimental data presented in this work. Using stimuli identical to those used experimentally, only two of the models, the Hodgkin-Huxley model [30] of the squid axon, using temperature rate coefficients suggested by Rattay and Aberham [64], and a model of bushy cells in the cochlear nucleus by Rothman, Young and Manis [69], offer simulations whose temporal and magnitude characteristics are comparable to the experimental data. Of the two models, the HH model more accurately recreates the temporal characteristics of subthreshold phenomena, while the RYM model is quite accurate at predicting the suprathreshold threshold-delay curve for a single conditioning pulse. The HH model more closely matches the trends of the data as the conditioner levels change.

Reasons for these model behaviors were discussed in terms of the state variables of the models; the initial sensitization for subthreshold conditioners is caused by an increase in the sodium activation variable, while the following desensitization can be explained by a combination of sodium inactivation and potassium rectification. The desensitization during the relative refractory period is caused by a decrease in the sodium activation variable.

Surprisingly, models of mammalian systems provided poor simulations of the experimental data. Both sub- and suprathreshold effects happen on a much shorter time scale than for HH, RYM, and experimental data.

The speed of the neural response to changes in the transmembrane potential may be the major difference between models from the viewpoint of how well their simulations resemble the experimental data. It is quite possible that through appropriate adjustments of the model rate constants a model could be evolved that would provide good simulations of the neural response to arbitrary stimuli, including the biphasic interleaved stimuli used in human implant systems.

Chapter 6

Conclusions

6.1 Summary

The initial goals of this study were to characterize the temporal interactions that occur while using non-simultaneous interactions as well as to investigate the physical basis for these interactions, and describe their possible implications for cochlear implants. The interactions were investigated using short cathodic current pulses to both condition and probe the response characteristics of the auditory nerve in cat. The neural response was characterized using measures of the threshold and the normalized dynamic range.

From these physiological studies, we conclude that following subthreshold conditioning pulses the neural threshold is decreased for a short time (up to 1 msec) to subsequent current pulses. Following this period of sensitization, there is a longer, smaller desensitization. For a single conditioning pulse, the sensitization decreases the threshold by an average of 5 dB, while the threshold increase seen during the desensitization period is between 0.5 and 1 dB. For conditioners of more than one pulse, the sensitization decreases sharply, being about 2 dB for a four pulse conditioner. The desensitization increases slightly. For short probe delays (less than 1 msec) there is an increase in the dynamic range of the neural response: there is a larger range of stimulus intensities for which the response is probabilistic. This range of intensities can be more than double that of the unconditioned neuron.

Following suprathreshold conditioners there is the classic relative refractory period: the threshold of the following probe pulse is elevated by about 2 dB at a delay of 2 msec. The probe threshold approximates its resting value after 5 msec. Additional conditioner pulses have little effect on these values. The dynamic range of the neuron following a suprathreshold pulse decreases; the time course of this decrease is longer than the threshold recovery.

Modeling studies examined the ability of Hodgkin-Huxley-like models to simulate the experimental results. All major changes in neural threshold and relative spread with probe delay are qualitatively simulated by this type of model. The models that were most effective were the Hodgkin-Huxley model of the squid giant axon and the Rothman-Young-Manis model of a cochlear nucleus bushy cell. Both these models exhibited strong sensitization periods followed by a weaker desensitization after a subthreshold pulse; the relative refractory periods following a suprathreshold pulse had similar amplitudes and time courses to the experimental data. The two mammalian models examined (the Schwartz-Eikhof model of rat sciatic nerve and the Chiu *et al.* model of rabbit sciatic nerve) showed surprisingly poor simulations for all stimuli investigated, most likely due to the very quick action of the state variables in these models.

6.2 Implications for CIS Processing Strategies

It is clear that temporal interactions have implications for present-day cochlear implant stimulation strategies. For CIS stimulation the interpulse interval for individual electrodes is less than 1 msec, while the interpulse interval across electrodes can be as short as 50μsec. The temporal interactions seen experimentally due to sub- and suprathreshold conditioners last much longer, typically 4–5 msec.

The magnitude of the effects also assure that temporal interactions are important. The magnitude of the sensitization (3–5 dB) and desensitization (3 dB) due to temporal interactions are a significant fraction of the 12 dB or less perceptual dynamic range of human cochlear implant subjects.

Determining how these temporal interactions affect neural activity in cochlear implant subjects using our experimental data is problematic due to the many differences between the two situations. First, charge-balanced pulses are used for human implant stimulation, as opposed to the monophasic stimuli used in this study. While there is no systematic study of temporal interactions using biphasic stimuli, results obtained by us using a single subthreshold biphasic conditioner and a monophasic probe indicate that for the anodic-phase first biphasic pulse used in human implant subjects, there exist temporal interactions much like those described for monophasic subthreshold pulses. Additionally, human implant subject psychophysical results using a single subthreshold biphasic masker followed by a biphasic probe also show temporal interactions resembling those of a single subthreshold monophasic pulse. It seems reasonable to infer from these results that, at a qualitative level, the perceptually-relevant physiological temporal interactions due to subthreshold conditioning stimuli are likely to behave as the monophasic interactions described in this work

Another difference is that human implants use many stimulating electrodes, while this study used a single electrode. While this is unlikely to alter the temporal interactions due to pulses, the stimulus that affects each neuron will be the sum of the current flows due to all electrodes, and will not resemble the stimuli used in this study.

Modification of Neural Responses

The stimuli used in this study are quite simple compared to the stimulus a typical neuron sees in the implanted ear: whereas our conditioners were either completely sub- or suprathreshold, neurons in the implanted ear that code changes in the stimulus amplitude are likely to see a 'mixed' stimulus, consisting of both sub- and suprathreshold pulses. This is due in part to the complex nature of the stimuli that result from CIS processing: the stimulus amplitudes change on multiple time scales, ranging from large changes in the stimulus for onsets in speech sounds, to smaller changes representing the fundamental frequency. Figure 6-1 shows these variations in a CIS stimulus resulting from the processing of "fa" in the word "father's".

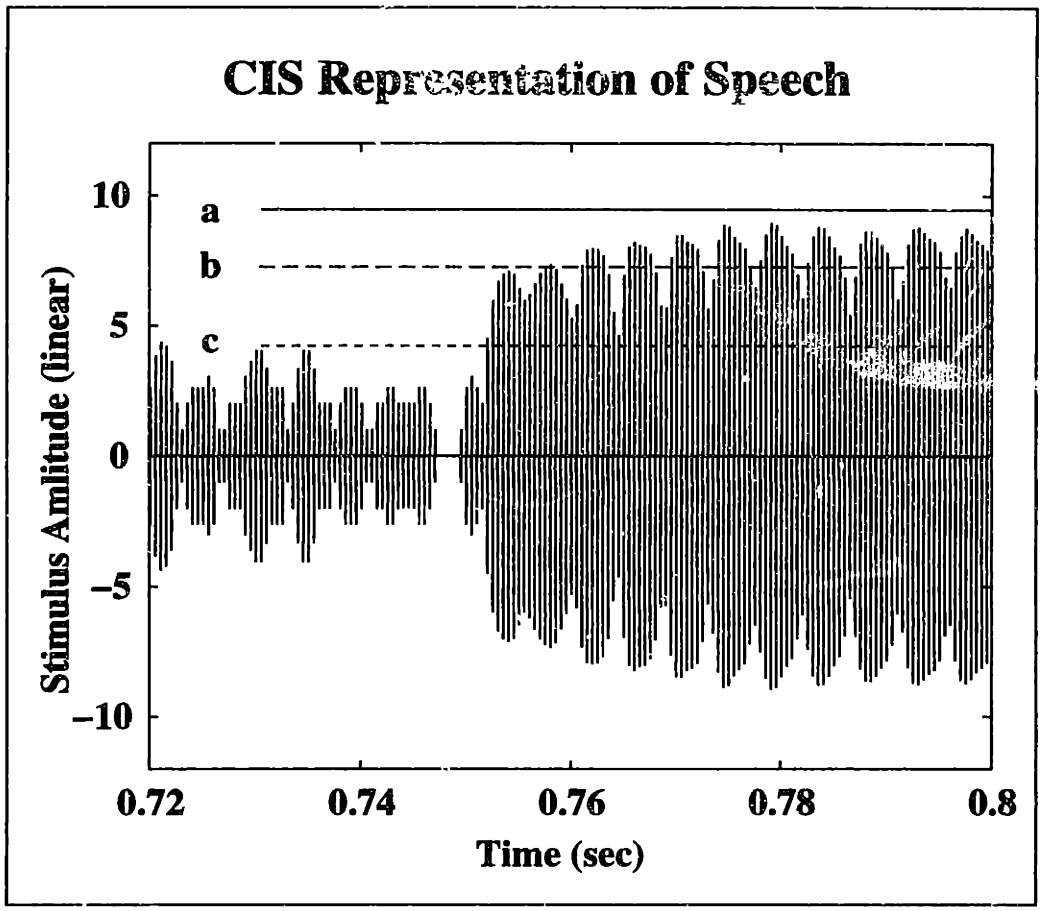

Figure 6-1: Speech processed using a six-channel CIS strategy. Shown is part of the stimulus amplitude in linear units resulting from processing the phrase "Joe took father's green shoe bench out"; the plot shows "fa" in "father's". The dominant periodicity of the right-hand portion is the 224 Hz glottal pulse rate of the female speaker. The three lines represent thresholds of three example fibers. The center frequency of the bandpass filter is 1050 Hz; the sampling frequency of the input is 32k samples/sec; the pulse rate to this particular channel is 1/6 that rate.

For a fiber whose threshold is greater than the maximum pulse amplitude (represented by 'a' in the figure), there would be no response in the absence of temporal interactions. However, if some subthreshold stimulus pulse is of sufficient amplitude to cause a large sensitization, the following pulse may result in a neural discharge. The increase in RS following subthreshold conditioners would increase the likelihood of this neural response to these subthreshold stimuli. These two effects tend to increase the dynamic range of the fiber for subthreshold stimuli; in the absence of the changes in the threshold and RS caused by temporal interactions, the neuron would never discharge to this stimuli.

If the fiber has a threshold corresponding to the 'b' line in the figure, there are alternating periods during which the stimulus pulses will be of sub- and suprathreshold intensity. The lack of experimental data regarding this 'mixed' stimulus (consisting of sub- and supra-threshold pulses) does not preclude us from predicting that the neuron will discharge, as the stimuli is often of suprathreshold amplitude.

A fiber with the 'c' threshold level would find all stimuli in the right portion of the figure to be above the resting threshold. Following a spike, the neuron would be in a refractory state, with the threshold elevated for a period of about 5 msec. The RS is also sharply decreased, resulting in a more deterministic neural response about the refractory threshold level. While the effect of this may be to reduce the apparent dynamic range of the fiber compared to the resting condition, the overall effect may be to increase the dynamic range of the neuron.

This comes about because in the absence of temporal interactions (the refractory period), the threshold would be at its resting value immediately following a spike. The next pulse (being suprathreshold) would cause another spike, and thus the neuron would respond with its maximal discharge rate for a train of even slightly suprathreshold pulses. Temporal interactions result in the relative refractory period, an elevation in the neural threshold following a spike. If the next several spikes are only slightly above the resting threshold, the neuron will not respond until the threshold has decreased to near its resting value, about 5 msec. Thus, temporal interactions result in a decrease in the discharge rate. Raising the level of the pulse train will result

in a higher discharge rate, unlike the case in the absence of temporal interactions. Thus, temporal interactions increase the dynamic range of the fiber for suprathreshold pulses.

From these examples it can be seen that overall, the effects of temporal interactions is to increase the dynamic range of the neural response. It is estimated that temporal interactions may increase the dynamic range from 2 dB (the dynamic range in response to a single pulse) to roughly 6 dB, and that this increase likely depends on the pulse rate, with higher pulse rates leading to larger dynamic ranges.

This increase in the dynamic range may well be a function of the interpulse interval. As shown in Figure 3-1 and Figure 3-5, the sensitization and desensitization effects grow as the second pulse approaches the first. One consequence of this may be that increasing the CIS pulse rate may result in larger dynamic ranges of neural response. Experimentally, increases in the CIS pulse rate is correlated with improved scores by human implant subjects for speech perception tasks (Eddington, pers. comm.). Whether this is a result of the increased temporal resolution of the stimulus, or an increase in the nerve's ability to code changes in the stimulus level, is unknown.

Although these issues will require further experimental data to resolve, the modeling results indicate that the Hodgkin-Huxley model or the Rothman-Young-Manis model provide qualitatively correct simulations of temporal interactions. This result, along with the results of Rattay and Aberham [64], suggest that these models may be useful as a tool to predict the neural response to arbitrary stimuli. This would be an invaluable aid to implant processor designers.

6.3 Future Directions

This study has laid the foundation for further studies into the effects of temporal interactions. The effects of basic temporal interactions were detailed, and it was determined that existing membrane models provide reasonable qualitative simulations of those interactions.

There are two avenues for extending these results: experimentally and through modeling studies.

Experimentally, the regime of mixed conditioners needs to be investigated. The neurons that experience these types of stimuli are those that likely code changes in the stimulus; it is important to understand how these neuron respond in this mixed conditioner situation.

Another area which needs to be explored is examining the effects of changing the interpulse interval for multi-pulse conditioners. This would detail the changes in the neural response to increasing the pulse rate of CIS processors, and test the hypothesis that the increase in human speech perception is due to an increase in the dynamic range of neural responses.

In order to relate these experimental results to the psychophysical results of human cochlear implant studies, it is imperative to replicate these studies using the biphasic stimuli used for the human studies.

These experimental results would be useful for the other avenue in which the results of this study could be extended: increasing the fidelity of models of the neural response to arbitrary stimuli. Previously it was noted that the rate constants for the Hodgkin-Huxley model may not be optimal for the auditory nerve. If a better fit between the model simulations and the experimental results could be found, the result would be a better tool for implant processor designers, and quite possibly a better understanding of the differences between the auditory and other neurons.

Indeed, if the model predictions are accurate enough, it would be quite advantageous to invert the model, such that instead of designers using the model to predict the neural response to a specific stimulus, the inverted model would be used to determine the stimulus needed to cause a desired pattern of activity on the auditory nerve. This would allow direct use of the large body of information on auditory nerve activity to acoustic stimuli, and would truly approach the goal of recreating the functionality of the cochlea through electrical stimulation.

Bibliography

[1] BERKINBLIT, M.B. *et.al.* "Modelling with Electronic Computor of the Behaviour of Nerve Fibre Membrane Under Rhythmic Stimulation" *Biofizikia* **15**, pp 147–155, 1970.

[2] BLACK, J.A., KOCSIS, J.D., and S.G. WAXMAN "Ion Channel Organization of the Myelinated Fiber" *Trends Neurosci.* **13**, pp 48–54, 1990

[3] BOSTOCK, H. "The Strength-Duration Relationship for Excitation of Myelinated Nerve: Computed Dependence on Membrane Parameters" *J. Physiol.* **341**, pp 59–74, 1983.

[4] BOSTOCK, H. and P. GRAFE "Activity-Dependent Excitability Changes in Normal and Demyelinated Rat Spinal Root Axons" *J. Physiol.* **365**, pp 239–257, 1985.es

[5] CARIANI, P. "As if time really mattered: temporal strategies for neural coding of sensory information" *Communication and Cognition — Artificial Intelligence.* **12**(2–3), pp 157–219, 1995.

[6] CHIU, S.Y., MROSE, H.E., and J.M. RITCHIE "Anamolous Temperature Dependence of the Sodium Conductance in Rabbit Nerve Compared with Frog Nerve" *Nature* **279**, pp 327–328, 1979.

[7] CHIU, S.Y. *et.al.* "A Quantitative Description of Membrane Currents in Rabbit Myelinated Nerve" *J. Physiol.* **292**, pp 149–166, 1979.

[8] CLARK, G.M. "The University of Melbourne-Nucleus multi-electrode cochlear implant" *Advances in Oto-Rhino-Laryngology* **38**, pp 1–189, 1987

[9] CLAY, J.R. and DEFELICE, L.J. "Relationship Between Membrane Excitability and Single Channel Open-Close Kinetics" *Biophys. J.* **42** (1983), 151–157

[10] COLOMBO, J. and C.W. PARKINS "A Model of Electrical Excitation of the Mammalian Auditory-Nerve Neuron" *Hear. Res.* **31**, pp 287–312, 1987.

[11] DELGUTTE, B. "Auditory Processing of Speech" in **The Handbook of Phonetic Sciences** W.J. Hardcastle and J. Laver, eds. Blackwell, Oxford. 1996

[12] DYNES, S.B.C. and B. DELGUTTE "Phase- locking of Auditory-nerve Discharges to Sinusoidal Electric Stimulation of the Cochlea" *Hear. Res.* **58**, pp 79--90, 1992.

[13] EDDINGTON, D.K., DOBELLE, W.H., BRACKMANN, D.E. *et. al.* "Auditory prostheses research with multiple channel intracochlear stimulation in man" *Ann. Otol. Suppl.* **53**, pp 5–39. 1978

[14] EDDINGTON, D.K. "Speech discrimination in deaf subjects with cochlear implants" *J. Acoustical Soc. Am.* **68**, pp 885-891. 1980

[15] ERLANGER, J. and E.A. BLAIR *Amer. J. Physiol.* **99**, 108, 1931.

[16] FRANKENHAEUSER, B. and A.F. HUXLEY "The Action Potential inthe Myelinated Nerve Fibre of *Xenopus Laevis* as Computed on the Basis of Voltage Clamp Data" *J. Physiol.* **171**, pp 302–315, 1964.

[17] FRIJNS, J.H.M., MOOIJ, J., and sc tem Kate, J.H. "A Quantitative Approach to Modelling Mammalian Myelinated Nerve Fibers for Electrical Prosthesis Design" *IEEE BME - to be published.* 1994.

[18] GARDNER-MEDWIN, A.R. "An Extreme Supernormal Period in Cerebellar Parallel Fibres" *J. Physiol.* **222**, pp 357–371, 1972.

[19] GASSER, H.S., and H. GRUNDFEST "Action and Excitability in Mammalian A Fibers" *Am. J. Physiol.* **117**, pp 113–133, 1936.

[20] GAUMOND, R.P., MOLNAR, C.E., and D.O. KIM "Stimulus and Recovery Dependence of Cat Cochlear Nerve Fiber Spike Discharge Probability" *J. Neurophys.* **48**, 3, pp 856–873, 1982.

[21] HARTMANN, R., TOPP, G. and R. KLINKE "Discharge patterns of cat primary auditory fibers with electrical stimulation of the cochlea" *Hear. Res.* **13** (1984), 47–62

[22] HARTMANN, R., and R. KLINKE "Impulse pattern in auditory nerve to extra- and intra-cochlear electrical stimulation" in: **Cochlear implant: current situation** International Cochlear Symposium, Düren, West Germany, 1987. P. Bonfai, ed. 73–86

[23] HILLE, B. *Ionic Channels of Excitable Membranes* Sinauer, Sunderland, Ma, 1992

[24] HINOJOSA, R., and M. MARION "Histopathology of profound sensorineural deafness" *Ann. N. Y. Acad. Sci.* **405** (1983), 459–484

[25] HOCHMAIR, E.S., and I.J. HOCHMAIR-DESOYER "Percepts elicited by different speech-coding strategies" in: **Cochlear prostheses: an international symposium** C.W. Parkins and S.W. Anderson, eds. *Ann. New York Acad. Sci.* **405** (1983) 268–279

[26] HOCHMAIR-DESOYER, I.J. *et al.* "Percepts from the vienna cochlear prostheses"in: **Cochlear prostheses: an international symposium** C.W. Parkins and S.W. Anderson, eds. *Ann. New York Acad. Sci.* **405** (1983) 295–306

[27] HODGKIN, A.L. and A.F. HUXLEY "Currents carried by sodium and potassium ions through the membrane of the the giant axon of *Logio.* " *J. Physiol.* **116**, pp 449–472, 1952.

[28] HODGKIN, A.L. and A.F. HUXLEY "The components of membrane conductance in the the giant axon of *Logio.* " *J. Physiol.* **116**, pp 473–496, 1952.

[29] HODGKIN, A.L. and A.F. HUXLEY "The dual effect of membrane potential on sodium conductance in the the giant axon of *Logio.* " *J. Physiol.* **116**, pp 497–506, 1952.

[30] HODGKIN, A.L. and A.F. HUXLEY "A Quantitative Description of Membrane Current and its Application to Conduction and Excitation in Nerve" *J. Physiol.* **117**, pp 500–544, 1952.

[31] HODGKIN, A.L. "The Conduction of the Nervous Impulse" Charles C. Thomas, Springfield, Illinois. 1964.

[32] HOUSE, W.F., and URBAN, J. "Long-term results of electrode implantation and electronic stimulation of the cochlea in man" *Ann. Otol. Rhinol. Laryngol.* **82**, (1973) 504–517

[33] JAVEL, E., TONG, Y.C., SHEPHERD, R.K. and G.M. CLARK "Responses of cat auditory nerve fibers to biphasic electrical current pulses" *Ann. Otol. Rhinol. Laryngol.* **96** , *Suppl.* **128** (1987) 26–30

[34] JAVEL, E. and J.B. MOTT "Physiological and Psychophysical correlates of temporal Processes in Hearing" *Hear. Res.* **34**, pp 275–294, 1988.

[35] JOHNSON, D.H. "The relationship of post-stimulus time and interval histograms to the timing characteristics of spike trains" *Biophys. J.* **22** (1978), 413–430

[36] JOHNSON, D.H. "The relationship between spike rate and synchrony in responses of auditory-nerve fibers to single tones" *J. Acoust. Soc. Am.* **68** (1980), 1115–1122

[37] KATZ, B. "The Time Course of the Excitatory Disturbance in Nerve Following a Short Shock" *Proc. Physiol. Soc.* , p. 6P, 1937.

[38] KATZ, B. "Experimental Evidence for a Non-conducted Response of Nerve to Subthrehsold Stimulation" *Proc. Roy. Soc. B* **124**, pp 244–276, 1937.

[39] KATZ, B. "Nerve Excitation by High-Frequency Alternating Current" *J. Physiol.* **96**, pp 202–224, 1939.

[40] KIANG, N.Y-S., WATANABE, T., THOMAS, E.C. and L.F. CLARK, "Discharge Patterns of Single Fibers in the Cat's Audtiory Nerve" (*Res. Monogr.* nr. **35**) M.I.T. Press, Cambridge (1965)

[41] KIANG, N. Y.-S., and E.C. MOXON "Physiological considerations in artificial stimulation of the inner ear" *Ann. Otol. Rhinol. Laryngol.* **81** pp. 714–730 (1972)

[42] KIANG, N. Y.-S., and E.C. MOXON "Tails of Tuning Curves of Auditory-nerve Fibers" *J. Acoust. Soc. Am.* **55**, 3 pp. 620–28 (1974)

[43] KILLIAN, M.J.P. "Excitability of the Electrically Stimulated Auditory Nerve" PhD. thesis, Univ. Utrecht. 1994.

[44] KOCSIS, J.D. *et.al.*, "Regenerating Mammalian Nerve Fibers: Changes in Action Potential Waveform and Firing Characteristics Following Blockage of Potassium Conductance" *Proc. R. Soc. Lond.* **217**, pp 77–87, 1982.

[45] LEAKE, P.A. *et al.* "Chronic Intracochlear Electrical Stimulation Induces Selective Survival of Spiral Ganglion Neurons in Neonatally Deafened Cats" *Hear. Res.* **54**, pp 251–271, 1991

[46] LECAR, H. and R. NOSSAL "Theory of Threshold Fluctuations in Nerves" *Biophys. J.* **11**, pp 1048–1067, 1971

[47] LIBERMAN, M.C. "The cochlear frequency map for the cat: labeling auditory-nerve fibers of known characteristic frequency" *J. Acoust. Soc. Am.* **72** (1982), 1441–1449

[48] LIBERMAN, M.C. and M.E. OLIVER "Morphometry of intracellularly labeled neurons of the auditory nerve: correlations with functional properties" *J. Comp. Neurol.* **223** (1984) 163–176

[49] LORENTE DE NÓ, R. and H.T. GRAHAM "Recovery of Mammalian Nerve Fibres in vivo" *Biophys. Soc. exp. Biol. Med.* **33**, pp 512–514 1936

[50] MANIS, P.B. and S.O. MARX "Outward Currents in Isolated Ventral Cochlear Nucleus Neurons" *J. Neurosci.* **11**, 9, pp 2865–2880, 1991

[51] MATLAB: High-Performance Numeric Computation and Visualization Software. The Mathworks, Inc. Natick, Massachusetts. info@mathworks.com 1992

[52] MCNEAL, D.R. "Analysis of a model for excitation of myelinated nerve" *IEEE Trans. Biomed. Eng.* **BME 23**, 4, pp 329–337, 1976

[53] MERZENICH, M.M., WHITE, M., VIVION, M.C., LEAKE-JONES, P.A.,and S. WALSH "Some considerations of multichannel electrical stimulation of the auditory nerve in the profoundly deaf; interfacing electrode arrays with the auditory nerve array" *Acta Otolaryngol.* **87** (1979), 196–203

[54] MOXON, E.C. "Neural and mechanical responses to electric stimulation of the cat's inner ear" Doctoral Dissertation, MIT, Cambridge, Mass. 1971

[55] NEWMAN, E.A. and S.A. RAYMOND "Activity Dependent Shifts in Excitability of Frog Peripheral Nerve Axons" *Q. Prog. Rep. Res. Lab. Elect. MIT* **102**, pp 165–189, 1971.

[56] PAINTAL, A.S. "The Influence of Diameter of Medullated Nerve Fibres of Cat on the Rising and Falling Phases of the Spike and its Recovery" *J. Physiol.* **184**, pp 791–811, 1966.

[57] PAINTAL, A.S. "Conduction Properties of Normal Peripheral Mammalian Axons" in: *Physiology and Pathobiology of Axons, S.G. Waxman, ed.* pp 131–144. Raven Press, New York. 1978.

[58] PARKINS, C.W. and J. COLOMBO "Auditory Nerve Single Neuron Thresholds to Electrical Stimulation from Scala Tympani Electrodes" *Hear. Res.* **31**, pp 267–285, 1987.

[59] PARKINS, C.W. "Temporal Response Patterns of Auditory Nerve Fibers to Electrical Stimulation in Deafened Squirrel Monkeys" *Hear. Res.* **41**, pp 137–168, 1989.

[60] PATRICK, J.F. and CLARK, G.M. "The Nucleus 22-channel cochlear implant system" *Ear and Hearing* **12** *Suppl. 1*, pp 3S–9S, 1991

[61] PFINGST, B.E. *et al.* "Psychophysical studies of cochlear implants in monkeys: clinical implications" in **Cochlear implants** R.A. Schindler and M.M. Merzenich, eds. Raven Press, New York. 1985

[62] PICKLES, J.M. An Introdution to the Physiology of Hearing. Academic Press, New York. (1982)

[63] RATTAY, F. "Analysis of Nodels for Extracellular Fiber Stimulation" *IEEE Trans. Biomed. Eng.* **36**, 7, pp 676–682, 1989

[64] RATTAY, F. and M. ABERHAM "Modeling Axon Membranes for Functional Electrical Stimulation" *IEEE Trans. Biomed. Eng.* **40**, 12, pp 1201–1209, 1993.

[65] RAYMOND, S.A. and J.Y. LETTVIN "Aftereffects of Activity in Peripheral Axons as a Clue to Nervous Coding" in: *Physiology and Pathobiology of Axons, S.G. Waxman, ed.* pp 203–225. Raven Press, New York. 1978.

[66] RAYMOND, S.A. "Effects of Nerve Impulses on Threshold of Frog Sciatic Nerve Fibers" *J. Physiol.* **290**, pp 273–303, 1979.

[67] REILLY, J.P., FREEMAN, V.T., and W.D. LARKIN "Sensory Effects of Transient Electrical Stimulation - Evaluation with a Neuroelectric Model" *IEEE Trans. Biomed. Eng.* **32**, 12, pp 1001–1011, 1985

[68] ROSE, J.E. *et.al.*, "Phase-locked response to low-frequency tones in single auditory nerve fibers of the squirrel monkey" *J. Neurophys.* **30** (1967), 769–793

[69] ROTHMAN, J.S., YOUNG, E.D., and P.B. MANIS "Convergence of Auditory Nerve Fibers Onto Bushy Cells in the Ventral Cochlear Nucleus: Implications of a Computational Model" *J. Neurophys.* **70**, 6, pp 2562–2583, 1993.

[70] RUBINSTEIN, J.T. "Analytical Theory for Extracellular Electrical Stimulation of Nerve with Focal Electrodes. II: Passive Myelinated Axon" *Biophys. J.* **60**, pp 538–555, 1991

[71] RUBINSTEIN, J.T. and S.B.C. DYNES "Latency, Polarity and Refractory Characteristics of Electrical Stimulation: Models and Single-unit Data" Abstract in *Sixteenth Midwinter Meeting of the Association for Research in Otolaryngology* 1993

[72] RUBINSTEIN, J.T. "Threshold Fluctuations in an N-channel Model of the Node of Ranvier" *to be published in IEEE BME* 1994.

[73] RUGGERO, M.A. *et al.* "Physiology adn Coding of Sound in the Auditory Nerve" in **The Mammalian Auditory Pathway: Neurophysiology** A.N. popper and R.R. Fay, eds. Springer-Verlag, New York. 1992

[74] SACHS, M.B. and P.J. ABBAS, "Rate versus level functions for auditory-nerve fibers in cats: tone-burst stimuli." *J. Acoust. Soc. Am.* **56** (1974), 1835–1847

[75] SANTOS-SACCHI, J. "Voltage-dependent Ionic Conductances of Type I Spiral Ganglion Cells from the Guinea Pig Inner Ear" *J. Neurosci.* **13**, 8, pp 3599–3611, 1993.

[76] SCHWARZ, J.R., and G. EIKHOF "Na Currents and Action Potentials in Rat Myelinated Nerve Fibres at 20 and 37 ." *Pflügers Arch.* **409**, pp 569–577, 1987.

[77] SHAMMA, S.A. "Speech processing in the auditory system I: The representation of speech sounds in the responses of the auditory nerve" *J. Acoust. Soc. Am.* **78**, pp 1612 – 1621, 1985.

[78] SHANNON, R.V. "Multichannel electrical stimulation of the auditory nerve in man. I. Basic psychophysics" *Hear. Res.* **11**, pp 157–189, 1983.

[79] SHANNON, R.V. "Multichannel electrical stimulation of the auditory nerve in man. II. Channel interaction" *Hear. Res.* **12**, pp 1–16 1983.

[80] SIEBERT, W.M. "Frequency discrimination in the auditory system: place or periodicity mechanisms?" *Proc. IEEE* **58**, pp 723–730 1970. 723–730

[81] SIGWORTH, F.J. "The Variance of Sodium Current Fluctuations at the Node of Ranvier" *J. Physiol.* **307**, pp 97–129, 1980

[82] SNYDER, R.L. *et al.* "Effects of Chronic Intracochlear Electrical Stimulation in the Neonatally Deafened Cat. I: Expansion of Central Spatial Representation" *Hear. Res.* **50**, pp 7–33, 1990

[83] SNYDER, R.L. *et al.* "Chronic Electrical Stimulation in the Neonatally deadfened cat. II: Temporal Properties of Neurons in the Inferior Colliculus." *Hear. Res.* **56**, pp 246–264, 1991

[84] TAYLOR, M.M, and C.D. CREEMAN "PEST: Efficient Estimates of Probability Functions" *J. Acoust. Soc. Am.* **41** pp. 782–87 (1967)

[85] TONG, Y.C., BLAMEY, P.J., DOWELL, R.C. and G.M. CLARK, "Psychophysical studies evaluating the feasibility of a speech processing strategy for a multiple-channel cochlear implant" *J. Acoust. Soc. Am.* **74** (1983), 73–81

[86] VAN DEN HONERT, C. and P.H. STYPULKOWSKI, "Physiological properties of the electrically stimulated auditory nerve. II. Single fiber recordings" *Hear. Res.* **14** (1984) 225–243

[87] VAN DEN HONERT, C. and P.H. STYPULKOWSKI, "Single fiber mappings of spatial excitation patterns in the electrically stimulated auditory nerve" *Hear. Res.* **29** (1987) 195–206

[88] VAN DEN HONERT, C. and P.H. STYPULKOWSKI, "Temporal response patterns of single auditory nerve fibers elicited by periodic electrical stimuli" *Hear. Res.* **29** (1987) 207–222

[89] VERVEEN, A.A. and H.E. DERKSEN "Fluctuation Phenomena in Nerve Membrane" *Proc. IEEE* **56**, 6, pp 906–916, 1968.

[90] WHITE, M.W., MERZENICH, M.M. and J.N. GARDI "Multichannel cochlear implants" *Arch. Otolaryngol.* **110** (1984), 493–501

[91] WIDROW, B. *et al.* "Adaptive noise cancelling: principles and applications" *Proc. IEEE* **63** (1975), 1692–1715

[92] WILSON, B.S. "Signal Processing" 35–85. Singular Publishing Group, San Diego, 1993.

[93] WILSON, B.S. *et. al.* "Better speech recognition with cochlear implants" *Nature* **352**, pp 236–238, 1991.

[94] WOOD, S.L., WAXMAN, S.G., and J.D. KOCSIS "Conduction of Trains of Impulses in Uniform Myelinated Fibers: Computed Dependence on Stimulus Frequency" *Neurosci.* **7**, 2, pp 423–430, 1982.

[95] XU, S.-A. *et. al.* , "Profound hearing loss in the cat following the single coadministration of kanamucin and ethacrynic acid" *Hear. Res.* **70** (1993) 205–215

[96] YOUNG, E.D., and M.B. SACHS "Representation of Steady-state Vowels in the Temporal Aspects of the Discharge Patterns of Populations of Auditory Nerve Fibers" *J. Acoust. Soc. Am.* **66**, 5 pp. 1381–1403 (1979)